



HAL
open science

Detection and real-time classification of abnormal bio-cells by image segmentation technique

Hawraa Haj-Hassan

► **To cite this version:**

Hawraa Haj-Hassan. Detection and real-time classification of abnormal bio-cells by image segmentation technique. Image Processing [eess.IV]. Université de Lorraine; Université libanaise, 2018. English. NNT : 2018LORR0043 . tel-01920276

HAL Id: tel-01920276

<https://hal.univ-lorraine.fr/tel-01920276v1>

Submitted on 1 Mar 2022

HAL is a multi-disciplinary open access archive for the deposit and dissemination of scientific research documents, whether they are published or not. The documents may come from teaching and research institutions in France or abroad, or from public or private research centers.

L'archive ouverte pluridisciplinaire **HAL**, est destinée au dépôt et à la diffusion de documents scientifiques de niveau recherche, publiés ou non, émanant des établissements d'enseignement et de recherche français ou étrangers, des laboratoires publics ou privés.



AVERTISSEMENT

Ce document est le fruit d'un long travail approuvé par le jury de soutenance et mis à disposition de l'ensemble de la communauté universitaire élargie.

Il est soumis à la propriété intellectuelle de l'auteur. Ceci implique une obligation de citation et de référencement lors de l'utilisation de ce document.

D'autre part, toute contrefaçon, plagiat, reproduction illicite encourt une poursuite pénale.

Contact : ddoc-theses-contact@univ-lorraine.fr

LIENS

Code de la Propriété Intellectuelle. articles L 122. 4

Code de la Propriété Intellectuelle. articles L 335.2- L 335.10

http://www.cfcopies.com/V2/leg/leg_droi.php

<http://www.culture.gouv.fr/culture/infos-pratiques/droits/protection.htm>

Détection et Classification temps réel de bio-cellules anormales par technique de segmentation d'images

Thesis

Présentée et soutenue publiquement le 30/01/2018

Pour l'obtention du

Doctorat de l'Université de Lorraine

(Discipline : Système électroniques)

Par

Hawraa HAJ HASSAN

Composition du jury

Rapporteurs : MCF HDR Jean-Philippe Blondé, Université de Strasbourg, France
MCF HDR Virginie Fresse, Université de Sainte-Etienne, France
Examineur : Prof. Youssef Harkouss, Université Libanaise, Liban
Prof. Ahmed Bouridane, Université Northumbria, UK
Dr. Ahmad Chaddad, McGill University, Canada
Prof. Camel Tanougast, Université de Lorraine, France

*To my parents,
To my brothers,
To my kids,
To my husband,
To all my family,
To all my friends...*

Acknowledgement

It is an honor to obtain my PhD degree from the University of Lorraine under the direction of Professor Camel Tanougast and the Lebanese University under the direction of Professor Youssef Harkouss. I would like to thank them for their hard work and dedication and for the great support throughout my thesis, also for allowing me to have new experiences by attending many international conferences, and their support in publishing my work a journal paper.

I would like to thank Dr. Ahmad Chaddad for supporting me during the thesis work stages, also for his interest and follow up through Skype meetings on a weekly basis which sometimes continued till midnight. I would like to thank him for his efforts that represented a big part of my context.

Many thanks to the president of the committee Professor Ahmed Boridane. In addition, a special thanks for the rapporteurs Dr. Jean-Philippe Blondé and Dr. Virginie Fresse and I am delighted they accepted my work. Thank again for Dr. Ahmad Chaddad, Professor Ahmed Bouridane, Professor Camel Tanougast and Professor Youssef Harkouss as being the examiners in the committee.

Thanks to my colleagues in LCOMS laboratory, especially Dr. Fadel Abdallah and Christophe Kizil, who were there for me and ready for continuous support and help.

Finally, big thanks for my family and my friends in Lebanon especially for my mother that supported me throughout the different stages of the thesis. Also dedicated for the memory of my father and grandfather who represented a father's support to me, all my wishes I would made them proud of me wherever they are now. Also big thanks for my brothers, my husband, and for my children who entered added happiness to my life.

Contents

List of Figures	9
List of Tables	11
List of Abbreviations	12
GENERAL INTRODUCTION	16
CHAPTER I INSTRUMENT NEEDED FOR DIGNOSIS OF TUMOR DISEASE	23
1. Introduction.....	23
2. Colon Cancer	25
2.1. What is Colon Cancer?	25
2.2. Causes, Symptoms and diagnosis	26
2.3. Colorectal cancer treatment	27
2.4. Colorectal cancer development	29
3. Types of abnormal tissues images	31
4. Conclusion	37
CHAPTER II - SEGMENTATION OF THE ABNORMAL TISSUES	39
1. Introduction.....	39
2. Methods and Materials	39
2.1. Thresholding.....	39
1) Inter-means algorithm	40
2) Minimum-error algorithm	42
3) K-mean clustering	45
2.2. Edge-based Segmentation	47
1) Gradient method.....	47
2) Zero crossings from a Laplacian-of-Gaussian filter	48
2.3. Region-based Segmentation	49
1) Seeded region method	49
2) Split and merge algorithm.....	50
2.4. Snake Method	51
2.5. Performance Metrics	53
2.6. Application of the segmentation methods on histopathological images	54
3. Conclusion	56
CHAPTER III- CLASSIFICATION OF MULTISPECTRAL COLORECTAL ABNORMAL TISSUES	59

1. Introduction.....	59
2. Classification using CNN	60
2.1. Machine Learning.....	60
2.2. Description of CNN.....	64
2.3. Implementation of CNN.....	74
3. Extraction of Features	80
3.1. Gray-level run length matrix	80
3.2. Gray-level size zone matrix.....	81
3.3. Scale Invariant Feature Transformation (SIFT)	82
3.4. Features extracted from CNN.....	83
4. SVM Classifier	83
4.1. Treebagger SVM	83
4.2. KNN SVM.....	84
5. Conclusion.....	84
CHAPTER IV - RESULTS AND DISCUSSION	87
1. Introduction.....	87
2. Classification Results.....	88
2.1. CNN.....	88
2.2. SVM	95
2.3. Comparison between CNN and SVM	98
2.4. Discussion.....	99
3. Conclusion	100
CONCLUSION AND PERSPECTIVES.....	102
List of Publications	104

List of Figures

Chapter I

Figure I. 1. Variation of the percentage of death (cancer) with respect to age [6].	23
Figure I. 2. Variation of the percentage of new cases (cancer) with respect to age [6].	24
Figure I. 3. The digestive system [7].	25
Figure I. 4. Various layers colonic tissues [10].	29
Figure I. 5. Gradation from polyps to cancer [10].	30
Figure I. 6. Microscopic images of normal and abnormal cells.	32
Figure I. 7. a) diagram of a simple microscope, b) diagram of a complex microscope.	34
Figure I. 8. Multispectral image.	35
Figure I. 9. Multispectral model of CCD camera (Hamamatsu C5985).	36
Figure I. 10. Proposed flowchart for automated detection of CRC progression using CNN comprises multispectral images of PT.	36

Chapter II

Figure II. 1. Inter-means algorithm	41
Figure II. 2. Minimum-error algorithm.	44
Figure II. 3. K-mean clustering algorithm.	46
Figure II. 4. Example of segmentation models based on: (a) The original image, (b) Prewitt, (c) Sobel, (d) Roberts, (e) Laplacian.	48
Figure II. 5. An example of seeded region method, (a) Original image, (b) 1st step, (c) 2nd step, (d)3rd step, (e) 4th step, (f) 5th step, (g) 6th step.	50
Figure II. 6. Quadtree for splitting, (a) Partition, (b) Split quadtree.	51
Figure II. 7. RAG with adjacency relations (in red) for big black region, (a) Merge tree, (b) Merge image.	51
Figure II. 8. Example of snake algorithm, (a): initial image, (b): contour after many iterations and (c): segmented image using snake method.	53
Figure II. 9. Automatic and manual segmentation of carcinoma cell type.(a) Three multispectral images of carcinoma cells, (b) Manual segmentation images, (c) Snake segmentation images, (d) Thresholding segmentation images, (e) Edge based segmentation images, (f) Region based segmentation images.	55

Chapter III

Figure III. 1. Traditional pattern recognition system	61
--------------------------------------------------------------	----

Figure III. 2. The perceptron	61
Figure III. 3. A multi-layer perceptron with 2 hidden layers	63
Figure III. 4. (a). Input neurons, (b). Local receptive field.	65
Figure III. 5. First convolution.	65
Figure III. 6. Second convolution.	66
Figure III. 7. Three feature maps.	68
Figure III. 8. A pooling unit.	69
Figure III. 9. CNN architectural model.	70
Figure III. 10. One plane of a convolution layer in CNN.	71
Figure III. 11. One plane of a sub-sampling layer in CNN.	72
Figure III. 12. Training system of the CNN classifier.	73
Figure III. 13. Proposed flowchart for automated detection of CRC progression using CNN comprises: 1) multispectral images of PT, and 2) Convolution neural network to classify each CRC image from segmented and non-segmented PT.	75
Figure III. 14. Example of the calculation of a run length matrix for a 4x4 image in 0° directions and for 4 gray levels.	81
Figure III. 15. Example of the calculation of a run length matrix for a 4x4 image with 4 gray levels.	81

Chapter IV

Figure IV. 1. Example of 256 non-segmented images of types ST, BH, IN and Ca.	89
Figure IV. 2. Variation of MSE during the training process of non-segmented images	90
Figure IV. 3. Example of 256 segmented images of types ST, BH, IN and Ca	92
Figure IV. 4. Variation of MSE during the training process of segmented images	93

List of Tables

Chapter II

Table II. 1: Comparative study of four segmentation techniques.	56
-----------------------------------------------------------------------------	----

Chapter III

Table III. 1: The composition of eight CNNs showing its accuracy and its mean squared error	78
----------------------------------------------------------------------------------------------------------	----

Chapter II

Table IV. 1: Summary of training and testing of the proposed CNN.....	94
Table IV. 2: Comparison of classification methods in the same type of data.	94
Table IV. 3: Comparison of tissue classification methods on the same data.	95
Table IV. 4: Performance metrics for multispectral texture of CRC cells using Treebagger SVM classifier.	96
Table IV. 5: Performance metrics for multispectral texture of CRC cells using KNN SVM Classifier.	97
Table IV. 6: Examples of some methods using different feature in the same type of data.	98
Table IV. 7: Comparison of CNN and SVM.	99

List of Abbreviations

CNN	:	Convolutional Neural Network
CRC	:	Colorectal Cancer
FPGA	:	field-programmable gate array
LCTF	:	liquid crystal tunable filter
CCD	:	Coupled Charged Device
SVM	:	Support Vector Machine
KNN	:	K-Nearest Neighbor
ST	:	Stroma
BH	:	Benign Hyperplasia
IN	:	Intra-epithelial Neoplasia
Ca	:	Carcinoma
PT	:	Pathology Tissue
JSC	:	Jaccard Similarity Coefficient
DSC	:	Dice Similarity Coefficient
FPR	:	False Positive Rate
FNR	:	False Negative Rate
ANN	:	Artificial Neural Network
NN	:	Multi-Layer Perceptron
MLP	:	Neural Network
GD	:	Gradient Descent
RPROP	:	Resilient Backpropagation
MSE	:	Mean Squared Error

GLRLM	:	Gray Level Run length Matrix
GLSZM	:	Gray Level Size Zone Matrix
SIFT	:	Scale Invariant Feature Transformation
DOG	:	Difference of Gaussians
GLCM	:	Gray Level Co-occurrence Matrix
DW	:	Discrete Wavelet
DWT	:	Discrete Wavelet Transforms
CCSM	:	Color Components based Statistical Moments

Abstract

Development of methods for help diagnosis of the real time detection of abnormal cells (which can be considered as cancer cells) through bio-image processing and detection are most important research directions in information science and technology. Our work has been concerned by developing automatic reading procedures of the normal and abnormal bio-images tissues. Therefore, the first step of our work is to detect a certain type of abnormal bio-images associated to many types evolution of cancer within a Microscopic multispectral image, which is an image, repeated in many wavelengths. And using a new segmentation method that reforms itself in an iterative adaptive way to localize and cover the real cell contour, using some segmentation techniques. It is based on color intensity and can be applied on sequences of objects in the image.

This work presents a classification of the abnormal tissues using the Convolution neural network (CNN), where it was applied on the microscopic images segmented using the snake method, which gives a high performance result with respect to the other segmentation methods. This classification method reaches high performance values, where it reaches 100% for training and 99.168% for testing. This method was compared to different papers that uses different feature extraction, and proved its high performance with respect to other methods. As a future work, we will aim to validate our approach on a larger datasets, and to explore different CNN architectures and the optimization of the hyper-parameters, in order to increase its performance, and it will be applied to relevant medical imaging tasks including computer-aided diagnosis.

Keywords: Abnormal tissues, Microscope, Multispectral images, Segmentation, Snake, Classification, Convolution Neural Network.

Résumé

Le développement de méthodes de la détection en temps réel de cellules anormales (peuvent être considérées comme des cellules cancéreuses) par captures et traitements bio-images sont des axes de recherche importants dans le domaine biomédical car cela contribue à diagnostiquer un cancer. C'est dans ce contexte que se situent ces travaux de thèse. Plus précisément, les travaux présentés dans ce manuscrit, se focalisent sur le développement de procédures de lecture, de détection et de classification automatiques de bio-images de cellules anormales considérées comme des cellules cancéreuses. Par conséquent, une première étape du travail consiste à déterminer une solution de détection, à partir d'images microscopiques multispectrales permettant une répétitivité d'images sur une gamme de longueurs d'ondes de certains types de bio-images anormales associées à différents stades ou évolutions de cellules cancéreuses. L'approche développée dans ces travaux repose sur l'exploitation d'une nouvelle méthode de segmentation basée sur l'intensité de la couleur et pouvant être appliquée sur des séquences d'objets dans une image en reformant de manière adaptative et itérative la localisation et la couverture de contours réels de cellules. Cette étape préalable de segmentation est primordiale et permet une classification des tissus anormaux en utilisant la méthode de réseau de neurones à convolution (CNN) appliqué sur les images microscopiques segmentées de type snake. L'approche permet d'obtenir de bons résultats comparativement à une approche basée sur d'autres méthodes de segmentation de la littérature. En effet, cette méthode de classification atteint des valeurs de performance de 100% pour la phase d'apprentissage et de 99.168 % pour les phases de test. Cette méthode est comparée à différents travaux antérieurs et basées sur différentes fonctionnalités d'extraction, et a prouvé son efficacité par rapport à ces autres méthodes. En termes de perspectives, les travaux futurs visent à valider notre approche sur des ensembles de données plus larges, et à explorer différentes architectures CNN selon différents critères d'optimisation.

Mots-clés: Tissus anormaux, Microscope, Images multispectrales, Segmentation, Serpent, Classification, Réseau de neurones convolutionnels.

GENERAL INTRODUCTION

Context

Our work represents a cotutelle between the University of Lorraine under the direction of Prof. Camel Tanougast, and the Lebanese University under the direction of Prof. Youssef Harkouss.

Where our work decomposed in two parts such as segmentation and classification, and it is based on five papers of dr. Ahmad Chaddad under the name of: “Multi Texture Analysis of Colorectal Cancer Continuum Using Multispectral Imagery”, “Extracted haralick’s texture features and morphological parameters from segmented multispectral texture bio-images for classification of colon cancer cells”, “Carcinoma cell identification via optical microscopy and shape feature analysis”, “Improving of colon cancer cells detection based on Haralick's features on segmented histopathological images” and “Improving Snake Method Using Canny Approach Implementation for Fast Cancer Cells Detection”.

We receive the data of the normal and abnormal tissues form dr. Chaddad which obtained from anatomical pathology at the CHU Nancy-Brabois Hospital, decomposed into normal tissue and three abnormal tissues according to the development of the disease. Also we set off from the snake method using a progressive division of the dimensions of the image in order to achieve faster segmentation, and the manual segmentation done by anatomists in order to evaluate our segmentation techniques. In addition, we based on SVM as a part of our classification, and searching for another features after comparing its results to the features studied by dr. Chaddad.

During our work, the time computation taken to extract the type of the input image are summed between the time needed for segmentation with the time needed for classification. Where the time computation of segmentation was decreased to 50% during using the progressive division of the dimensions of the image reaching about two minutes. In addition, the time computation for the classification reaches about three minutes to indicate the category of the input image. where we are going to decrease the time computation as a next work using many estimations based on previous work such as FPGA implementation as Chaddad et al. study in their work that proposed proving good performances in term of time processing and logic area consumption during segmentation, and an Adaptive Drop-weight technique to solve the problems of speed and storage capacity during applying Convolution Neural network.

Motivation

The electronic devices and instruments for the medical applications play an important role today in the diagnosis and the treatment of the diseases, and it is developed with the evolution of the integrated microelectronic circuits and systems especially for the medical imaging such as scanner, X-Ray, and many others. This development presents a push for clarification and evolution of the cancer diagnosis and also cancer types and stages, which presents using the analysis of histopathological images, that detects many cancer types using computer aided, such as lung [1], prostate [2, 3], breast [4, 5] for more than 38% of cancers in the western world, including in France and the United Kingdom. Many hospitals have a different opinion about the surgical pathology material, which results in major therapeutic and prognostic modifications for patients; this opinion is not new where it began at the early years of 1970s, where the opinion tends to reduce the unwarranted elective surgeries and to decrease the number of unnecessary medical procedures.

In our work, we are concerned in the detection of colorectal cancer cells from multispectral images, which represents, a collection of many monochrome images where each one has its different frequency. This type of image is an important tool for understanding the image formation, and it helps in capturing the information, which is not available to the human observer. In other side, it has a drawback, which is the time computation, and it needs more memory, since it has to process additional data. The multispectral image is taken by a microscope and a CCD camera that is integrated to it with a liquid crystal tunable filter (LCTF) using an optical microscopy system. Microscope which is an instrument used to see the small objects that is invisible to the eye has many types, but the most common and the oldest one is the optical microscope which uses the visible light and lenses to magnify and improve the resolution of the images.

The selection of a good camera is important, where many reasons will affect in choosing it, such as:

- Cost and Size: not the most expensive or the biggest one is always the best one, where we need to choose the camera which is convenient to our work,
- Field of view: where it is determined by the focal length of the telescope, and the size of the CCD sensor, knowing that the camera with shorter focal length and larger pixels is preferred,
- Sensitivity: which is determined by many things such as, focal ratio, pixel size and quantum efficiency of the detector,
- Resolution: which is corresponding to the number of pixels used in the device,
- Guiding: where it is a very important function in CCD images, and you will not get a very good images without good guiding,

- Noise: camera should be designed to minimize the impact of the noise and sky background
- Software: every CCD camera is operated with a computer, so it needs a good software in order to have a good one.

LCTF, which is an optical filter that uses liquid crystal to transmit the wavelength of light, it is usually used with the CCD camera to enable very high image quality, and easy integration. Some LCTFs are designed to a limited number of wavelengths, and others can be required over a wide range of wavelengths.

A good capture of the images helps the segmentation process to reach its aim by better performance. The image segmentation is a process that locates objects and boundaries in an image according to certain specifications that varies with the variation of the methods used. For each application, many segmentation methods are studied and updated in order to ameliorate the segmentation results. Therefore, each method improves its strength in a certain type of images, where in our colorectal cancer applications many segmentation methods applied on it, such as threshold, edge, region and snake methods. It is clear that segmentation is naturally taking place in the human visual system, where we are congenitally looking initially for lines, edges and shapes in a certain image in order to find objects inside it [6]. Image segmentation has a long history, beginning from Brice and Fenema (1970), Pavlidis 1972 that takes the image pixels as regions, and choosing λ to determine the number of regions needed. Knowing that these methods face a main problem, which is how to choose the convenient value of λ , Morel-Solimini 1995, solves this problem by choosing it as scale parameter. In 1985, 1989 Mumford-Shah formulized the region growth where it decomposed the energy associated with a segmentation into three parts, which lead to minimal segmentations made of a finite set of curves [7]. Snake method which is an automatically detecting contours of objects is studied by Kass-Witkin-Terzopoulos (1987), where it minimizes the energy using Euler-Lagrange equations. Today, many scientists update the snake method in a way to increase its performance and decrease its time implementation, and many applications are now depending in its work on it.

After segmenting the image and determining the objects inside it, a good classification is needed in order to get a good result in many applications especially in the medical domain, which plays an important role in the diagnosis and the treatment of the diseases. Many classification methods which depend on the extraction of many types of features are studied, where these features change and increase with time in a way to increase the performance of the classification method according to the type of application. Chaddad et al. [8], uses Laplacian of Gaussian filter, Discrete wavelets and GLCM as features where they apply it on LDA, Decision trees and Nearest neighbors classifiers. Also, Peyret et al. [9], apply Local binary patterns, GLCM and Local

intensity order patterns on SVM and Random forest classifiers. Clinically significant and biologically features are used by Kumar et al. [10], where they are applied on Nearest neighbors and SVM classifiers. Where Rathore et al. [11], used SVM as a classifier and applied Statistical moments and GLCM on it. Also Elgamal et al. [12], extract Discrete wavelets features and applied it on Nearest neighbors and Neural Networks.

Another type of classification is the neural network technique, which plays an important role in the diagnosis of the disease, since it uses machine learning and visualization. It depends on the records of the data, and comparing their classification to it, where it measures the error and update its network characteristic till decreasing the error to its minimum value. As an initial advantage, neural network is a self-adaptive method, where it updates its characteristics according to the given data, and also it can approximate any function with arbitrary accuracy. Also neural network represents a non linear one, which makes it flexible in modeling, and it is able to estimate the posterior probabilities that are important in establishing the classification rules. Over the years, it has been applied successfully in many applications such as medical diagnosis, fault detection and recognition [13]. The self-organization of neural networks give it an important role especially in the classification of medical images which make it involved in diagnosis decision.

Convolution Neural Network (CNN) which is proposed originally by LeCun [14] is one type of machine learning which improves its high performance, where it automatically learns local feature extractors and classifies it. CNN is trained initially by taking data, compare it and measure the error, then it updates its characteristics in order to decrease the error. This process is repeated until reaching a minimum error, and in order to measure the performance of CNN, it will be tested by another data. CNN is used in many applications such as classifying the face recognition [15], visual inputs arising from documents [16], in medical image [17] [18], and in the detection of abnormal tissues [14].

In our work we are going to capture the multispectral images, and apply the snake segmentation on it, and we will classify the segmented and non segmented images using CNN as a classifier, and using different types of classification applied on many types of features including the features extracted from CNN. Then the comparison will be done for each type of classification after applying it on the segmented and non segmented images in order to determine the importance of segmentation. Next step is to make comparison between the classification types that depend on the features extracted, including the features extracted from CNN. Finally all these methods will be compared to the classification that depends on CNN in order to improve the high performance of it. This comparison is important in the medical diagnosis, especially in our case which concerns the colorectal cancer.

Organization of the thesis

The thesis manuscript is divided into four chapters. The rest of the paper is organized in the following sequence:

- Chapter 1 introduces the research scope of this thesis and the basic concepts related to the Histological observation based on microscope observations through visual magnifications samples conditioned tissue of abnormal cells (Colorectal cancer). Firstly, the overview of the establishment of an instrumental bench multi-spectral image capturing histologies based on the combination of a microscope, a LCTF filter and a CCD camera to digitize, automate and perform extraction and analysis of information textural is presented. Then, the chapter specifies the choice of multi-spectral images based on the quality and the sufficient quantity of textural information, and the digital acquisition based on acquisition and image processing by specific architectures or computers. The main contributions of this thesis are presented in the following chapters 2, 3, and 4.
- Chapter 2 presents the proposed snake segmentation of the digital image in order to get in one hand an automatic and effective method of treatment detection and classification of images from multi-spectral microscope device to capture digital images. Some numerical simulations are made to test the validity and robustness of the proposed segmentation schemes. A comparative study between different segmentation methods is studied on the same number and types of images. Snake segmentation was demonstrated highest similarity metrics by comparison with other approaches, which give it the priority to be chosen as a segmented method in our work.
- Chapter 3 presents a brief description of machine learning, and then CNN is studied after showing its importance in machine learning. Then, this chapter proposes to work with CNN as a colon cancer cells classifier that automatically learns local feature extractors. We have implemented several network architectures, and compared their performances, to find the CNN that provides the highest accuracy reaching 100% during the training phase, and 96.97% during the test phase. In this chapter, we also compare SVM to the CNN classifier in order to evaluate the better method, where it will be applied on 40 multi-spectral image textured sound like cells (ST) or abnormal (BH, IN and Ca), which will be described in the next chapter.

- Chapter 4 presents a method for the classification of CRC tissues from multispectral biopsy images, based on active contour segmentation and on three classifiers such as: CNN, treebagger- SVM and KNN- SVM after extracting features from the proposed CNN, which learn a discriminative representation directly from the data. Experiments of these methods are done on multispectral images of 40 patients, and CNN outperform traditional approaches when using pre-segmented images, and also outperform the two other classifiers which scored the top ranking in the last century. Moreover, the testing accuracy of our proposed approach is compared with that of other methods applied either on the same type of data or not, and in both cases, it proves the strength of the CNN classifier over other used classifiers. CNN improves its strength in extracting its features and also in classifying it.
- In the conclusion chapter, conclude about the main contribution of these works and discuss performance of proposed automated segmentation step suitable for hyperspectral image. This chapter introduces future works by given several useful investigations allowing to improve the proposed contributions.

References

- [1] K. Hagiwara, K. Hikasa, K. Nakamura, M. Tanabashi, M. Aguilar-Benitez, C. Amsler, *et al.*, "Review of particle properties," *Physical Review D*, vol. 66, p. 010001, 2002.
- [2] R. Seager, M. Ting, I. Held, Y. Kushnir, J. Lu, G. Vecchi, *et al.*, "Model projections of an imminent transition to a more arid climate in southwestern North America," *Science*, vol. 316, pp. 1181-1184, 2007.
- [3] J. Doyle, W. Ge, and S. McVay, "Determinants of weaknesses in internal control over financial reporting," *Journal of accounting and Economics*, vol. 44, pp. 193-223, 2007.
- [4] S. Saigal and L. W. Doyle, "An overview of mortality and sequelae of preterm birth from infancy to adulthood," *The Lancet*, vol. 371, pp. 261-269, 2008.
- [5] M. B. Dickerson, K. H. Sandhage, and R. R. Naik, "Protein-and peptide-directed syntheses of inorganic materials," *Chemical reviews*, vol. 108, pp. 4935-4978, 2008.
- [6] G. L  th  n, "Segmentation Methods for Medical Image Analysis," Thesis, 2010.
- [7] D. A. Forsyth and J. Ponce, "A modern approach," *Computer vision: a modern approach*, pp. 88-101, 2003.
- [8] A. Chaddad, C. Desrosiers, A. Bouridane, M. Toews, L. Hassan, and C. Tanougast, "Multi Texture Analysis of Colorectal Cancer Continuum Using Multispectral Imagery," *PloS one*, vol. 11, p. e0149893, 2016.
- [9] R. Peyret, A. Bouridane, S. A. Al-Maadeed, S. Kunhoth, and F. Khelifi, "Texture analysis for colorectal tumour biopsies using multispectral imagery," in *Engineering in Medicine and Biology Society (EMBC), 2015 37th Annual International Conference of the IEEE*, 2015, pp. 7218-7221.
- [10] R. Kumar, R. Srivastava, and S. Srivastava, "Detection and Classification of Cancer from Microscopic Biopsy Images Using Clinically Significant and Biologically Interpretable Features," *Journal of Medical Engineering*, vol. 2015, 2015.

- [11] S. Rathore, M. Hussain, M. A. Iftikhar, and A. Jalil, "Ensemble classification of colon biopsy images based on information rich hybrid features," *Computers in biology and medicine*, vol. 47, pp. 76-92, 2014.
- [12] M. Elgamal, "Automatic skin cancer images classification," *IJACSA) International Journal of Advanced Computer Science and Applications*, vol. 4, 2013.
- [13] G. W. Jiji, L. Ganesan, and S. S. Ganesh, "Unsupervised texture classification," *Journal of Theoretical and Applied Information Technology*, vol. 5, pp. 373-81, 2009.
- [14] Y. LeCun, L. Bottou, Y. Bengio, and P. Haffner, "Gradient-based learning applied to document recognition," *Proceedings of the IEEE*, vol. 86, pp. 2278-2324, 1998.
- [15] S. Lawrence, C. L. Giles, A. C. Tsoi, and A. D. Back, "Face recognition: A convolutional neural-network approach," *Neural Networks, IEEE Transactions on*, vol. 8, pp. 98-113, 1997.
- [16] P. Y. Simard, D. Steinkraus, and J. C. Platt, "Best practices for convolutional neural networks applied to visual document analysis," in *null*, 2003, p. 958.
- [17] S.-C. B. Lo, S.-L. A. Lou, J.-S. Lin, M. T. Freedman, M. V. Chien, and S. K. Mun, "Artificial convolution neural network techniques and applications for lung nodule detection," *Medical Imaging, IEEE Transactions on*, vol. 14, pp. 711-718, 1995.
- [18] D. Stutz, "Understanding Convolutional Neural Networks," 2014.

CHAPTER I INSTRUMENT NEEDED FOR DIGNOSIS OF TUMOR DISEASE

1. Introduction

Cancer is a group of diseases involving abnormal cell growth with the potential to invade or spread to other parts of the body, it begins when cells in a part of the body start to grow out of control and crowd out normal cells, and it can start any place in the body. Cancer can start projected to be breast cancer, lung and bronchus cancer, prostate cancer, colon and rectum cancer, bladder cancer, melanoma of the skin, non-Hodgkin lymphoma, thyroid cancer, kidney and renal pelvis cancer, leukemia (cancer of the blood), endometrial cancer, and pancreatic cancer. Most cancers form a lump called a "tumor" or a growth, and some aren't like leukemia which grow in the blood cells or other cells of the body [1-5].

Many studies work on the variation of the cancer percentages with the variation of the age, National Center Institute made many researches between 2009 and 2013 which showed that the percentage of deaths in cancer reaches a small value for those of less than 20 years old (0.3%), where this percentage increases to reach 26.9% for the ages between 75 and 84 years, then start to decrease for those whom are greater than 84 years old (figure I.1). The percentage of death is affected by many other reasons, where it is higher in case of males than that of females, and in case of black people than white ones [6].

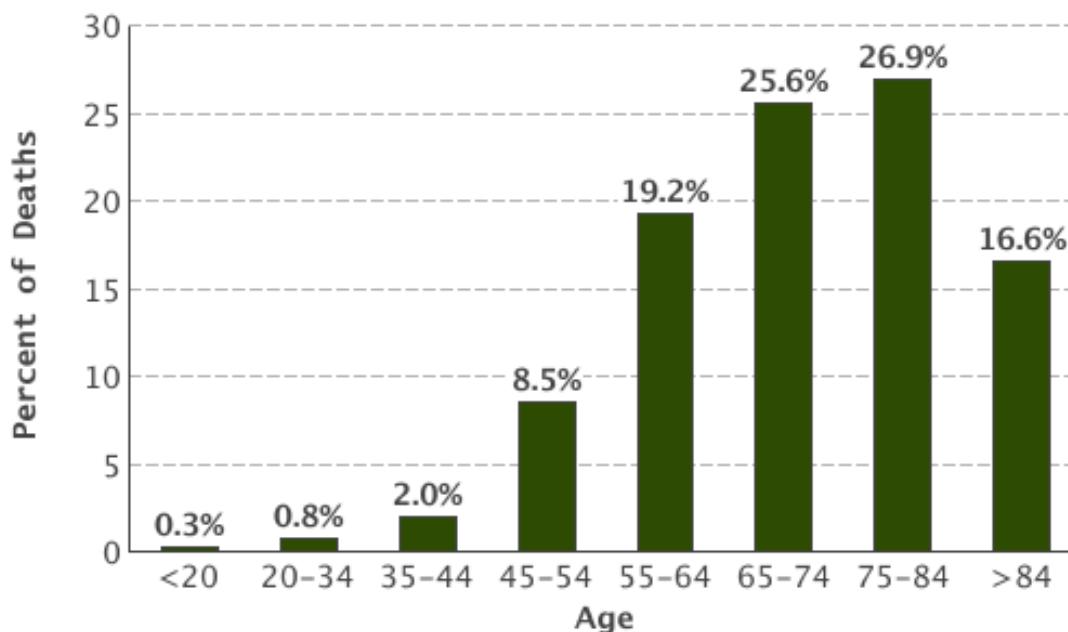


Figure I. 1. Variation of the percentage of death (cancer) with respect to age [6].

Also it shows the variation of the new cases with respect to age (figure I.2), where the probability of those infected in cancer is very low for small ages (<20 years) which is 1%, and the danger of being infected increases with age till it reaches its highest percentage between 65 and 74 years, then decrease in case of those greater than 74 years. Also the danger of getting infected in cancer is greater for males than females, and for black males than white males, while it's greater for white females than black females [6].

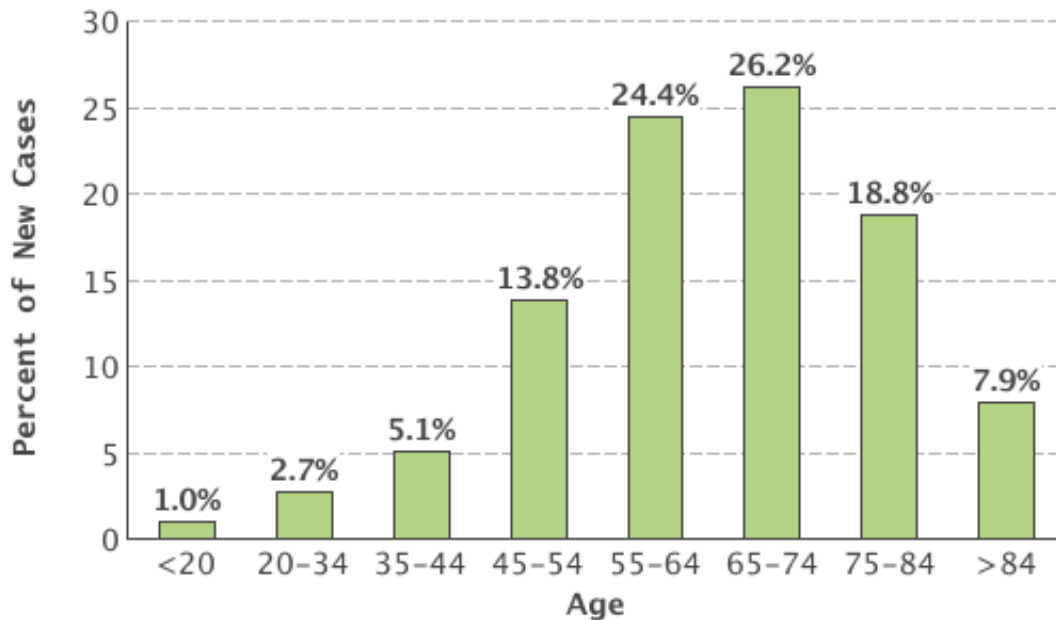


Figure I. 2. Variation of the percentage of new cases (cancer) with respect to age [6].

A family history of certain cancers is associated with an increased risk of developing cancer. At the beginning during the 15th century, scientists like Galileo and Newton began to use the scientific method and the autopsies which was done by Harvey (1628) and led to an understanding of the circulation of the blood through the heart which was later used to study the disease. The first study of cancer was done in 1761 by Giovanni Morgagni of Padua, where he did autopsies to relate the patient's illness to pathologic findings after death. The famous sentence for the Scottish surgeon John Hunter (1728-1793): "There is no impropriety in removing it", in case tumor had not invaded nearby tissue and was "moveable" which can be cured by surgery. The 19th century attends the use of the modern microscopic techniques in studying diseased tissues, where Rudolf Virchow, provided the scientific basis for the modern pathologic study of cancer. So as Morgagni had linked autopsy findings seen with the unaided eye with the clinical course of illness, so Virchow reconditioned microscopic pathology to illness.

2.Colon Cancer

2.1. What is Colon Cancer?

The colon beside to rectum represents parts of the digestive system, which make up the large intestine (large bowl), where most of the large intestine is made of the colon and a muscular tube [7]. After the remaining food matter goes through small intestine, the colon absorbs water and salt from it, where the waste matter continues its pass through the rectum, where it is stored in order to pass out of the body (figure I.3).

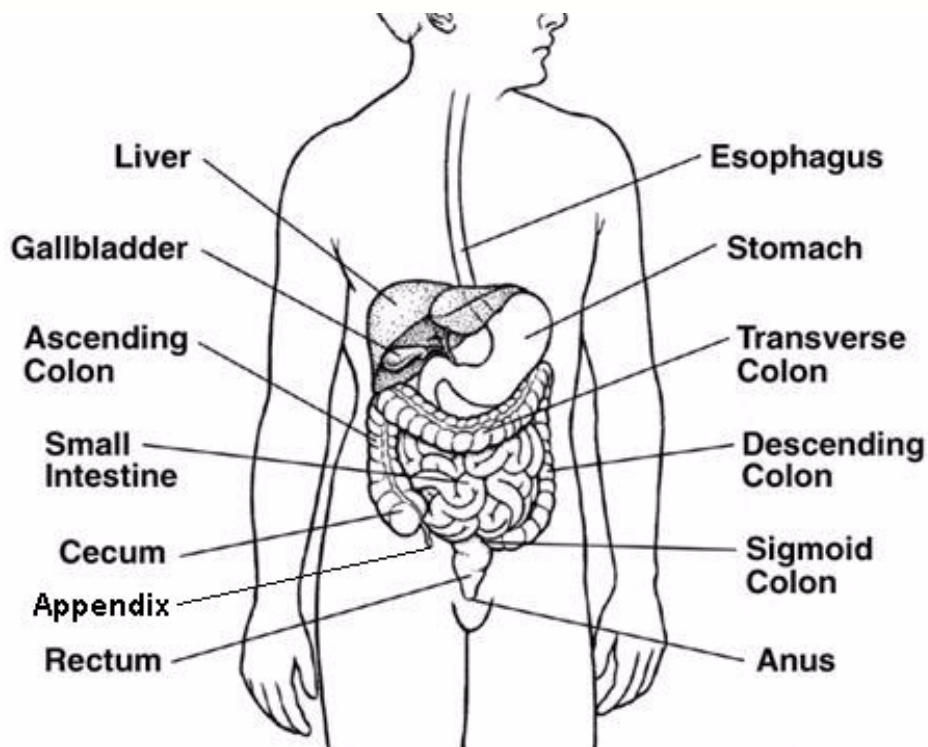


Figure I. 3. The digestive system [7].

The colon cancer is a cancer of the large intestine, and it exist in the lower part of the digestive system. Where Colorectal cancer (CRC), which is also known as bowel cancer, is the development of the cancer from the colon or rectum, which is due to the abnormal growth of cells that have the ability to invade to different parts of the body. Most of the colon cancers begin from noncancerous tumors (benign) that form on the inner walls of the large intestine called *polyps* which have two main types [7], **adenomatous polyps** (adenomas) where it could turns into cancer and **hyperplastic and inflammatory polyps** where they are pre-cancerous.

Colorectal cancer is the third most common cancer in USA, where The American Cancer Society's estimates for the number of colorectal cancer cases in the United States for 2016 are 95,270 new cases of colon cancer, and 39,220 new cases of rectal cancer. And the risk of developing is about 4.7% for men and 4.4% for women. Also the Colorectal cancer is the third leading cause of cancer-related deaths in USA, and it is expected to cause about 49,190 deaths during 2016.

2.2. Causes, Symptoms and diagnosis

Having a risk or chance of getting a disease, does not mean that you will get it. And on other side, many people get a disease without having any risk of it. There are many causes for getting the colorectal cancer that can be changed such as: overweight, physical inactivity, diets, smoking and alcohol. And that can't be changed [8], such as: being older, a history of colorectal cancer, a history of inflammatory bowel disease, having an inherited syndrome.

Actually, the above factors increase a person's risk of colorectal cancer, but it's not clear how. Scientifically, cancer is produced by the changes in DNA, which makes our genes that control our cell function. Some genes help cells grow, divide and stay alive called "*oncogenes*", and others cause cells to die at right time are called "*tumor suppressor genes*". Where cancers can be caused by DNA defects, that turn on "*oncogenes*" or turn off "*tumor suppressor genes*".

It is important to find the colorectal cancer early, since it become most likely to be curable. It might not cause symptoms, but rarely it may cause one or more of the following symptoms [8]:

- A change in bowel habits, such as diarrhea, constipation, or narrowing of the stool, that lasts for more than a few days
- Rectal bleeding
- Blood in the stool, which may make it look dark
- Cramping or abdominal pain
- Weakness and fatigue
- Unintended weight loss
- Iron deficiency (anemia)

It is important to make an appointment with your doctor in order to find it early if it is exist. Knowing that an early colorectal cancer doesn't have symptoms of disease, it is important to get the recommended screening test. Where many tests used to screen for colorectal cancer, such as: Guaiac-based fecal occult blood test (gFOBT) and fecal immunochemical test (FIT), Stool DNA test, Sigmoidoscopy, Colonoscopy, Double-contrast barium enema and CT colonography.

It is important to know the stage of the cancer the patient have, in order to decide how to treat the cancer and how successful treatment might be. In colorectal cancer, the stage is based on how far the cancer has grown into the wall of the intestine, if it has reached nearby structures, and if it has spread to the nearby lymph nodes. When the stage is based on the results the tests done (test for colorectal cancer) it is called clinical stage, while if it is based on the surgery it is called pathologic stage. It is clear that the pathologic stage is more advanced than the clinical one, since sometimes during surgery; the doctor finds more cancer than was seen on imaging test.

2.3. Colorectal cancer treatment

There are several ways to treat colorectal cancer depending on its stage, but the treatment decision should consider many factors [10], such as:

- a. The medical conditions of the patient
- b. The treatment of the side effects
- c. The medicine that the patient takes if exist
- d. The nutritional status of the patient

After taking the treatment decision, many treatments could be used, such as:

Surgery

This is the most common treatment for colorectal cancer, knowing that there are many types of the surgeries, where they are applied according to its need [10], such as: surgical resection, laparoscopic surgery, colostomy for rectal cancer and radiofrequency ablation (RFA) or cryoablation. On other side, these surgeries have side effects, which include pain and tenderness in the operation area.

Radiation therapy

It is the use of high-energy x-rays in order to destroy cancer cells, where its schedule consists of a specific number of treatments over periods of time. Many types of these radiations are used, such as: external-beam radiation therapy, stereotactic radiation therapy, intraoperative radiation therapy, and brachytherapy.

These methods have many side effects like fatigue, mild skin reactions, upset stomach, loose bowel movements and bloody stools from bleeding through the rectum or blockage of the bowel. Also it has sexual problems and the inability to have a child in both men and women may occur.

Chemotherapy

It is an operation that use drug to stop the ability of growing and divide for the cancer cells. It can gets into bloodstream, an intravenous tube placed into a vein using a capsule that is swallowed to reach the cancer cells. It can be given before surgery to reduce the size of a rectal tumor and reduce the chance of the cancer returning or after surgery to eliminate any remaining cancer cells. It has many types such as: Capecitabine, Fluorouracil, Irinotecan, Oxaliplatin and Trifluridine/tipiracil.

It has side effects that may cause vomiting, nausea, diarrhea, neuropathy, mouth sores, tired and hair loss. If side effects are particularly difficult, the dose of the drug may be lowered or a treatment session may be postponed.

Targeted therapy

It is a treatment that targets the cancer's specific genes, proteins, or the tissue that contributes to cancer growth and survival, but not all tumors have the same targets. For that, there are many tests done in order to identify the genes. It has many types such as: Anti-angiogenesis therapy, Bevacizumab, Regorafenib, Ziv-aflibercept and ramucirumab, Epidermal growth factor receptor (EGFR) inhibitors, Cetuximab, Panitumumab. The side effects of targeted treatments can include a rash to the face and upper body, which can be prevented or reduced with various treatments.

Symptoms caring

Caring helps in decreasing a person's symptoms and side effects, which is called palliative or supportive care. This care is better as it begins early as needed in cancer treatment process. Its treatments vary widely and often include medication, nutritional changes, relaxation techniques, emotional support, and other therapies, such as treatments that help to eliminate the cancer, such as radiation therapy, chemotherapy, or surgery.

Remission and The chance of recurrence of the colorectal cancer

For many patients with colorectal cancer, treatment may remove or destroy the cancer, but it's hard not to worry about cancer coming back. And for other patient's colorectal cancer may never go away completely, which is difficult and very stressful. A remission is when the cancer cannot be detected in the body, where we call recurrent cancer the ones that does return after the first treatment. Also we call local recurrence the one that could come back in the same place, regional recurrence that is nearby and distant recurrence that is

in another place. Then there is a need to make the tests again in order to know more about the recurrence, and to make the treatment plan which may include radiation therapy, chemotherapy and surgery and the clinical trials that are studying new ways to treat this type of recurrent cancer may occur.

But on other side, recovery from cancer is not always possible, and if the cancer cannot be controlled, the disease may be advanced, and these patients have advanced cancer and could live less than 6 months.

2.4. Colorectal cancer development

Usually colorectal cancer starts in the mucosa the innermost lining of the large intestine, which consists of five layers [10]. The first layer is the mucosa where nutrients, fats and proteins are absorbed from the foods we eat. The next layer represents the muscularis mucosa that forms a barrier between the mucosa and the third layer called the submucosa, where it is rich in vessels that provide the intestines with their blood supply while carrying the digested nutrients away to other vital organs. The fourth layer is the muscularis propria, that acts to propel food through the intestines, and the outermost layer is the serosa (figure I.4).

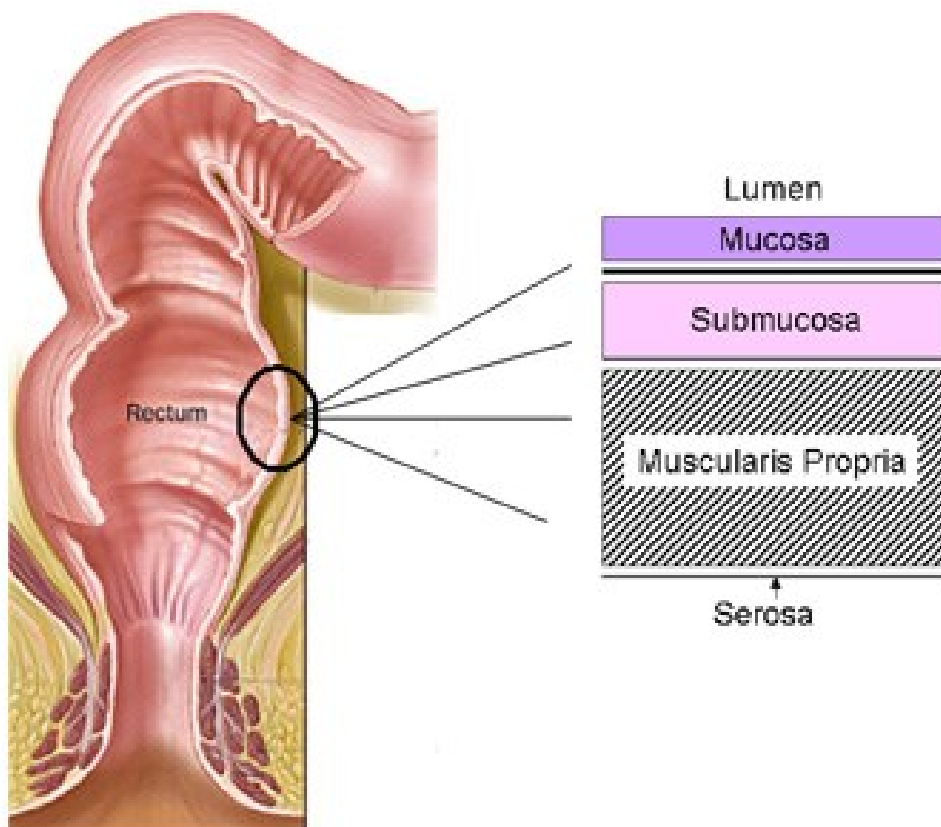


Figure I. 4. Various layers colonic tissues [10].

Usually, colorectal cancer begins as benign polyps that grow from the mucosa, but some people that have the ability or high risk factor to have cancer especially that with personal or family history of polyps are likely to develop polyps. Most polyps remain benign are often termed hyperplastic polyps, and its percentage to be cancer is very low. These polyps are not malignant, but it has a chance of becoming cancerous if not removed, and it may have invaded one or more layers of the intestine, and may spread the cancer to other organs such as the liver and lungs. These adenomas grow slowly over a decade or more, and the risk of developing into cancer increases as the size of the adenoma increases and with the amount of time they have been growing in the colon and adenomas that are malignant are called adenocarcinomas (figure I.5). The growth of the abnormal cell can be another precancerous condition of the colorectal tissue, and is known as dysplasia.

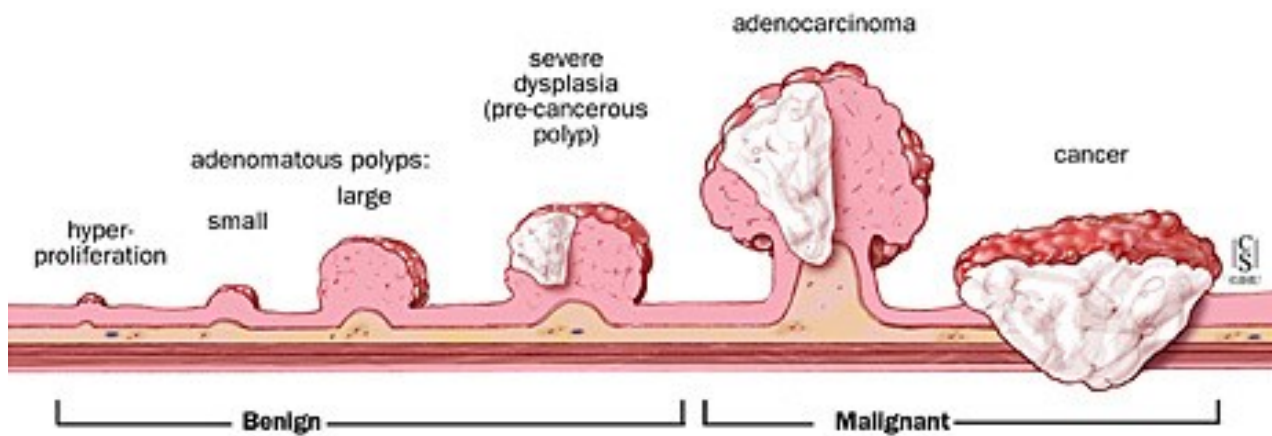


Figure I. 5. Gradation from polyps to cancer [10].

Knowing that the percentage of the adenomas become cancerous is less than 10%, more than 95% of colorectal cancers develop from adenomas. Also some polyps long considered to be benign may also become cancerous as well, so doctor should remove all polyps during a colonoscopy screening. Small polyps are easily and painlessly removed, also very small polyps may be destroyed with an instrument that delivers heat to the polyps, but very large polyps may require surgery, whether they are benign or cancerous.

The progression of a polyp to a colorectal cancer is first described by Scientists at Johns Hopkins, where Dr. Bert Vogelstein discovered that colorectal polyps and colorectal cancer develops as a result of genetic

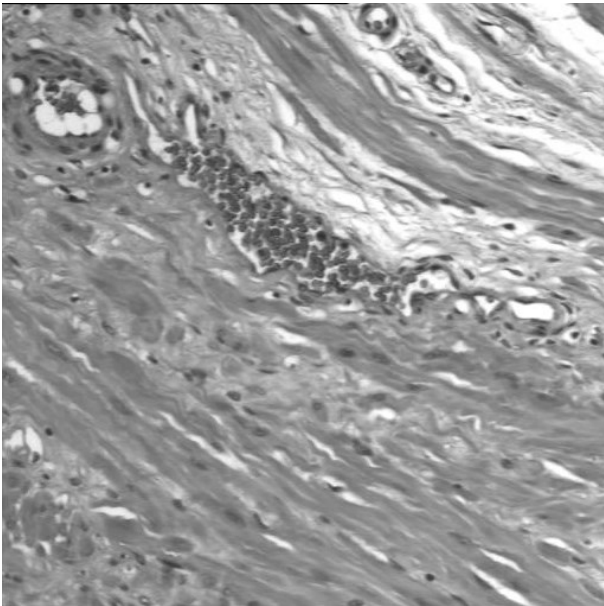
mutations or other chemical modifications, causing inactivation or promotion of specific genes known as tumor suppressor and tumor promoter genes.

3.Types of abnormal tissues images

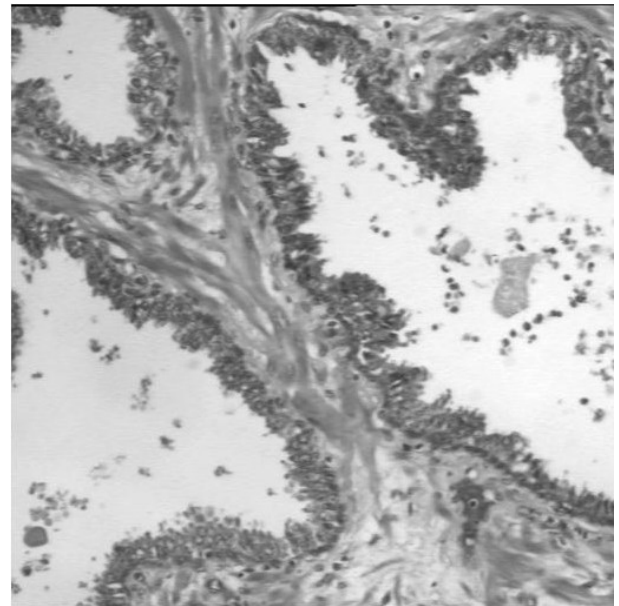
In our work, in order to help in detection and identification of the abnormal cells that could be considered cancerous cells, we consider three main types of abnormal cells that can characterize an evolution progression of a normal cell. The normal tissue and the three abnormal tissues images are studied and taken as reference of our work. Where the cells are classified as:

- 1) Stroma (ST), which corresponds to normal tissues,
- 2) Benign Hyperplasia (BH), which represents an abnormal increase in the number of non-cancerous cells,
- 3) Intra-epithelial Neoplasia (IN), which is an abnormal growth of tissue that can form a mass (tumor),
- 4) Carcinoma (Ca), in which the abnormal tissue develops into cancer.

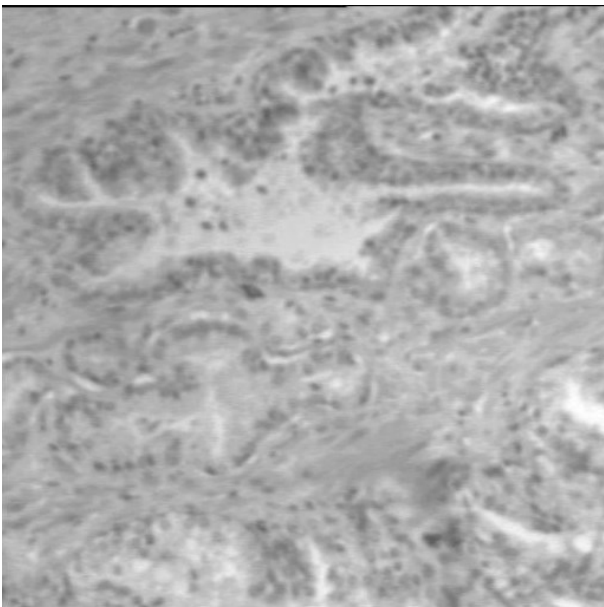
Figure I.6 give an example of microscopic image of one normal and three abnormal tissues (malignant different degree). Abnormal cells are characterized by the increase in their size caused by epithelial hyperplasia of Stroma cells. While intraepithelial neoplasia (IN) cells may have different sizes or shapes, and have an abnormal form in their contour, which are no longer smooth. Usually this type of abnormal cells are not cancerous, nevertheless it has a risk to increase its abnormal evolution towards a more pronounced cancerous. IN can develop into carcinoma cell (Ca), which has a big size and a huge lack of the base compared to normal cells.



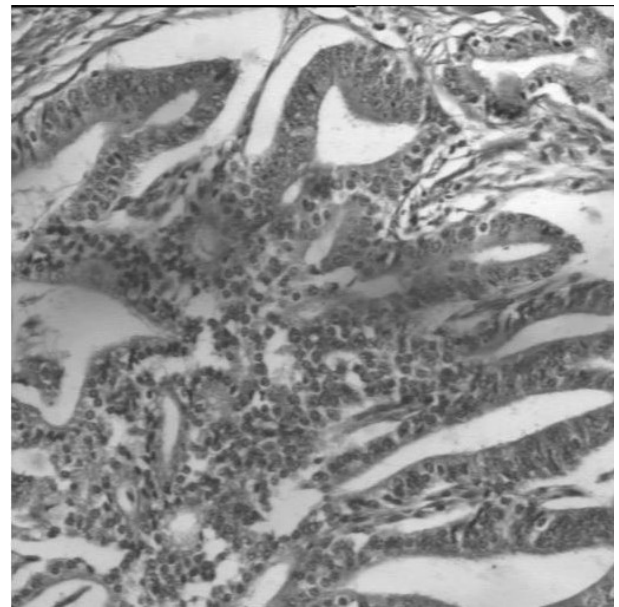
Stoma



Benign Hyperplasia



Intra-epithelial Neoplasia



Carcinoma

Figure I. 6. Microscopic images of normal and abnormal cells.

The diagnosis of the cancer in its early stages is very important (have a high treatment percentage), so the detection of it can be done by the observation of histological cells from biopsies and in an automated manner by recognition of cell abnormalities using specific instruments which are based on optical microscope with a high resolution camera using a convenient filter taking it in different frequencies in order to extract

information that can't be taken in usual image. Where the important step lies in good selection of these instruments, such as:

a. Microscopic image

The microscopic image give a speed visualization of the image in a good quality and allow to give very accurate information about the objects in the bio-images, which has an advantage for diagnosis normal and abnormal tissue by detecting cell forms. One of the important types of microscope which is convenient in our work is the optical microscope which is also known as light microscope; it uses visible light and a lenses system to magnify images. It is the oldest design of microscope and was possibly invented in their present compound form in the 17th century, and it is static to focus at different focal depths the lens to sample distance is adjusted, and to get a wider or narrower field of view a different magnification objective lens [11]. It has two basic configurations which are:

- Simple microscope: which is a microscope that uses a lens or set of lenses in order to enlarge an object, it give the viewer an erect enlarged virtual image. Its use is still found in simple magnification devices such as the magnifying glass, loupes, and eyepieces for telescopes and microscopes (figure I.7.a),
- Compound microscope: which is a microscope that uses lens close to the object being viewed to collect light that called the objective lens, which focuses a real image of the object inside the microscope. It use a combination between objective and eyepiece to allow much higher magnification, reduced chromatic aberration, exchangeable objective lenses to adjust the magnification and enables more advanced illumination setups (figure I.7.b).

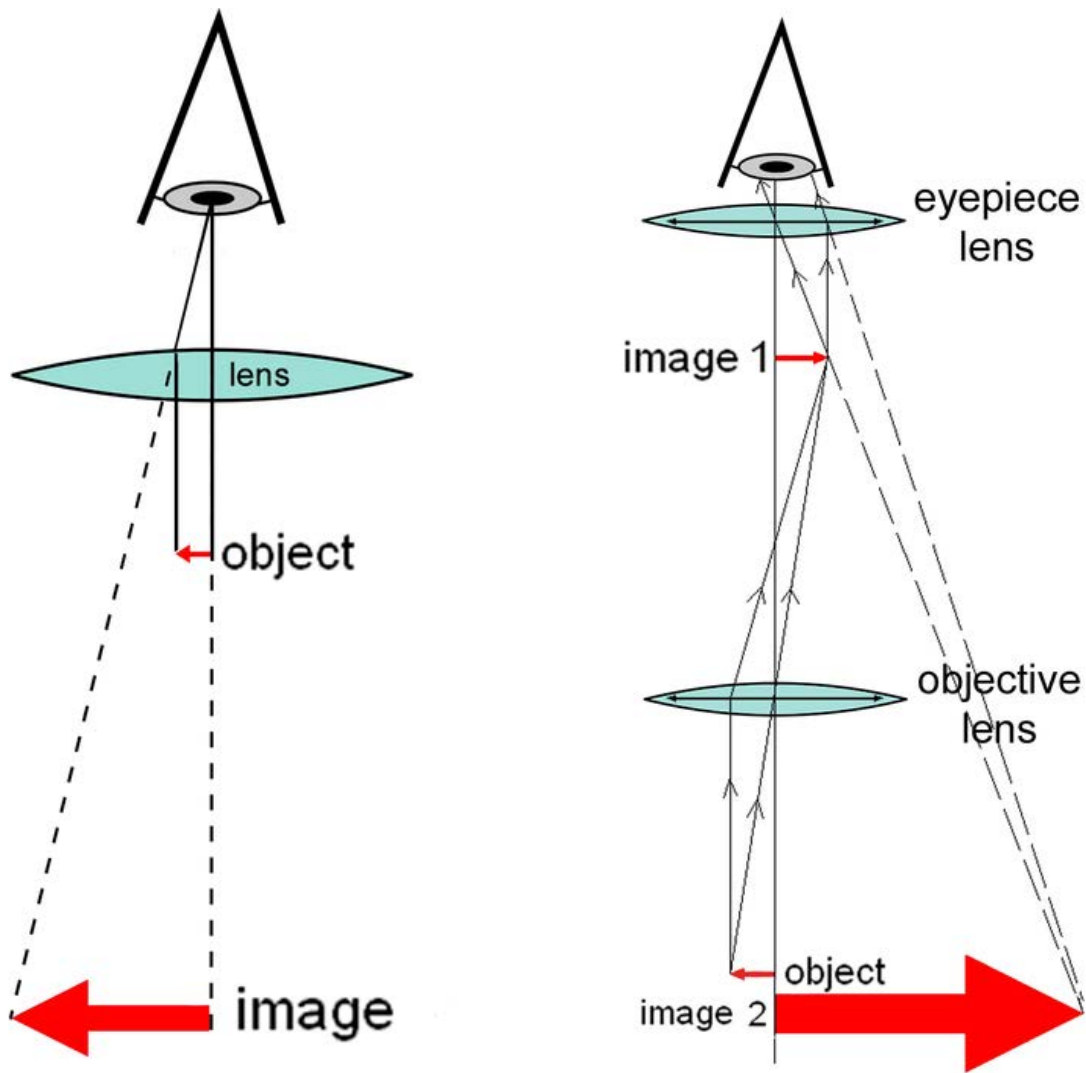


Figure I. 7. a) diagram of a simple microscope, b) diagram of a complex microscope.

b. Multispectral image

The microscope helps in distinguishing between the different regions in the medical image and extract textual information contributing to a diagnosis, so it is difficult to extract and characterize all information textured in a single spectrum of capturing medical images. In order to highlight all the features textured information, the image should be captured in different bands of spectrum, which is called multi-spectral image [12-14]. Each image can be seen as an image beam intensity to represent a length of the particular wavelength as shown in Figure I.8, and the textured images are distributed over a spectral band of wavelengths generally between 500 and 650 nm which is for visible light and sometimes beyond to infrared, and the number of its sub-bands is between 4 and 20. We propose to set up a system for acquiring multi-spectral images from a wide field microscope and a sampling of the spectrum into 16 sub-bands equidistant from a variable light source [15].

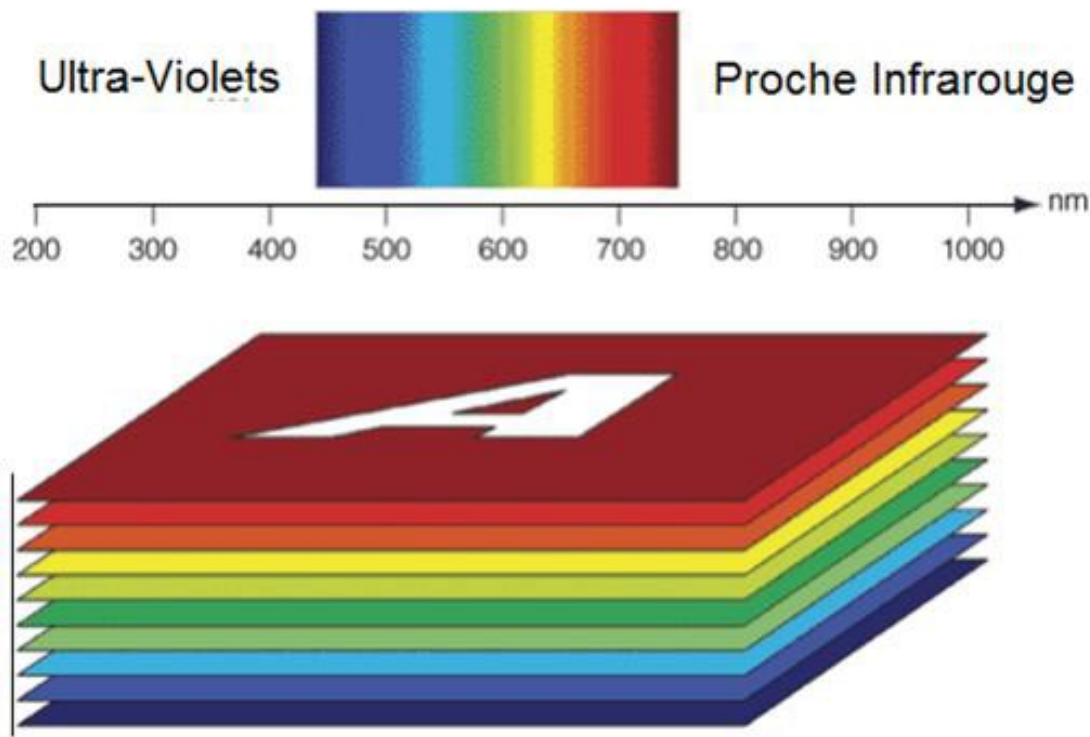


Figure I. 8. Multispectral image.

c. CCD camera with filter

Multispectral images are then provided from a charge coupled device CCD camera (figure I.9), which has a resolution of 5000x5000 pixels/image. It scans the multi-spectral images which is stored in an image format of n (n is an integer between 1 and 16) multispectral bands, corresponding to a sequential tape format ".bsq". CCD camera is integrated with a liquid crystal tunable filter (LCTF) in the optical microscopy system [16], where it has a precision of sub-bands up to 5 nm. The LCTF technology offers a reasonably wide field of view ($\pm 7^\circ$ from the normal axis) but, nevertheless, the limitation in field-of-view is a parameter that has to be treated with care for imaging applications [17].



Figure I. 9. Multispectral model of CCD camera (Hamamatsu C5985).

Our needed instruments are based on optical microscope, the LCTF filter, the microscope image sensor to obtain a spectral image in 16 separate bands and an image-type CCD camera sensor (figure I.10). Also the size of the image is an important point for study, where it is obvious that as the image size decrease, the image may lose many of its information, so in our study we study an image of size 512x512 pixels. This approach usually gives very accurate results in terms of textured images and spectra, but its acquisition is slow, costly and requires specific equipment.

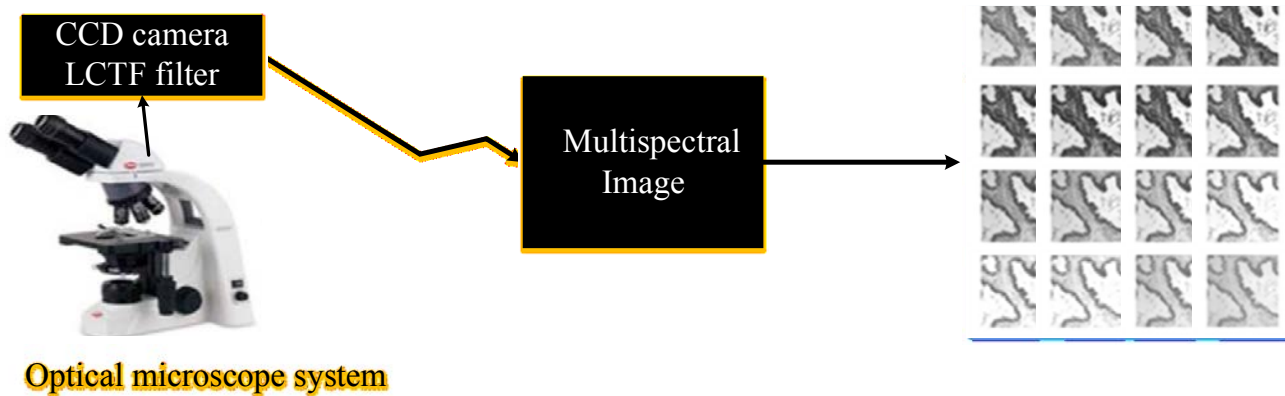


Figure I. 10. Proposed flowchart for automated detection of CRC progression using CNN comprises multispectral images of PT.

These images are then ready to be segmented using many segmentation methods and comparing its performance results to find the better one in such application, in order to prepare it to the next step which is the classification of its type.

4. Conclusion

Colorectal cancer is the third most common cancer in USA, and it is expected to cause about 49,190 deaths during 2016. This type of cancer is silent, since it doesn't shows symptoms until an advanced stage of the disease, and there is need for its screening as early as possible to increase the chances of recovery, thus reduce mortality from this cancer, and fight against it. Such diagnosis can usually be carried out by step and is suitable for automated detection using a system for capturing and processing of the images. So we propose the development of instrumentation to aid in the detection and effective automatic classification of healthy cells (Stroma) or abnormal malignant considered to varying degrees (Benign Hyperplasia, epithelial neoplasia Intra and Carcinoma).

Histological observation is primarily based on an observation by a microscope, through visual magnifications samples conditioned tissue. But in our work, we proposed the establishment of an instrumental bench multi-spectral image capturing histologies based on the combination of a microscope, a LCTF filter and a CCD camera to digitize, automate and speed the extraction and analysis of information textural. Choosing the multi-spectral images is based on the quality and the sufficient quantity of textural information, and choosing of a digital acquisition based solely on acquisition opportunities and rapid image processing by computers, specific architectures or computers.

After this detection, there is a need to make segmentation of the digital image which will be our work in the next chapter, in order to get in one hand an automatic and effective method of treatment detection and classification of images, on the other hand an architectural design of a microelectronic system to accelerate all image processing to complete and integrate or embark on a multi-spectral microscope device to capture digital images.

References of Chapter I

- [1] R. A. Smith, D. Manassaram - Baptiste, D. Brooks, M. Doroshenk, S. Fedewa, D. Saslow, *et al.*, "Cancer screening in the United States, 2015: A review of current American Cancer Society guidelines and current issues in cancer screening," *CA: a cancer journal for clinicians*, vol. 65, pp. 30-54, 2015.
- [2] K. Swapnil, S. Vijay, and M. Chandrakant, "Targeted Drug Delivery: A Backbone for Cancer Therapy," *Asian Journal of Pharmacy and Technology*, vol. 3, pp. 40-46, 2013.
- [3] A. This, "The History of Cancer."
- [4] M. G. Kris, S. I. Benowitz, S. Adams, L. Diller, P. Ganz, M. S. Kahlenberg, *et al.*, "Clinical cancer advances 2010: annual report on progress against cancer from the American Society of Clinical Oncology," *Journal of Clinical Oncology*, vol. 28, pp. 5327-5347, 2010.

- [5] E. Winer, J. Gralow, and L. Diller, "American Society of Clinical Oncology. Clinical cancer advances 2008: major research advances in cancer treatment, prevention, and screening—a report from the American Society of Clinical Oncology," *J Clin Oncol*, vol. 27, pp. 812-826, 2008.
- [6] B. D. Cheson, J. M. Bennett, M. Grever, N. Kay, M. J. Keating, S. O'Brien, *et al.*, "National Cancer Institute-sponsored Working Group guidelines for chronic lymphocytic leukemia: revised guidelines for diagnosis and treatment," *Blood*, vol. 87, pp. 4990-4997, 1996.
- [7] B. Levin, D. A. Lieberman, B. McFarland, R. A. Smith, D. Brooks, K. S. Andrews, *et al.*, "Screening and surveillance for the early detection of colorectal cancer and adenomatous polyps, 2008: a joint guideline from the American Cancer Society, the US Multi-Society Task Force on Colorectal Cancer, and the American College of Radiology*†," *CA: a cancer journal for clinicians*, vol. 58, pp. 130-160, 2008.
- [8] R. A. Smith, A. C. von Eschenbach, R. Wender, B. Levin, T. Byers, D. Rothenberger, *et al.*, "American Cancer Society guidelines for the early detection of cancer: update of early detection guidelines for prostate, colorectal, and endometrial cancers: Also: update 2001—testing for early lung cancer detection," *CA: a cancer journal for clinicians*, vol. 51, pp. 38-75, 2001.
- [9] S. B. Edge and C. C. Compton, "The American Joint Committee on Cancer: the 7th edition of the AJCC cancer staging manual and the future of TNM," *Annals of surgical oncology*, vol. 17, pp. 1471-1474, 2010.
- [10] J. H. Bortz and H. Friedrich-Nel, "The Adenoma-Carcinoma Sequence, Management and Treatment of Colon Cancer," in *CT Colonography for Radiographers*, ed: Springer, 2016, pp. 211-219.
- [11] A. Kilian, W. Metzger, E. Mutschelknauss, G. Kabagambe, P. Langi, R. Korte, *et al.*, "Reliability of malaria microscopy in epidemiological studies: results of quality control," *Tropical Medicine & International Health*, vol. 5, pp. 3-8, 2000.
- [12] J. Y. Hardeberg, F. Schmitt, and H. Brettel, "Multispectral color image capture using a liquid crystal tunable filter," *Optical engineering*, vol. 41, pp. 2532-2548, 2002.
- [13] H. Huang, "Acquisition of multispectral images using digital cameras," *Asian Association on Remote Sensing (ACRS)*, pp. 42-49, 2004.
- [14] J.-I. Park, M.-H. Lee, M. D. Grossberg, and S. K. Nayar, "Multispectral imaging using multiplexed illumination," in *2007 IEEE 11th International Conference on Computer Vision*, 2007, pp. 1-8.
- [15] N. Everdell, I. Styles, E. Claridge, J. Hebden, and A. Calcagni, "Multispectral imaging of the ocular fundus using LED illumination," in *European Conferences on Biomedical Optics*, 2009, pp. 73711C-73711C-6.
- [16] A. Chaddad, C. Tanougast, A. Dandache, and A. Bouridane, "Extracted haralick's texture features and morphological parameters from segmented multispectral texture bio-images for classification of colon cancer cells," *WSEAS Trans Biol Biomed*, vol. 8, pp. 39-50, 2011.
- [17] J. Y. Hardeberg, F. J. Schmitt, and H. Brettel, "Multispectral image capture using a tunable filter," in *Electronic Imaging*, 1999, pp. 77-88.

CHAPTER II - SEGMENTATION OF THE ABNORMAL TISSUES

1. Introduction

Image segmentation is a process used to locate objects or boundaries in an image which is distinguished between forward and backward pixels according to many characteristics like a pixel's intensity. We summarized four principal techniques as follows:

Thresholding based segmentation is a technique used in image processing in order to detect the objects within image. It uses a threshold value of the pixels to determine if it belongs to the object or to the background [1]. This makes it an easy method but also effective to separate objects from background. Many applications use thresholding method, for example, counting of blood cells using thresholding based segmentation [2], and multi-thresholding model for brain tumor detection [1, 3].

Edge-based method: it uses the derivative functions to detect the maximum variance which have intensity greater than the ones in the background. Positive effect of this technique showed off anatomical structure detection and in particular the biomedical images [4].

Region-based method: is used as a type of segmentation which decomposes the image of multi regions; each region contains pixels that have similar characteristics (e.g. color, intensity and texture). This approach has a high accuracy to detect the abnormal shapes of objects within the image, like the cancer cells detection in multispectral bio-images [5, 6]. This approach combined scene structure and semantic in an energy function (e.g. external energy and internal energy).

Active contour: It is a deformable method, which is independent from the three previous techniques. However, this paper presents the most popular segmentation techniques used in medical images [5]. The real data (cancer's patients' images) will be used to evaluate the performance for each of the segmentation techniques.

2. Methods and Materials

2.1. Thresholding

It can discriminate between foreground & background of the image based on the threshold value t [1]. This latter can be the average for all pixels intensity within an image. Moreover, all the pixels that have a gray level less than t will be classified as black "0"; otherwise it will be white "1". Given an image $g(x, y)$, segmentation is performed according to the following expressions:

$$g(x,y)=\begin{cases} 1 & \text{if } f(x,y) > t \\ 0 & \text{if } f(x,y) \leq t \end{cases} \quad (1)$$

where, t is the threshold value, x and y are the coordinates of the pixel and $f(x, y)$ represents the gray level image pixels. Thresholding t computed according to many techniques proposed like inter-means, minimum-error and k-means clustering algorithms.

1) *Inter-means algorithm*

Inter-means algorithm which is also known as “*Histogram-based thresholding*”, will take an initial value of t as a center of the pixels, the next step is to calculate the mean value of the two categories that are identified as a black “0” or white “1”, then calculate t to be the midpoint of the two mean values of these categories. It repeats these steps till the value t shows no difference between iterations [7]. Mathematically, the algorithm can be specified as shown in the figure II.1.

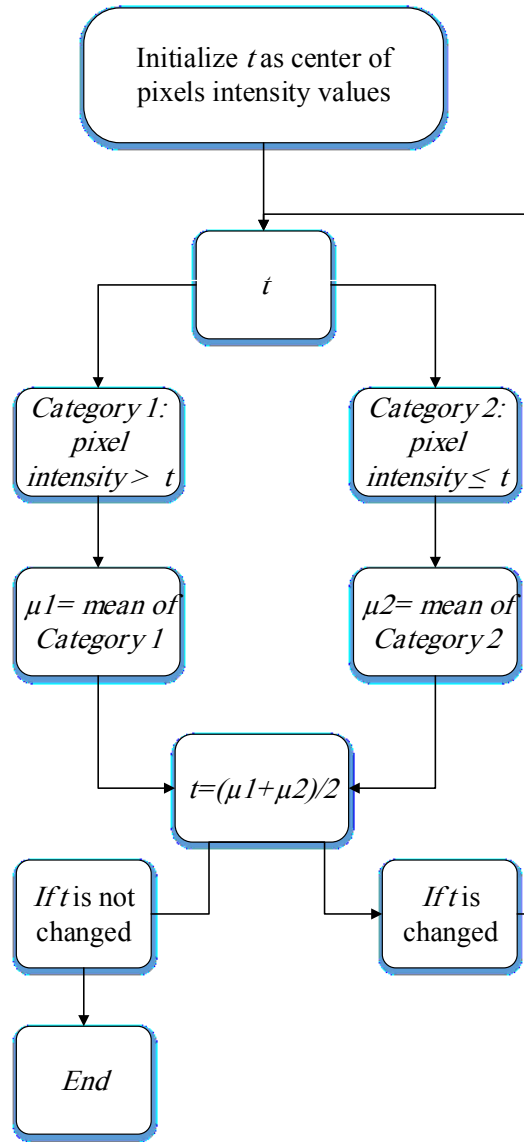


Figure II. 1. Inter-means algorithm

- a. Calculate the mean pixel value in each category. For values less than or equal to t such as follows:

$$\mu_1 = \frac{\sum_{k=0}^t kh_k}{\sum_{k=0}^t h_k} \quad (2)$$

Whereas, for values greater than t , it is given by:

$$\mu_2 = \frac{\sum_{k=t+1}^N kh_k}{\sum_{k=t+1}^N h_k} \quad (3)$$

- b. Re-estimate t as half-way between the two means as follows:

$$t = \left\lceil \frac{\mu_1 + \mu_2}{2} \right\rceil \quad (4)$$

c. Repeat steps (a) and (b) till t stops changing value between consecutive evaluations.

where μ_1 and μ_2 are the average of the above categories 1 and 2 respectively, h_k : specifies the number of pixels in an image with gray scale value k , N is the maximum pixel value.

2) Minimum-error algorithm

Given the histogram h_k which is performed to:

$$h_k = n^2 \{p_1 \phi_1(k) + p_2 \phi_2(k)\} \quad (5)$$

Where p_1 and p_2 are proportions (such that $p_1 + p_2 = 1$), k is the ray scale value of k^{th} pixel, $\phi(k)$ is the probability density of a Gaussian distribution which is performed according to:

$$\phi_l(k) = \frac{1}{\sqrt{2\pi\sigma_l^2}} \exp\left\{-\frac{(k - \mu_l)^2}{2\sigma_l^2}\right\} \quad (6)$$

For $l=1, 2$

where μ_l and σ_l^2 are the mean and variance respectively of pixel values in category l .

The best classification criterion, which is the one misclassifies the least number of pixels, allocates pixels with value k to category 1 if

$$p_1 \phi_1(k) \geq p_2 \phi_2(k) \quad (7)$$

where $\phi_1(k)$ and $\phi_2(k)$ are the probability density of categories 1 and 2 respectively; Otherwise classifies them as category 2.

After substituting for ϕ and taking logs, the inequality becomes:

$$k^2 \left\{ \frac{1}{\sigma_1^2} - \frac{1}{\sigma_2^2} \right\} - 2k \left\{ \frac{\mu_1}{\sigma_1^2} - \frac{\mu_2}{\sigma_2^2} \right\} + \left\{ \frac{\mu_1^2}{\sigma_1^2} - \frac{\mu_2^2}{\sigma_2^2} + \log \frac{\sigma_1^2 p_2^2}{\sigma_2^2 p_1^2} \right\} \leq 0 \quad (8)$$

The left side of the inequality is a quadratic function in k . Let:

$$A = \left\{ \frac{1}{\sigma_1^2} - \frac{1}{\sigma_2^2} \right\} \quad (9)$$

$$B = \left\{ \frac{\mu_1}{\sigma_1^2} - \frac{\mu_2}{\sigma_2^2} \right\}, \quad (10)$$

Then the criterion for value k to category 1 is:

$$C = \left\{ \frac{\mu_1^2}{\sigma_1^2} - \frac{\mu_2^2}{\sigma_2^2} + \log \frac{\sigma_1^2 p_2^2}{\sigma_2^2 p_1^2} \right\} \quad (11) \quad \text{allocating pixels with}$$

$$k^2 A - 2kB + C \leq 0 \quad (12)$$

If $A=0$, then $2kB \geq C$, (If, in addition, $p_1 = p_2$ and $\mu_1 < \mu_2$, the criterion becomes $k \leq 1/2 \{\mu_1 + \mu_2\}$). Note that this is the inter-means criterion.

Otherwise, denote the roots t_1 and t_2 :

$$t_1, t_2 = \frac{B \pm \sqrt{B^2 - AC}}{A} \quad (13)$$

The criteria for category 1 is expressed according to the following expressions:

$$\begin{aligned} t_1 < k \leq t_2 & \quad \text{if } A > 0 \\ k \leq t_1 \text{ or } k > t_2 & \quad \text{if } A < 0 \end{aligned}$$

Then it belongs to category 1 if the pixel value is:

$$k \leq \frac{B \pm \sqrt{B^2 - AC}}{A} \quad (14)$$

Minimum-error algorithm which can be regarded as a generalization of the *inter-means* algorithm, based on this threshold criteria [7]. From an initial guess at the threshold, the proportions, means and variances of the pixels values in the two categories are calculated. The threshold is repositioned according to the above criterion, and proportions, means and variances are calculated until t stops changing value between consecutive evaluations. Mathematically, the algorithm can be specified as shown in the figure II.2.

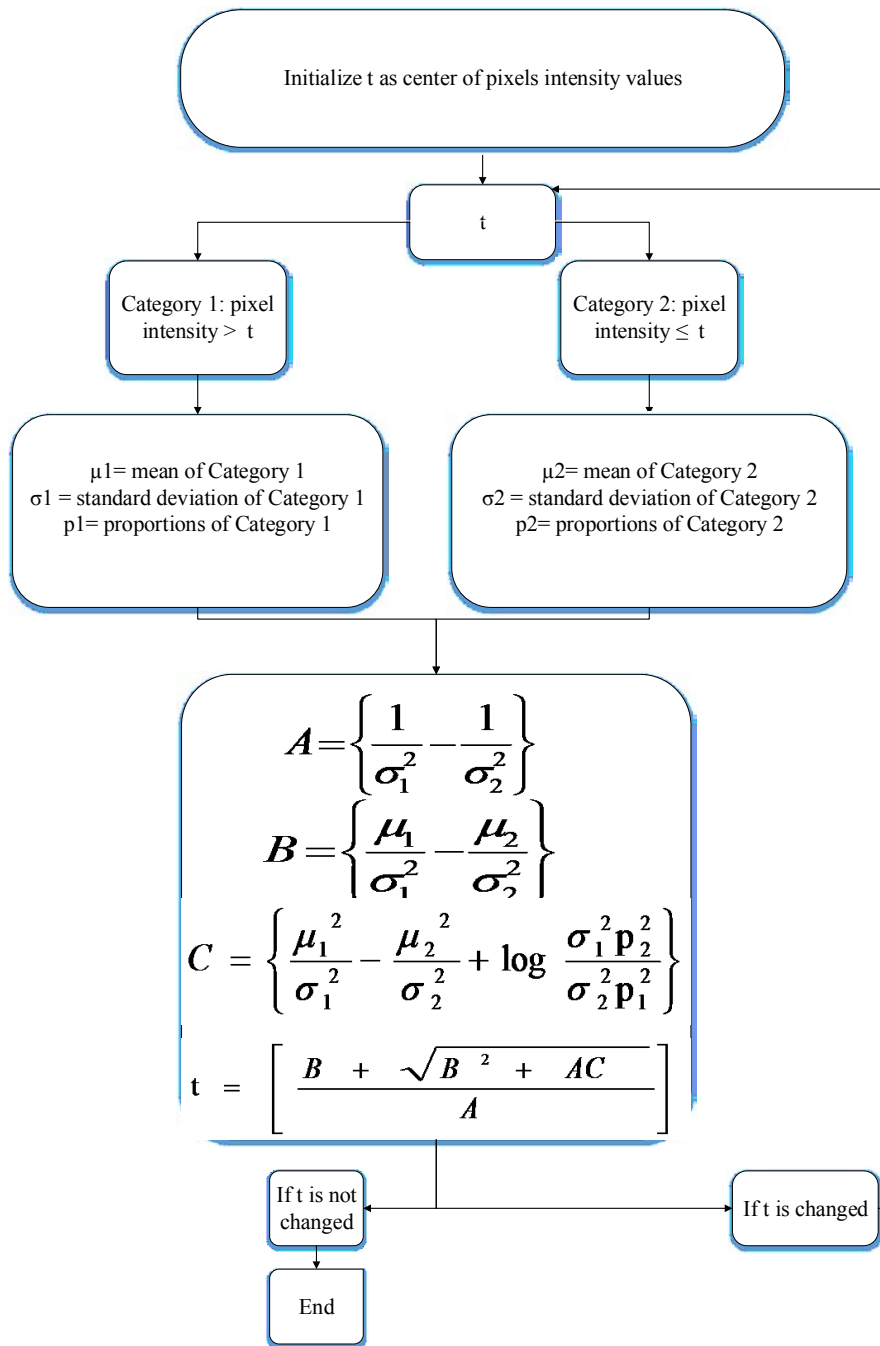


Figure II. 2. Minimum-error algorithm.

- a. Make an initial guess at a value for t
- b. Calculate p_1, μ_1 and σ_1^2 for pixels, by

$$P_1 = \frac{1}{n^2} \sum_{k=0}^t h_k \quad (15)$$

$$\mu_l = \frac{1}{n^2 p_1} \sum_{k=0}^t k h_k \quad (16)$$

Similarly,

$$\sigma_1^2 = \frac{1}{n^2 p_1} \sum_{k=0}^t k^2 h_k - \mu_1^2 \quad (17)$$

estimate p_2 , μ_2 and σ_2^2 for pixels in the range $t + 1$ to N , k are the pixels gray scale value.

c. Re-estimate t by the following expression:

$$t = \left\lceil \frac{B + \sqrt{B^2 - AC}}{A} \right\rceil \quad (18)$$

Repeat the steps (b) and (c) until t stops changing value between consecutive evaluations.

3) K-mean clustering

This algorithm works with multivariate criteria, which are more difficult. In order to define the k-means clustering, the linear discrimination should be defined first; suppose that the image is decomposed to R categories, then it will deal with R regions $\{B_1, \dots, B_R\}$. Calculate squared Mahalanobis distance between pixel value f_{ij} and the r^{th} category which is expressed as follows:

$$(f_{i,j} - \mu_r)^T V^{-1} (f_{i,j} - \mu_r) \quad (19)$$

where, T is the threshold value, i and j are the pixel coordination, μ_r is the mean value in a region r which is performed as follows:

$$\mu_r = \frac{1}{N_r} \sum \sum_{(i,j) \in B_r} f_{i,j} \quad (20)$$

for, $r=1, \dots, R$ and N_r is the number of pixels in region r , V^{-1} is the inverse of the variance-covariance matrix, where V can be estimated as follows:

$$V = \sum_{r=1}^R (\sum \sum_{(i,j) \in B_r} f_{i,j} f_{i,j}^T - N_r \mu_r \mu_r^T) / \sum_{r=1}^R N_r \quad (21)$$

Then, put the pixel in the category that has a minimum distance with its mean value; this is the linear discrimination [7]. K-means clustering is an automatic version of linear discrimination; the steps applied in this method can be summarized in the figure II.3.

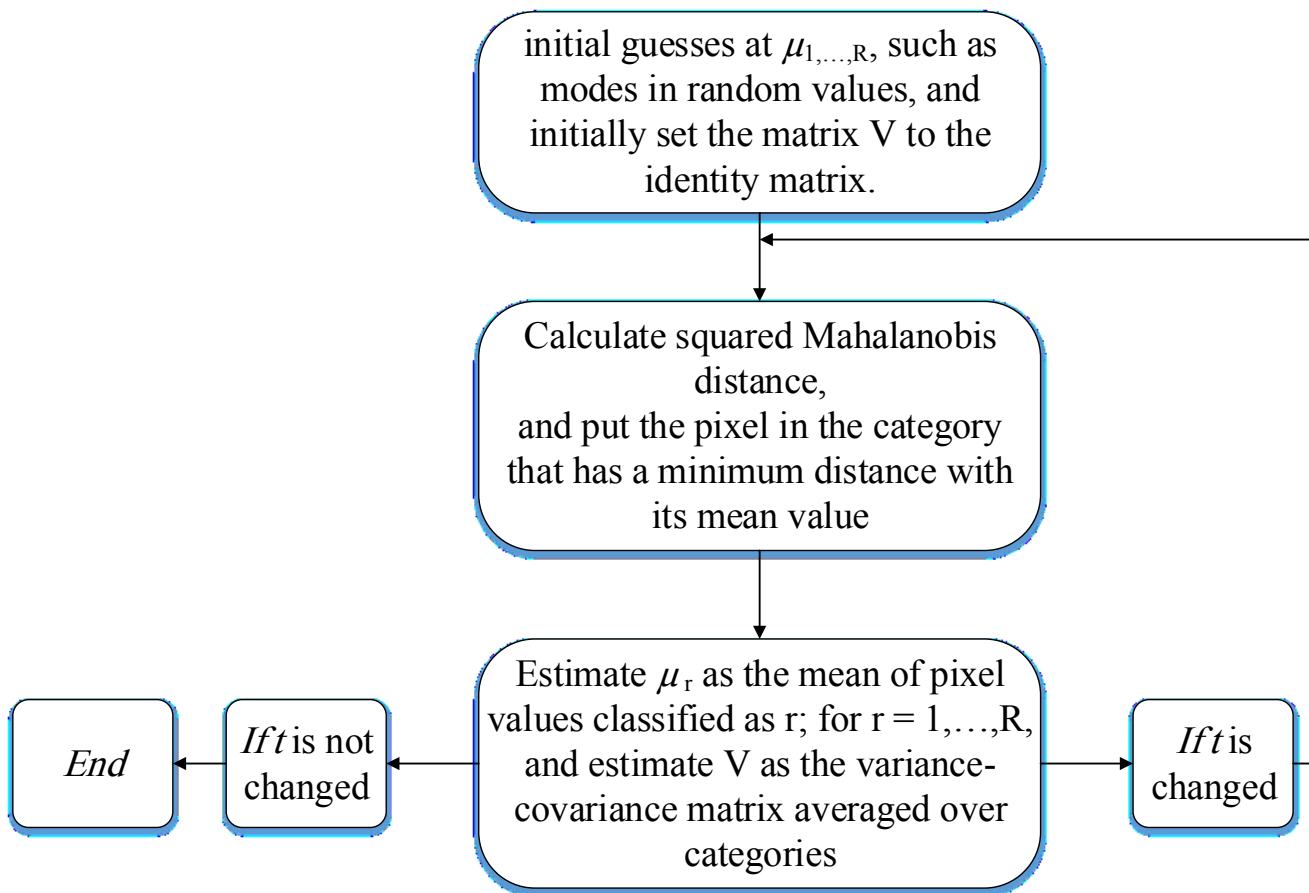


Figure II. 3. K-mean clustering algorithm.

- Make initial guesses at $\{\mu_1, \dots, \mu_R\}$, such as modes in random values, and initially set the matrix V to the identity matrix.
- Segment the image according to the linear discrimination criterion.
- Estimate μ_r as the mean of pixel values classified as r ; for $r = 1, \dots, R$, and estimate V as the variance-covariance matrix averaged over categories, using the equations already given.
- Repeat the last two steps until t stops changing value between consecutive evaluations.

A drawback of the k-means algorithm is that the number of clusters k is an input parameter.

Thresholding algorithm is an important algorithm, but its accuracy still depends on the value of the threshold value " t ".

2.2. Edge-based Segmentation

Edge based segmentation is used to detect an edge which have higher intensity than its surrounds in at least one direction [8]. Two most popular methods used for edge detection namely “Gradient method and Laplacian zero-crossings method”.

1) Gradient method

It uses the derivative, which detects the maximum or minimum values in a function to get a vector; its magnitude is invariant with respect to translations and rotations [8].

Initially find the gradient vector which represents the 1st derivative of the signal at position (x,y) of function $f(x,y)$ and expressed as follows:

$$\vec{\nabla}f = \begin{bmatrix} G_x \\ G_y \end{bmatrix} = \begin{bmatrix} \partial f / \partial x \\ \partial f / \partial y \end{bmatrix} \quad (22)$$

Where the vector ∇f represent the first order derivative vector G_x , G_y represent the gradient vector components, $\delta f / \delta x$, $\delta f / \delta y$ represent the first derivative of the function f with respect to x and y respectively.

It's magnitude (∇f) and phase $\alpha(x,y)$ of the gradient $(\vec{\nabla}f)$ can be expressed according to the following expressions :

$$\nabla f \approx |G_x| + |G_y| \quad (23)$$

$$\alpha(x,y) = \tan^{-1} \left(\frac{G_y}{G_x} \right) \quad (24)$$

The steps done are:

- Filtering of an image I separately with the discrete difference operators G_x , G_y and (in 3D) G_z ,
- Calculation of the square root,
- Looking for maxima in the magnitude of the gradient.

There are many types of filtering an image such as Roberts, Sobel and Prewitt [9]; each one depends on a matrix H , which differs from one to another. The main function of filtering is expressed as follows:

$$\begin{cases} f \otimes H_1 \\ f \otimes H_2 \end{cases} \rightarrow \sqrt{(f \otimes H_1)^2 + (f \otimes H_2)^2} \quad (25)$$

In the case of Roberts filter H_1 and H_2 represented as follows:

$$H_1 = \begin{bmatrix} 0 & -1 \\ 1 & 0 \end{bmatrix}, \quad H_2 = \begin{bmatrix} -1 & 0 \\ 0 & 1 \end{bmatrix};$$

In the case of Prewitt filter H_1 and H_2 represented as follows:

$$H_1 = \begin{bmatrix} -1 & 0 & 1 \\ -1 & 0 & 1 \\ -1 & 0 & 1 \end{bmatrix}, \quad H_2 = \begin{bmatrix} -1 & -1 & -1 \\ 0 & 0 & 0 \\ 1 & 1 & 1 \end{bmatrix};$$

In the case of Sobel filter H_1 and H_2 represented as follows:

$$H_1 = \begin{bmatrix} -1 & 0 & 1 \\ -2 & 0 & 2 \\ -1 & 0 & 1 \end{bmatrix}, \quad H_2 = \begin{bmatrix} -1 & -2 & -1 \\ 0 & 0 & 0 \\ 1 & 2 & 1 \end{bmatrix};$$

Figure II.4 represents an example of edge-based technique applied on carcinoma cell type, using four different filters.

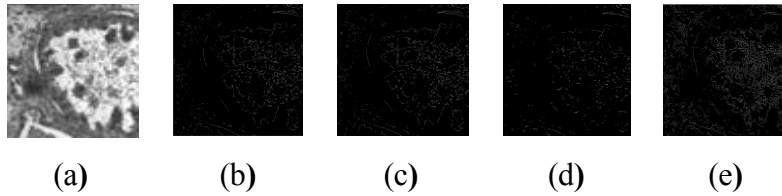


Figure II. 4. Example of segmentation models based on: (a) The original image, (b) Prewitt, (c) Sobel, (d) Roberts, (e) Laplacian.

2) Zero crossings from a Laplacian-of-Gaussian filter

The second order derivative of a function gives a zero value on the highest rise or fall; Laplacian method uses the second order derivative of the image to detect the edge, this means that the second order derivate must be zero at the point which has a maximum in the first order derivate. Initially the Laplacian operator represented as follows:

$$L(x,y) = \nabla^2[G(x,y) * f(x,y)] \quad (26)$$

where ∇^2 represents the second order derivative, $G(x,y)$ represents the Gaussian function as follows:

$$G(x,y) = \exp\left(-\frac{x^2 + y^2}{\sigma^2}\right) \quad (27)$$

where exp represents the exponential operation, σ^2 represents the standard deviation.

Apply a *Laplace* operator on the image, and then observe each pixel: If its value is equal to 0, this pixel is on the edge; otherwise, it has a neighbor with a different sign. The pixel with smaller magnitude is on the edge. Note that from the magnitudes with different sign the sub pixel position of the edge can be calculated.

2.3. Region-based Segmentation

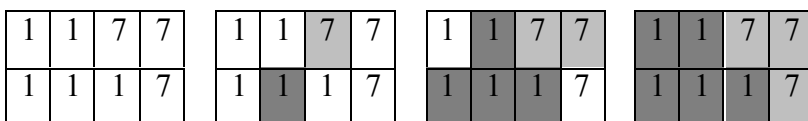
Region based technique used to divide an image into regions or categories according to common properties, such as intensity values of original image, or values computed based on an image operator, or patterns that are unique to each type of region, or spectral profiles that provide multi-dimensional image data [10]. The aim of region detection is to provide the possibility to characterize the detected object by parameter analysis (shape, position, size, etc...). Two most popular methods used for region detection namely “Seeded region and Split-merge methods”.

1) Seeded region method

Seeded region algorithm used to detect region by “initially” choosing seed points and a threshold value, then examining its neighboring pixels in order to determine if the pixel neighbor should be added to the region or not [11].

The algorithm for seeded region based method is:

- a. Select the initial seed points say, $\{p_1, p_2, \dots, p_n\}$,
- b. Compute difference between the pixel values of initial seed points and its neighboring points,
- c. If the computed difference is less than the threshold, add the neighboring point to the cluster where seed point belonged,



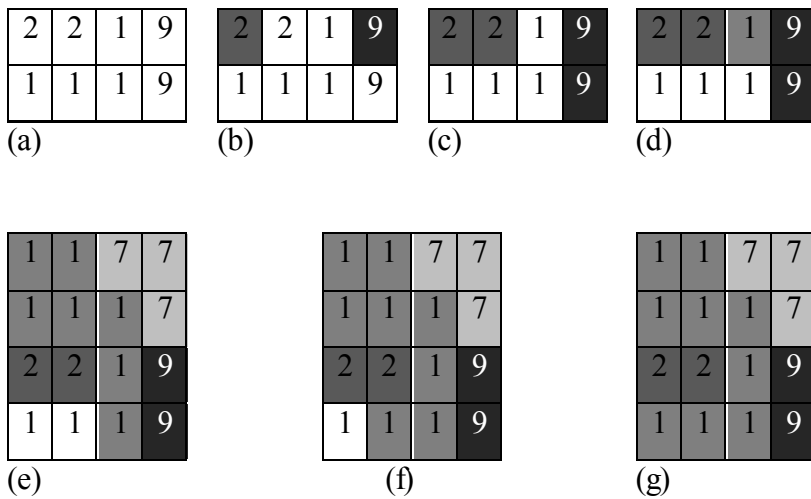


Figure II. 5. An example of seeded region method, (a) Original image, (b) 1st step, (c) 2nd step, (d) 3rd step, (e) 4th step, (f) 5th step, (g) 6th step.

- d. Re-compute the boundary of the cluster and set the boundary points as new seed points,
- e. Re-compute the mean pixel values of the clusters,
- f. Repeat the steps (b) to (e) for all pixels until they are allocated to a cluster.

An example about the seeded region is represented in (Figure II.5), which shows how to add each pixel to its region according to the nearest.

2) Split and merge algorithm

Split and merge algorithm uses the pixel intensity to split and merge pixels after comparing its value to a threshold “ t ”. There are two data structure in this algorithm[12]:

- *Quadtree for splitting:* splitting is done from top to down procedure which will create regions that may be adjacent and homogeneous but not merged. Figure II.6 shows an example of image that was decomposed into four parts, the parts that have the same color such as black or white will be represented by its color node, while the other parts which have different colors will be decomposed each to four parts and continue this decomposition till no parts have different colors.

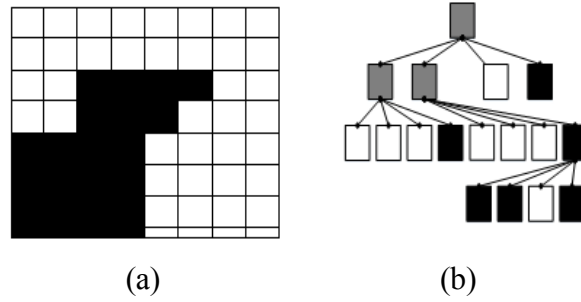


Figure II. 6. Quadtree for splitting, (a) Partition, (b) Split quadtree.

- *RAG (region adjacency graph) for splitting and merging*: splitting and merging work together iteratively of quadtree partitioning, (Figure II.7). It has an embedded quadtree for splitting that represents four containment relations and represents four adjacency relations (one per square side).

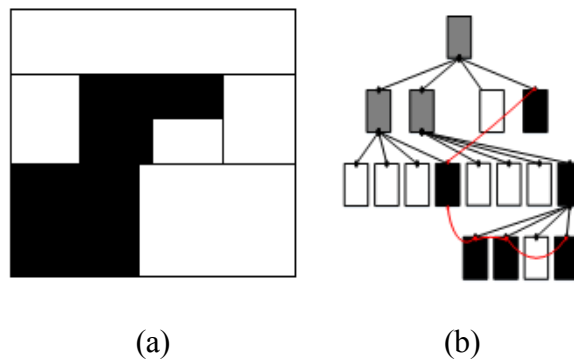


Figure II. 7. RAG with adjacency relations (in red) for big black region, (a) Merge tree, (b) Merge image.

Algorithm:

- If a region R is inhomogeneous $\{P(R) = \text{False}\}$, then R is split into four sub-regions.
- If two adjacent regions R_i and R_j are homogeneous $\{P(R_i \cup R_j) = \text{True}\}$, they are then merged.
- The algorithm stops when no further splitting or merging is possible.

2.4. Snake Method

Snake method which is also called active contour method, is defined as edge detection which depends on its shape and location in medical image using energy minimization [13]. Knowing that the initial contour represents a square, this energy uses a parametric vector $p(s) = (x(s), y(s))$, where the value of s varies between 0 and 1, and it depends on the internal forces which acts as smoothing constraint for the snake, and the external

forces of the contour which guide the snake towards the features in the image, this energy which should be minimized on the contour C_0 is expressed as follows:

$$E_{snake} = \int_0^1 E_{int}(p(s)) + E_{ext}(p(s)) ds \quad (28)$$

where,

$$E_{int} = \frac{1}{2} \{ \alpha |p'(s)|^2 + \beta |p''(s)|^2 \} \quad (29)$$

where $|p'(s)|$ is the magnitude of the first derivative which it keeps the snake short, $|p''(s)|$ is the magnitude of the second derivative which it keeps it straight, α and β are constants which have a relative importance with these derivatives terms. And then :

$$E_{ext} = -|\nabla(G_\sigma(x, y)) * I(x, y)|^2 \quad (30)$$

where, $I(x, y)$ represent the intensity function, and $G_\sigma(x, y)$ represent the two-dimensional Gaussian function, with standard deviation σ and gradient operator ∇ . Note that as σ should be large in order to increase the external energy to push the snake towards the edges.

Figure II.8 gives an example of the snake algorithm, where the initial contour which is represented as square, pushed toward the final one C_0 . Where (a) represents a carcinoma image, (b) the contour after many iterations (>2000 iteration) and (c) the segmented image.

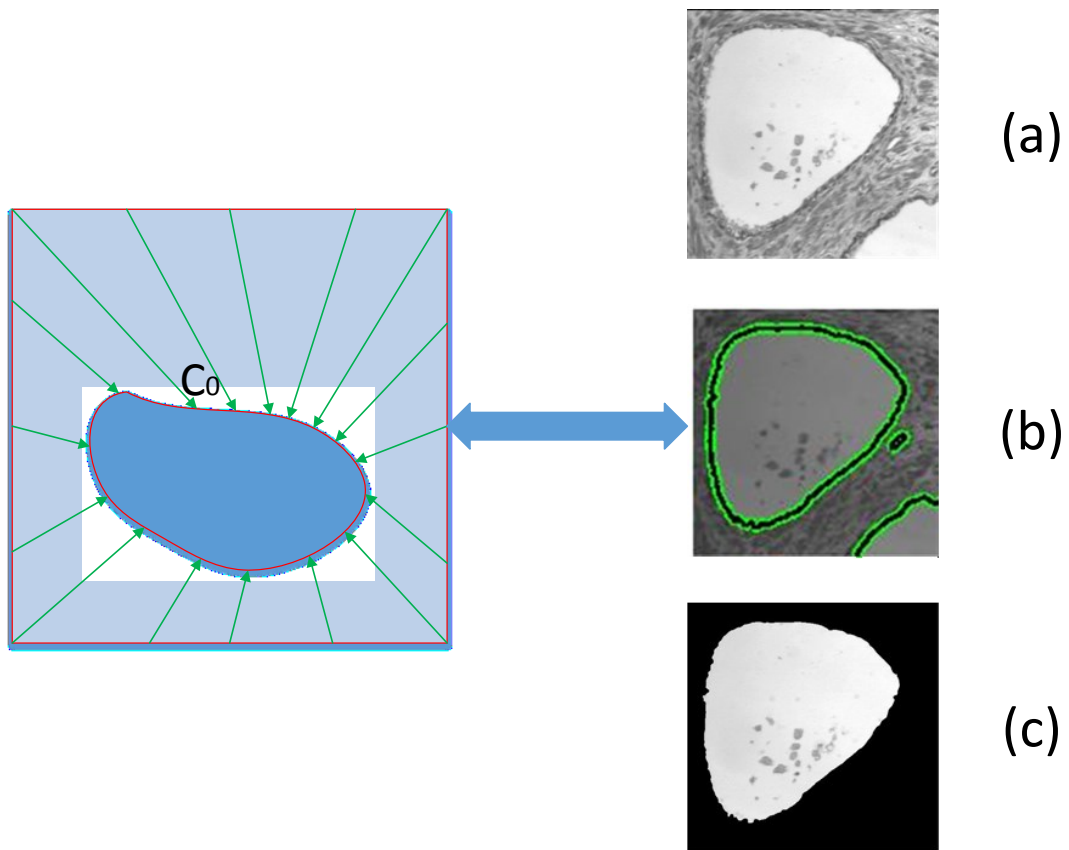


Figure II. 8. Example of snake algorithm, (a): initial image, (b): contour after many iterations and (c): segmented image using snake method.

Knowing that this method can be easily manipulated using external image forces, can be made sensitive to image scale by incorporating Gaussian smoothing in the image energy function and can be used to track dynamic objects in temporal as well as the spatial dimensions, its accuracy is governed by the convergence criteria used in the energy minimization technique and it often overlooks minute features in the process of minimizing the energy over the entire path of their contours.

2.5. Performance Metrics

The performance matrices can be described by many coefficients, in our paper we discussed Jaccard similarity coefficient (*JSC*), Dice similarity coefficient (*DSC*), false positive rate (*FPR*) and false negative rate (*FNR*). *JSC* and *DSC* measure the degree of the correspondence between two segmentations, where *JSC* can be formulated according to the following expression:

$$JSC(A, B) = (A \cap B) / (A \cup B) \quad (31)$$

And *DSC* can be formulated according as follows:

$$DSC(A, B) = 2(A \cap B) / |A \cup B| \quad (32)$$

where *A* and *B* are the two compared images. Additionally *FPR* and *FNR* are calculated according to the following expressions:

$$FPR(A, B) = (A/B) / (A \cup B) \quad (33)$$

$$FNR(A, B) = (B/A) / (A \cup B) \quad (34)$$

Therefore, algorithms were further tested on data obtained using different cancer patients' images (see Figure II.9) which are taken in the size of 256×256 pixels. Image format is ".*bsq*", which represents multispectral image type provided from charge-coupled device camera of optical microscopy [6, 14]. Note that we employed the images in mid-frequency band which is situated in wavelength range of 500–650nm. Manual segmentation is applied on a carcinoma cell, which are represented by complex and irregular shapes done by anatomist. Cells segmented using threshold, edge, region and snake methods are compared with the manual method to assess the performance metrics of these methods which is reported in Table II.1. These data should be extracted on the highest performance conditions for enhanced accuracy and diagnosis precision.

2.6. Application of the segmentation methods on histopathological images

The four segmentation methods are applied on multispectral images, of size 512x512 pixels, of type ".*bsq*" with 16 bands. A computer system with an Intel Core i5-3570 CPU 3.4 GHz processor was used for software implementation and the performance test. All of the segmentation techniques were simulated using MATLAB R 2013a (Mathworks Inc., Novi, MI, USA), in accordance with the predefined format. Validation of the proposed technique was done by comparative study based on similarity metrics using 160 carcinoma images, of four type's stroma (ST), benign Hyperplasia (BH), Intraepithelial Neoplasia (IN) and Carcinoma (Ca).

Figure II.9 shows an example of segmentation of three carcinoma images, using the four segmentation, and manual segmentation techniques. Snake technique clearly was demonstrated highest similarity metrics than the other techniques.

In order to assess the performance of these segmentation methods, a comparative study was done on carcinoma cell type. Table II.1 shows the performance metrics for each of the four segmentation techniques.

It gives the mean and standard deviation values of the similarity metrics. We observed that snake technique showed the best metrics with a *JSC*, *DSC*, *FPR* and *FNR* value of 76.00, 83.00, 05.00 and 18.00% respectively, which improves its validity and strength. While the other methods give less performance results, such as threshold which reaches 56.00 and 58.00 as *JSC* and *DSC* values, since its accuracy still depends on the value of the threshold value "*t*". Thus, region segmentation method showed 52.00 and 42.00 as *JSC* and *DSC* values, since it is unusual, and the lighting affects the appearance. Also, edge based segmentation showed 34.00 and 38.00 as *JSC* and *DSC* values, since it is sensitive to noise. While in other side, computation of time is one of the snake technique limitations, where its average was 116 seconds. However best time computation of edge, thresholding and region segmentation showed with value of 15, 24 and 56 seconds, respectively.

It was demonstrated that the snake method is highly detecting the abnormal cells, and showed a feasibility computation time with maximum of three minutes [14]. Also it was demonstrated that the snake technique based on active contour was not affected by the image noise [15]. This technique has been used both often and successfully, and that the active contour model can converge to the edge of the image even with the non-homogeneity intensity [16].

Based on our findings, the snake method since its invention by Kass et al. provides a high performance of abnormal cells segmented.

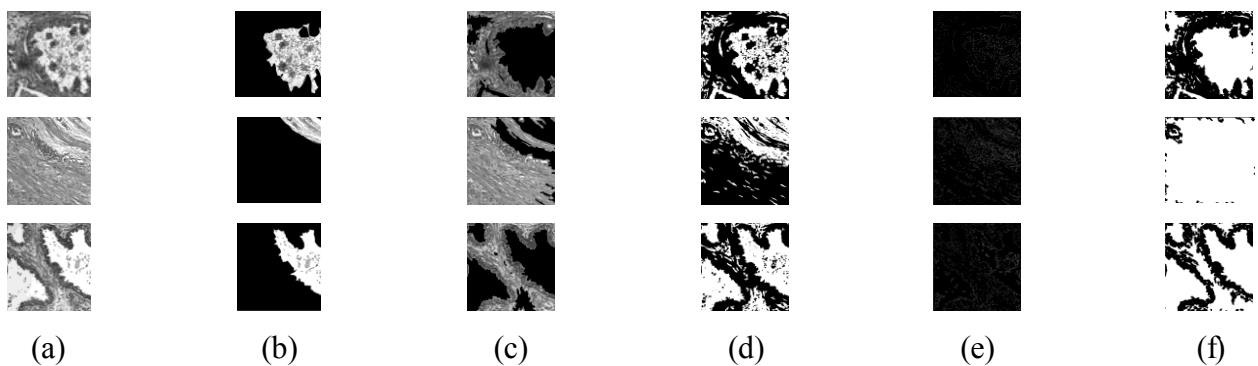


Figure II. 9. Automatic and manual segmentation of carcinoma cell type.(a) Three multispectral images of carcinoma cells, (b) Manual segmentation images, (c) Snake segmentation images, (d) Thresholding segmentation images, (e) Edge based segmentation images, (f) Region based segmentation images.

Metrics	Snake	Thresholding	Edge	Region
JSC				
Mean	0.76	0.56	0.34	0.52
Standard deviation	0.03	0.07	0.15	0.22
DSC				
Mean	0.83	0.58	0.38	0.42
Standard deviation	0.01	0.03	0.04	0.08
FPR				
Mean	0.05	0.16	0.13	0.12
Standard deviation	0.01	0.03	0.02	0.06
FNR				
Mean	0.18	0.28	0.75	0.25
Standard deviation	0.03	0.05	0.11	0.12
Time (second)				
Mean	116.76	24.01	15.05	56.24
Standard deviation	12.7	0.66	0.85	0.75

Table II. 1: Comparative study of four segmentation techniques.

It can be a good technique to segment many object types, but the performance of computation time is still limited, where it is less than two minutes.

3. Conclusion

We have presented in this chapter a brief study on four segmented methods, such as: Threshold, Edge-based, region and snake segmentation. Each one has its importance in certain type of images, but we apply these four methods in one type of images. Where it is applied on multi-spectral image textured sound like cells (*ST*) or abnormal (*BH*, *IN* and *Ca*) of 16 bands each, in order to segment healthy or malignant abnormal cells. The variation of the frequency of each image during the segmentation leads to the change of the performance values too. Also the size of the images (512x512) increases the performance too, since as the image size decrease the data of the images disappeared. A comparative study between these segmentation methods is studied on the same number and types of images. Snake segmentation was demonstrated highest similarity

metrics by comparison with other approaches, which give it the priority to be chosen as a segmented method in our work. The segmented images will be studied and applied on many classification methods in order to identify if the image is not cancer image (ST), or to classify the phase of the cancer image in the case of abnormal (BH, IN and Ca), where this is the subject of the next chapter.

References of Chapter II

- [1] M. Sezgin and B. Sankur, "Selection of thresholding methods for nondestructive testing applications," in *Image Processing, 2001. Proceedings. 2001 International Conference on*, 2001, pp. 764-767.
- [2] Y. M. Alomari, S. N. H. Sheikh Abdullah, R. Zaharatul Azma, and K. Omar, "Automatic Detection and Quantification of WBCs and RBCs Using Iterative Structured Circle Detection Algorithm," *Computational and Mathematical Methods in Medicine*, vol. 2014, p. 17, 2014.
- [3] A. Chaddad, P. O. Zinn, and R. R. Colen, "Brain tumor identification using Gaussian Mixture Model features and Decision Trees classifier," in *Information Sciences and Systems (CISS), 2014 48th Annual Conference on*, 2014, pp. 1-4.
- [4] P. Mesejo, A. Valsecchi, L. Marrakchi-Kacem, S. Cagnoni, and S. Damas, "Biomedical image segmentation using geometric deformable models and metaheuristics," *Computerized Medical Imaging and Graphics*, vol. 35, pp. 3-10, 2014.
- [5] A. Chaddad, C. Tanougast, A. Dandache, and A. Bouridane, "Extracted Haralick's texture features and morphological parameters from segmented multispectral texture bio-images for classification of colon cancer cells," *WSEAS Trans. Biol. Biomed*, vol. 8, pp. 39-50, 2011.
- [6] A. Chaddad, C. Tanougast, A. Golato, and A. Dandache, "Carcinoma cell identification via optical microscopy and shape feature analysis," *Journal of Biomedical Science and Engineering*, vol. 6, p. 1029, 2013.
- [7] S. S. Al-Amri and N. V. Kalyankar, "Image segmentation by using threshold techniques," *arXiv preprint arXiv:1005.4020*, 2010.
- [8] T. Uemura, G. Koutaki, and K. Uchimura, "Image segmentation based on edge detection using boundary code," *Int. J. Innovative Computing*, vol. 7, pp. 765-778, 2011.
- [9] S. Milyaev and O. Barinova, "Learning graph laplacian for image segmentation," in *Transactions on Computational Science XIX*, ed: Springer, 2013, pp. 92-106.
- [10] F. M. Abubakar, "A Study OF REGION-BASED AND CONTOUR-BASED IMAGE SEGMENTATION," *Signal & Image Processing*, vol. 3, pp. 15-22, 2012.
- [11] M. Abdelsamea, "An Automatic Seeded Region Growing for 2D Biomedical Image Segmentation," in *Proceedings of International Conference on Environment and Bio-Science*, 2011.
- [12] D. Kelkar and S. Gupta, "Improved quadtree method for split merge image segmentation," in *Emerging Trends in Engineering and Technology, 2008. ICETET'08. First International Conference on*, 2008, pp. 44-47.
- [13] M. Kass, A. Witkin, and D. Terzopoulos, "Snakes: Active contour models," *International journal of computer vision*, vol. 1, pp. 321-331, 1988.
- [14] A. Chaddad, C. Tanougast, A. Dandache, A. Al Houseini, and A. Bouridane, "Improving of colon cancer cells detection based on Haralick's features on segmented histopathological images," in *Computer Applications and Industrial Electronics (ICCAIE), 2011 IEEE International Conference on*, 2011, pp. 87-90.
- [15] S. Lankton and A. Tannenbaum, "Localizing region-based active contours," *Image Processing, IEEE Transactions on*, vol. 17, pp. 2029-2039, 2008.

- [16] G. Wang, J. Xu, Q. Dong, and Z. Pan, "Active Contour Model Coupling with Higher Order Diffusion for Medical Image Segmentation," *International journal of biomedical imaging*, vol. 2014, p. 8 pages, 2014.
- [17] A. Chaddad, C. Tanougast, and A. Dandache, "Improving Snake Method Using Canny Approach Implementation for Fast Cancer Cells Detection," in *International Joint Conference on Biomedical Engineering Systems and Technologies (France)*, 2014, pp. 187-192.

CHAPTER III- CLASSIFICATION OF MULTISPECTRAL COLORECTAL ABNORMAL TISSUES

1. Introduction

The earlier detection by imaging feature of colorectal cancer (CRC) can offer a great deal of chance for treatment from this disease. Previous studies have been investigated to assess and classify the CRC tissue. For example, a computer-aided diagnostic system was developed to classify the type of the colorectal polyps. It considered a feature selection based on sequential forward selection and sequential floating forward selection model, and the accuracy of detecting polyps by types achieved 96% using SVM classifier [1]. A framework for automated detection and classification of cancer from microscopic biopsy images using clinically significant and biologically interpretable features is proposed. It includes enhancement of microscopic images, segmentation of background cells, features extraction, and finally classification [2]. Another study based on textural features of the oral mucosal epithelium to discriminate normal and oral sub-mucous fibrosis (OSF) has been proposed, and it showed the important role to characterize the oral images, and lead to a performance of 96.43% degree of accuracy [3]. And a study for classifying the colorectal cancer based on correlation of clinical, morphological and molecular features has also been proposed and it showed the impact of features for accelerating the clinical management in diagnosis and treatment [4]. Using a new feature type like geometric feature has been also studied to detect CRC, it showed that the hybrid feature space encompassing diverse knowledge about the tissues' characteristics is capable to classify colon biopsy images with an accuracy classifier of 98.07% and 99.18% for testing and training, respectively [5]. In this term, another study showed its feasibility to classify colon biopsy images using structural feature [6]. Another method of colon biopsy image classification achieved an accuracy classifier value of 98.85% using hybrid feature spaces [7]. A new study for assessing the continuum of CRC tissue has showed a good performance metrics using a 3D- gray-level co-occurrence matrices approach [8]. But a new classification still needed to improve the classifier accuracy, most specifically for characterizing the continuum of CRC tissues.

To best characterize the CRC tissues, we hypothesize to use convolution neural network (CNN) model as a classifier based on convolution operation. Since CNN model has been used in many applications such as detection of abnormal tissues [9], for example CNN showed a good result in classifying the face recognition [10]. Also it is used to classify 1.3 million high-resolution images in the LSVRC-2010 Image Net training set into 1000 different classes [11], and classification of mass and normal breast tissue, where it investigates the classification of regions of interest on mammograms as either mass or normal tissue using CNN. The receiver

operating characteristic methodology was used to evaluate the classification accuracy, where it reached 0.87 [12]. CNN is used also for classifying visual inputs arising from documents [13], and showed a significant potential in medical image pattern recognition [14]. CNN in medical images can be a feasible technique to characterize an image using spatial information between the pixels [15].

In CRC tissues, no study yet used CNN to characterize the continuum of tissues, for this reason, this study aims to investigate the effect of CNN in order to classify four pathological tissues, namely: ST, BH, IN and Ca. We present the effect of CNN model employed on multispectral images of normal and three abnormal pathology tissues. In this context, we classify the segmented and non-segmented images using CNN, and using Support Vector Machine (SVM) after extracting some types of features. These methods will be compared in order to evaluate the performance of CNN for evaluating the continuum of CRC.

2. Classification using CNN

2.1. Machine Learning

Machine learning acquires a type of artificial intelligent discipline, that give the computer the ability to learn without being programmed, it focuses on the computer programs which can teach themselves to change when they are prone to new data. Over the past several years, machine learning techniques, particularly when applied to neural networks, have played an increasingly important role in the design of pattern recognition systems. In the matter of fact, it could be set that the availability of learning techniques has been a critical factor in the recent success of pattern recognition applications. Machine learning techniques automatically learn from a set of examples how to classify new instances of the same type of data. The capability to generalize, i.e. the capacity to successfully classify unknown data and possibly posses generic rules or functions, is an important property of these approaches and is sought to be maximized.

The usual method of recognizing individual patterns consists in splitting the system into two main modules as shown in figure III.1. The first module, called the feature extractor, transforms the input patterns so that they can be represented by low-dimensional vectors or short strings of symbols that can be easily matched or compared, and relatively stable with respect to transformations and distortions of the input patterns that do not change their nature. The feature extractor contains most of the prior knowledge and is rather specific to the task. It is also the focus of very most of the design effort, because it's often entirely hand-crafted. The classifier, on the other hand, is often general-purpose and trainable. In this scheme, fully-connected multi-layer networks can be used as classifiers.



Figure III. 1. Traditional pattern recognition system

One of the essential problems with this approach is that the recognition accuracy is highly determined by the ability of the designer to create an appropriate set of features. This turns out to be a daunting task which, unfortunately, must be redone for each new problem. A potentially more interesting scheme is to rely as much as possible on learning in the feature extractor itself, i.e. feeding the network with raw inputs. While this can be done in a regular fully connected feed-forward network with some success for certain tasks, there are problems. Convolution Neural Networks (CNN) are an approach that tries to reduce these problems, where both feature extraction and classification modules are integrated into one structure and are fully adaptive. Artificial Neural Networks (ANN), short Neural Networks (NN), denote a machine learning technique that has been guided by the human brain and its capacity to perform complex tasks by means of inter-connected neurons performing each a very simple operation. Likewise, a NN is a trainable structure consisting of a set of inter-connected units, each implementing a very simple function, and together eventually performing a complex classification function or approximation task.

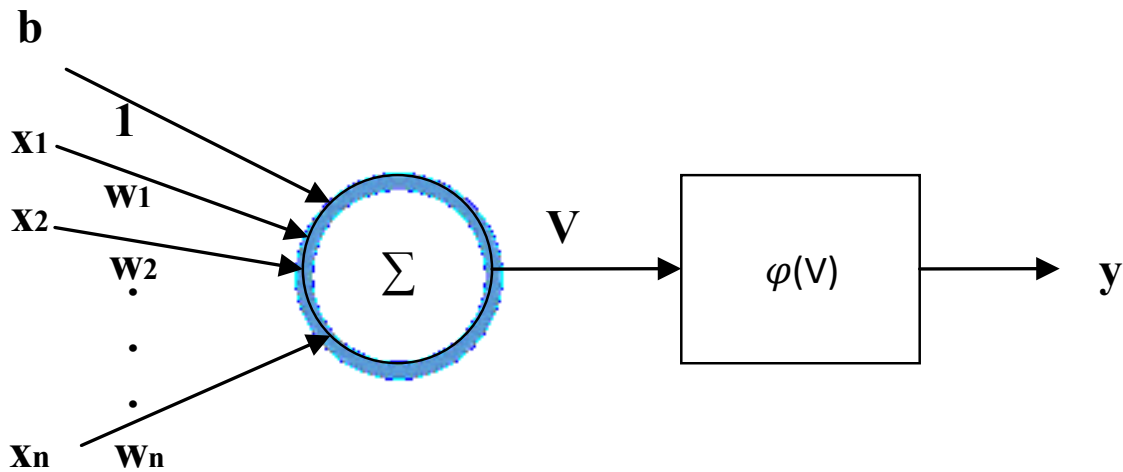


Figure III. 2. The perceptron

The most very well-known type of neural unit is called perceptron and has been introduced by Rosenblatt. Its basic structure is illustrated in figure III.2. It has n inputs and one output where the output is a simple function of the sum of the input signals x weighted by w and an additional bias b . Thus,

$$y = \varphi(x \cdot w + b) \tag{III.1}$$

Often, the bias is put inside the weight vector w such that $w_0 = b$ and the input vector x is extended correspondingly to have $x_0 = 1$. The equation (III.1) becomes:

$$y = \varphi(x \cdot w) \tag{III.2}$$

where φ is the Heavy-side step function:

$$\varphi(x) = \begin{cases} 1 & \text{if } x > 0 \\ 0 & \text{else} \end{cases} \tag{III.3}$$

The Perceptron implements a simple two-class classifier where $w \cdot x \geq 0$ for examples from one class and $w \cdot x < 0$ for examples from the other one. In 1962, Rosenblatt introduced the perceptron convergence theorem [16], a supervised training algorithm capable of learning an arbitrary two-class classification problems. However, Minsky and Papert showed that there are very simple classification problems where the perceptron doesn't work, specifically when the two classes are not linearly separable like in the XOR-problem, where the patterns (0, 0) and (1, 1) belong to one class and (0, 1) and (1, 0) to the other one. This encouraged the use of several interconnected perceptrons which are able to form more complex decision frontiers by combining many hyperplanes. The most common type of these NNs is the Multi-Layer Perceptron (MLP). Where MLP are able of approximating arbitrarily complex decision functions [16]. With the introduction of a practicable training algorithm in the 1980's, the so-called Back propagation algorithm, they became the most common widely used form of NNs.

Figure III.3 illustrates the structure of a MLP. There is an input layer, one or more hidden layer(s) and an output layer of neurons, where each neuron implements a perceptron except the input neurons as described in the previous section. Also, each neuron of one layer (hidden or input layer) is connected to each neuron in the following layer. We call this type of network: feed-forward network, or fully connected network.

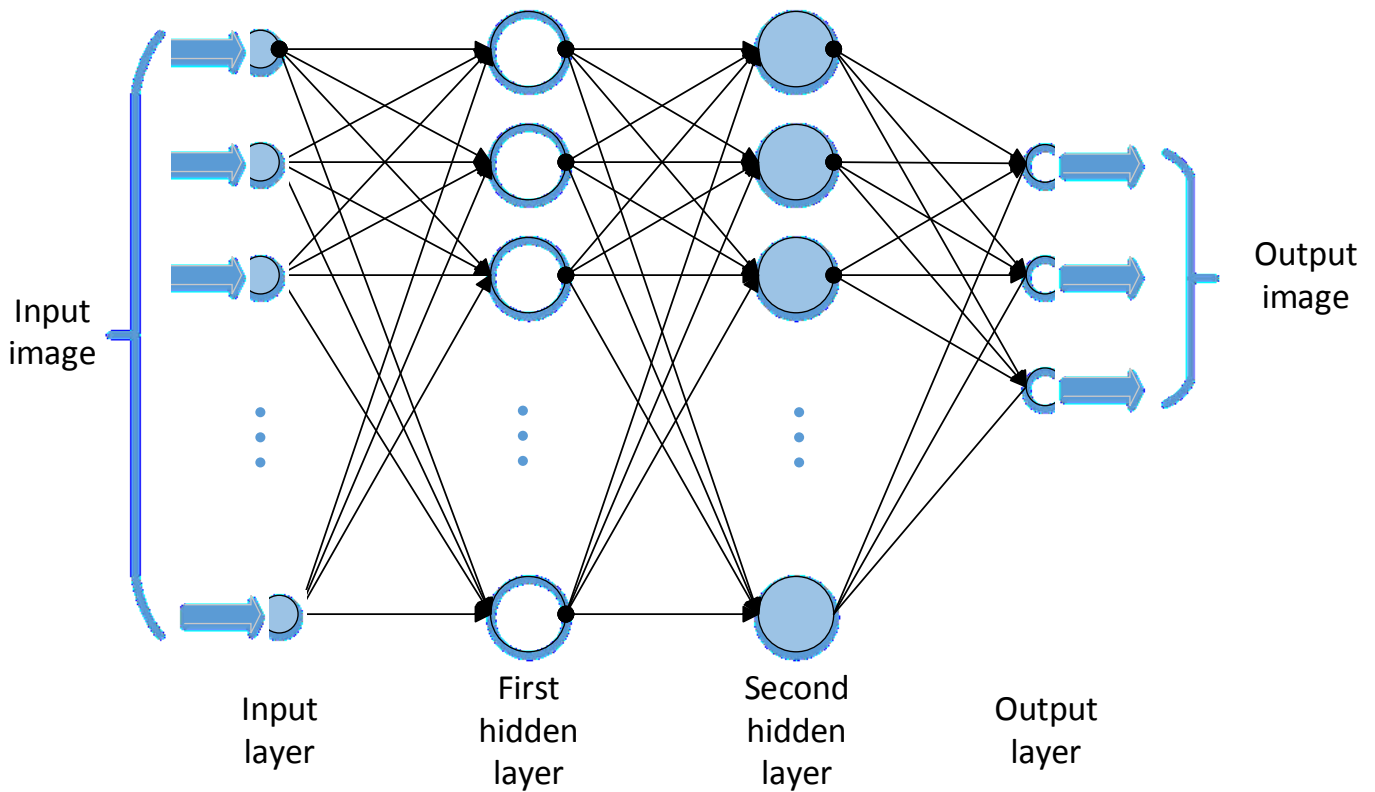


Figure III. 3. A multi-layer perceptron with 2 hidden layers

Multi-layer feed-forward Neural Networks (NN) have shown to be a very efficient machine learning technique as they can be trained to make complex non-linear functions approximate from high-dimensional input examples. Virtually, standard MLP have been used in pattern recognition systems to categorize signatures coming from a different separate feature extraction algorithm working on the input data. However, the manual selection of the feature extraction algorithm and the features to be distinguished is often empirical and therefore sub-optimal. Thus, a possible solution would be to directly imply the NN on the “raw” input data and make the training algorithm, e.g. Back propagation, seek the best feature extractors by adjusting the weights accordingly.

The problem with this approach is that when the input dimension is becomes high, as in images, the number of connections will be also high because each hidden neuron (in the first hidden layer) would be fully attached to the input layer. Typically, this number may be close to the order of several 10,000 or rather several 100,000 according to the application. The number of training example might be relatively small compared to the pattern dimension, which means that the NN would have a very high complexity and, thus, would tend to be over-fit with respect to the data.

Another disadvantage of this type of MLP is that its input layer has a fixed size and the input patterns have to be presented like well aligned and/or normalized to this input window, which, practically, is a rather complicated task. Thus, there is no built-in invariance with respect to small translations and local distortions. Finally, fully-connected NN architectures do not take into consideration correlations of neighboring input data. However, in pattern recognition problems there is generally a high amount of local correlation. Thus, it would be preferable to extract local features and combine them thereafter in order to perform the detection or recognition.

Actually, CNN are an approach that tries to rectify the above mentioned problems. That is, they automatically learn local feature extractors, they are stable to small translations and distortions in the input pattern, and they implement the principle of weight sharing which radically reduces the number of free parameters (weights and biases), and thus increases their generalization ability compared to NN architectures without this property.

2.2. Description of CNN

CNN has three key architectural notions [9] as described belows.

a. Local receptive fields

In the fully-connected layers shown earlier, the inputs were portrayed as a vertical line of neurons. In a convolution net, it'll help to think instead of the inputs as, say, for example, a 60×60 square of neurons, whose values relate to the 60×60 pixel consistencies we're using as inputs. An example of this is shown in figure III.4.a. As per usual, we'll connect the input pixels to a layer of hidden neurons. But we won't connect every input pixel to every hidden neuron. Instead, we only make connections in small, localized areas of the input image. More precisely, each neuron in the first hidden layer will be connected to a small area of the input neurons, say, for example, a 5×5 region, relating to 25 input pixels. For a specific hidden neuron, we might have connections as shown in the figure III.4.b.

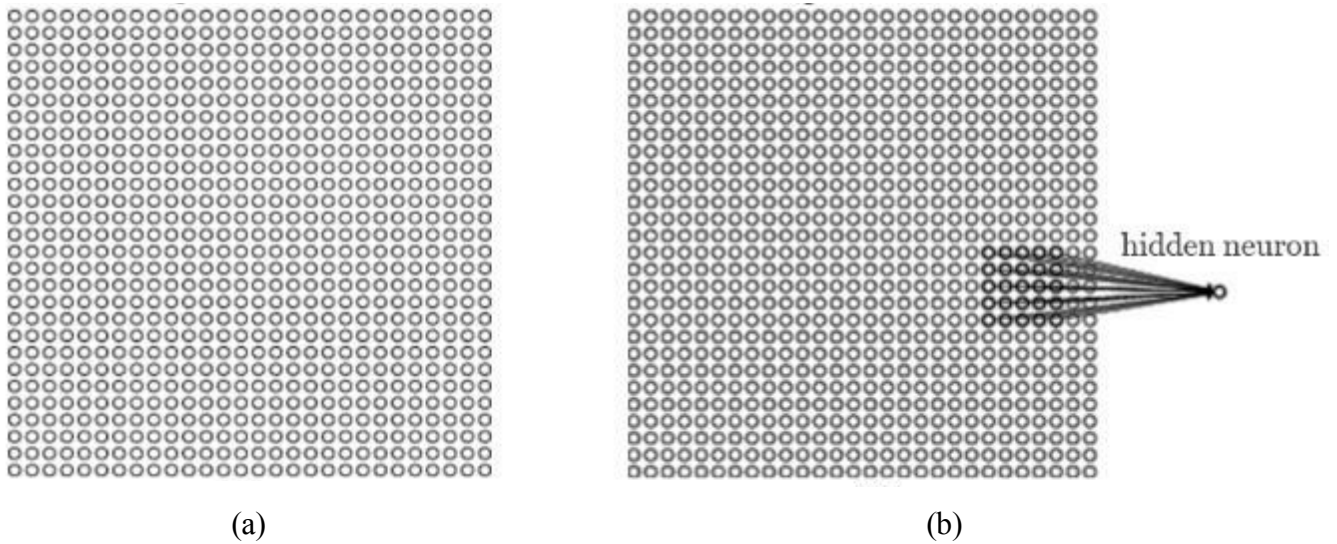


Figure III. 4. (a). Input neurons, (b). Local receptive field.

That region within the input image is called the local receptive field for the hidden neuron. It is a little window on the input pixels. Each connection learns a weight. And the hidden neuron learns an overall bias too. You can think of that particular hidden neuron as learning to analyze its specific local receptive field. We then slide down the local receptive field across the entire input image. For each local receptive field, there is a different hidden neuron in the first hidden layer. To clarify this concretely, let's start with a local receptive field in the top-left corner as shown in figure III.5.

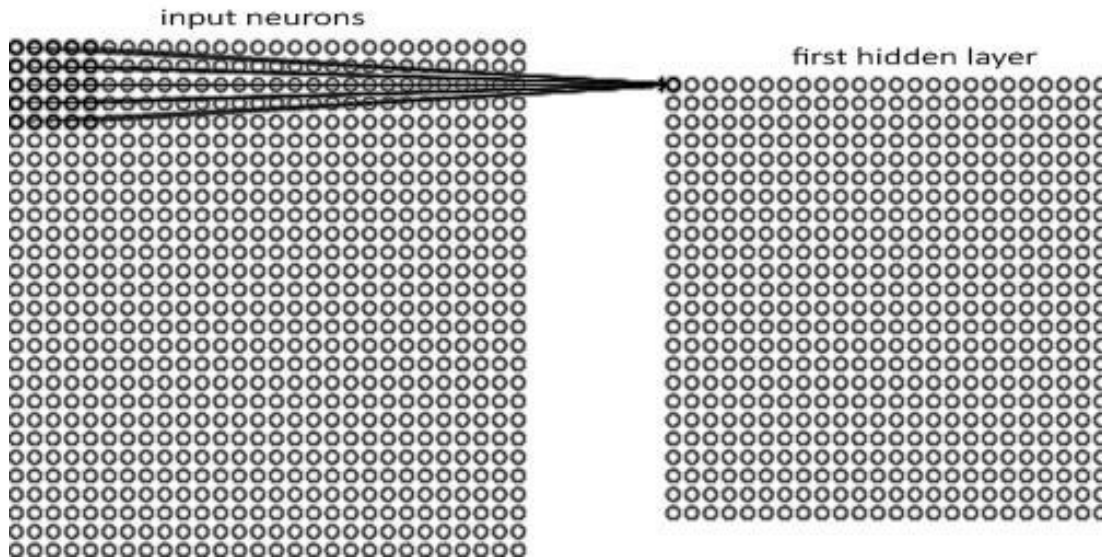


Figure III. 5. First convolution.

Then we slide the local receptive field by one pixel to the right to connect to a second hidden neuron as shown in figure III.6.

And so on, building up the first hidden layer, note that if we have a 60×60 input image, and 5×5 local receptive fields, then there will be 56×56 neurons in the hidden layer. This is because we can only wag the local receptive field 55 neurons across (or 55 neurons down), prior to colliding with the right-hand side (or bottom) of the input image.

Each neuron in a layer receives inputs from a set of neurons located in a small neighborhood in the previous layer. The idea of connecting neurons to local receptive fields on the input relate to the perceptron in the early 60s, and was almost done at the same time with Hubel and Wiesel's [17] discovery of locally-sensitive, orientation-selective neurons in the cat's visual system. Local connections have been used many times in neural models of visual learning. With local receptive fields, neurons can extract elementary visual features such as end points, oriented edges and corners. These features are then combined by the thereafter layers in order to detect higher-order features.

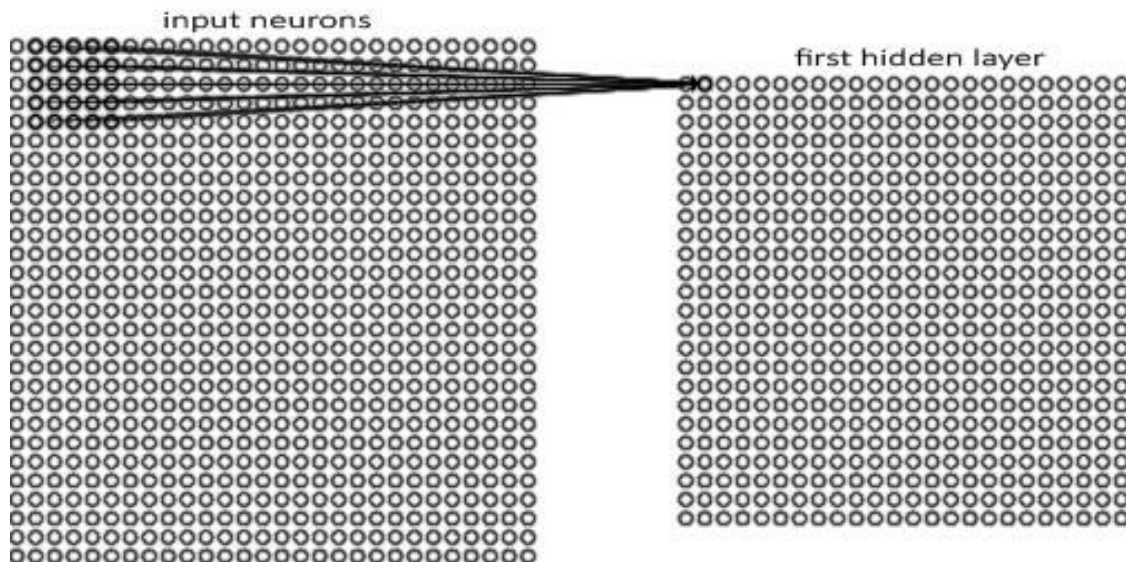


Figure III. 6. Second convolution.

Thus, images have a strong 2D local structure: variables (or pixels) that are temporally nearby are enormously correlated. Local correlations are the reasons for the well-known advantages of extracting and combining local features before perceiving spatial or temporal objects, because the arrangements of neighboring variables can be classified into a small number of categories (e.g. edges, corners, etc..). CNN force the extraction of local features by enclosing the receptive fields of hidden neurons to be local.

b. Weight Sharing

As stated earlier, distortions or shifts of the input can cause the position of protruding features to vary. In addition, elementary feature detectors that are beneficial on one part of the image are likely to be useful across the entire image. This knowledge can be applied by implementing a set of units, whose receptive fields are found at different places on the image, to have identical weight vectors. Thus, neurons in a layer are ordered in planes within which all the neurons share the same set of weights. The shared weights and bias are often said to determine a kernel or filter. The set of outputs of the neurons in such a plane is called a feature map. Neurons in a feature map are all known to perform the same operation on different parts of the image. A complete convolution layer is formed of several feature maps (with different weight vectors), so that multiple features can be extracted at each location.

Going back to the previous example, each hidden neuron has a bias and 5×5 weights connected to its local receptive field. We're going to use the same weights and bias for each of the 56×56 hidden neurons. This means that all the neurons in the first feature map of the hidden layer reveal exactly the same feature, just at different locations in the input image. To see why this makes sense, suppose the weights and bias is such that the hidden neuron can pick out, say, a vertical edge in a specific local receptive field. That ability is also likely to be useful at other places in the image. And so it is useful to apply the same feature detector everywhere in the image. To put it in slightly more abstract terms, convolution networks are well convenient to the translation invariance of images: move a picture of a dog (say) a little ways, and it's still an image of a dog.

The network structure described so far can reveal just a single kind of localized feature. To do image recognition we'll need more than one feature map. And so a complete convolution layer composed of several different feature maps. In the example shown in figure III.7, there are 3 feature maps. Each feature map is defined by a set of 5×5 shared weights, and a single shared bias. The result is that the network can detect 3 different types of features, with each feature being detectable across the entire image. A big advantage of sharing weights and biases is that it greatly reduces the number of parameters involved in a convolution network.

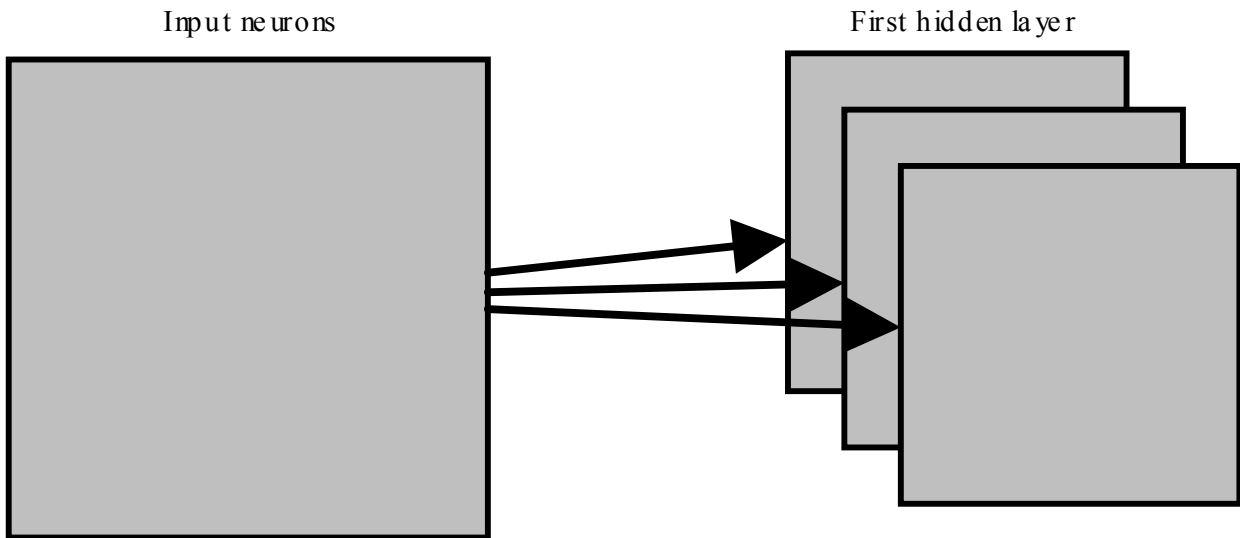


Figure III. 7. Three feature maps.

c. Sub-sampling in the spatial domain

Once a feature has been detected, its exact location becomes less substantial. Only its approximate position relative to other features is relevant. Not only is the precise position of each of those features irrelevant for recognizing the pattern, it is potentially baleful because the positions are likely to vary for different instances of the pattern. A simple way to reduce the accuracy with which the position of distinctive features is encoded in a feature map is to reduce the spatial resolution of the feature map. This can be achieved with so-called sub-sampling layers which execute a local averaging and a sub-sampling, reducing the resolution of the feature map, and reducing the sensitivity of the output to shifts and distortions.

In details, a sub-sampling layer takes each feature map precipitated from the convolution layer and prepares a condensed feature map. For instance, each unit in the sub-sampling layer may epitomize a region of (say) 2×2 neurons in the previous layer. As a concrete example, one common procedure for sub-sampling is known as max-pooling. In max-pooling, a pooling unit simply outputs the maximum activation in the 2×2 input region, as illustrated in figure III.8.

Contiguous units have non-overlapping adjoining receptive fields. Consequently, a sub-sampling layer feature map has half the number of rows and columns as the feature maps in the previous layer.

We can think of max-pooling as a way for the network to ask whether a given feature is found anywhere in a region of the image. It then throws away the exact positional information. The conjecture is that once a feature has been found, its exact location isn't as important as its rough location relative to other features. A big

benefit is that there are many fewer pooled features, and so this helps reduce the number of parameters needed in upcoming layers.

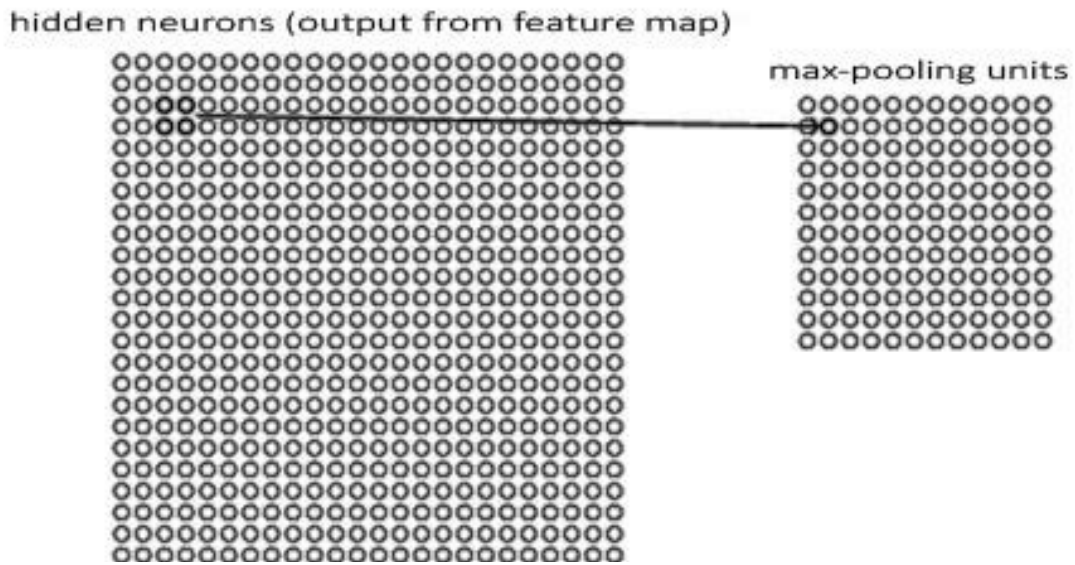


Figure III. 8. A pooling unit.

These connotations, all together, are the key ideas behind the evolution toward the use of the CNN instead of the fully-connected multilayer perceptron in pattern recognition problems. As in most CNN-based classification approaches, we adopted an architecture consisting of three types of layers: convolution layers, sub-sampling (max-pooling) layers and a fully-connected output layer [18]. They are arranged in a form such that each convolution layer is followed by a sub-sampling layer, and the last convolution layer is followed by the output layer (see figure III.9).

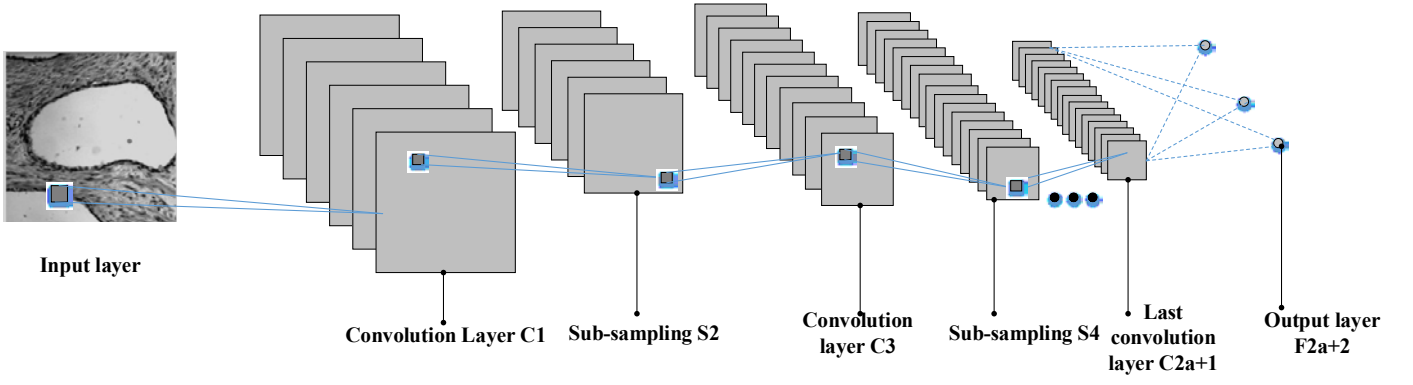


Figure III. 9. CNN architectural model.

Convolution layer: this layer type receives as input either the image to classify or the output of the previous layer, and applies a set of N_l convolution filters to this input. The output of the layer corresponds to N_l feature maps, each one of the results of a convolution filter and some additive bias as illustrated in figure III.10. The parameters learned during training correspond to the convolution filter and bias weights. Note that the convolution process trims output maps by a border of $M_l - 1$ pixels, where $M_l \times M_l$ is the size of convolution filters.

The feature map n of convolution layer l (Figure III.10) is expressed as follows:

$$y_n^l = f_l \left(\sum_{m \in v_n^l} y_m^{l-1} \otimes w_{m,n}^l + b_n^l \right) \quad (\text{III.4})$$

Where,

$$w_{m,n}^l = \{w_{m,n}^l(i, j)\} \quad (\text{III.5})$$

Knowing that i & j represent the coordinates of the pixels, f_l represents the sigmoid activation function of layer l , y_m^{l-1} is the feature map m in layer $(l-1)$, where $l = 1, 3, \dots, 2a+1$, b_n^l represents the bias term associated with feature map n , v_n^l represents the list of all planes in layer $(l-1)$ that are connected to feature map n , and \otimes represents the 2-D convolution operator. Note that $L=2a+2$ is the number of network layers.

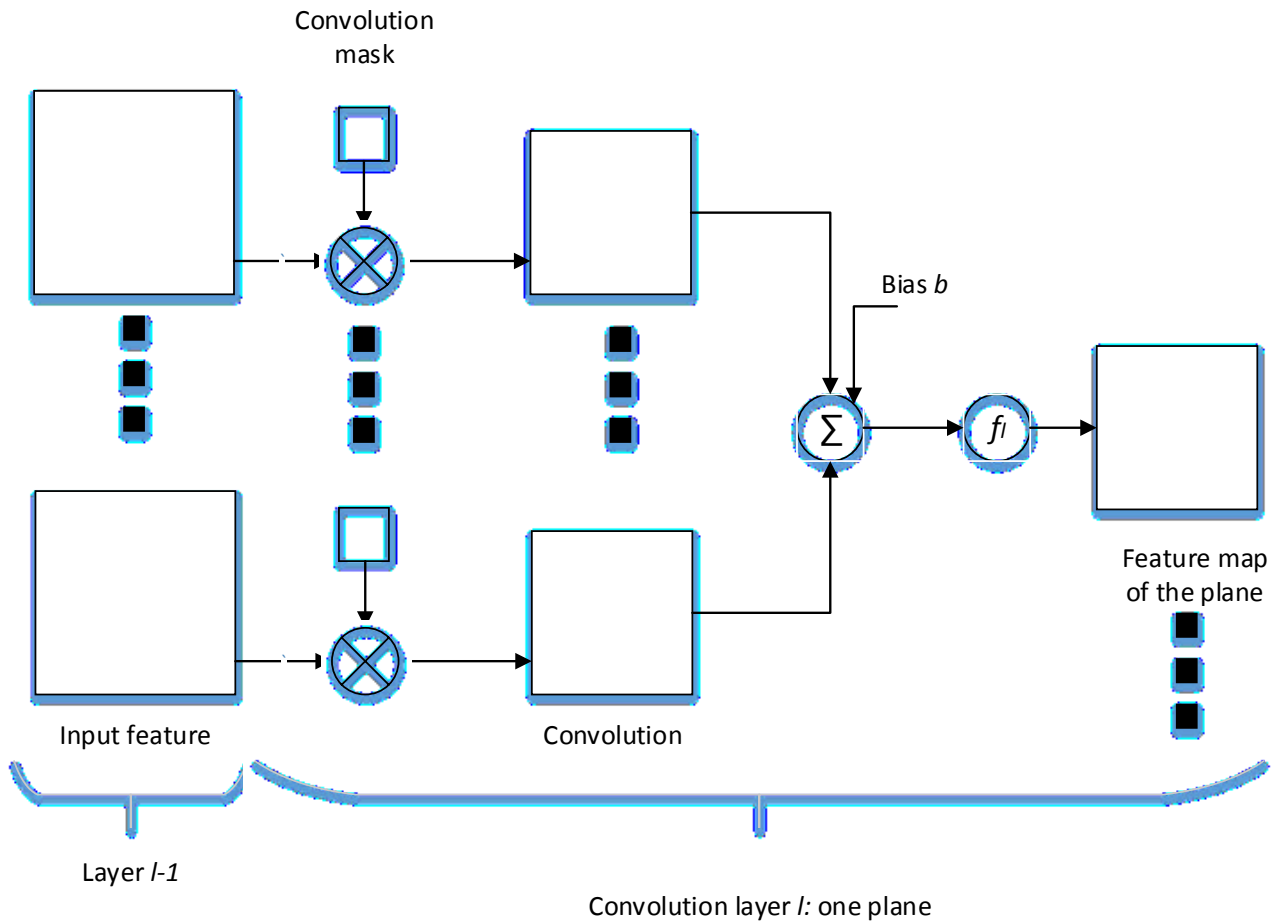


Figure III. 10. One plane of a convolution layer in CNN.

Sub-sampling (pooling) layer: this parameter-less type of layer reduces the size of input feature maps via sub-sampling, thereby supporting local spatial invariance. It divides the input maps into non-overlapping sub-regions, and applies a specific pooling function to each one of them as illustrated in figure III.11. In our architecture, we considered the max-pooling strategy, which outputs the maximum value of each sub-region. Note that the pooling process reduces the feature maps by a factor of M_l , where $M_l \times M_l$ is the size of pooling sub-regions.

The feature map n of sub-sampling layer l ($l=2, 4, 6, \dots, 2a$) is expressed as follows (Figure III.11):

$$y_n^l = f_l(z_n^{l-1} \times w_n^l + b_n^l) \quad (III.6)$$

Where, z_n^{l-1} represents a matrix that is expressed as follows:

$$z_n^{l-1}(i, j) = y_n^{l-1}(2i - 1, 2j - 1) + y_n^{l-1}(2i - 1, 2j) \\ + y_n^{l-1}(2i, 2j - 1) + y_n^{l-1}(2i, 2j) \quad (\text{III.7})$$

b_n^l represents the bias term associated with feature map n , and w_n^l represents its weight.

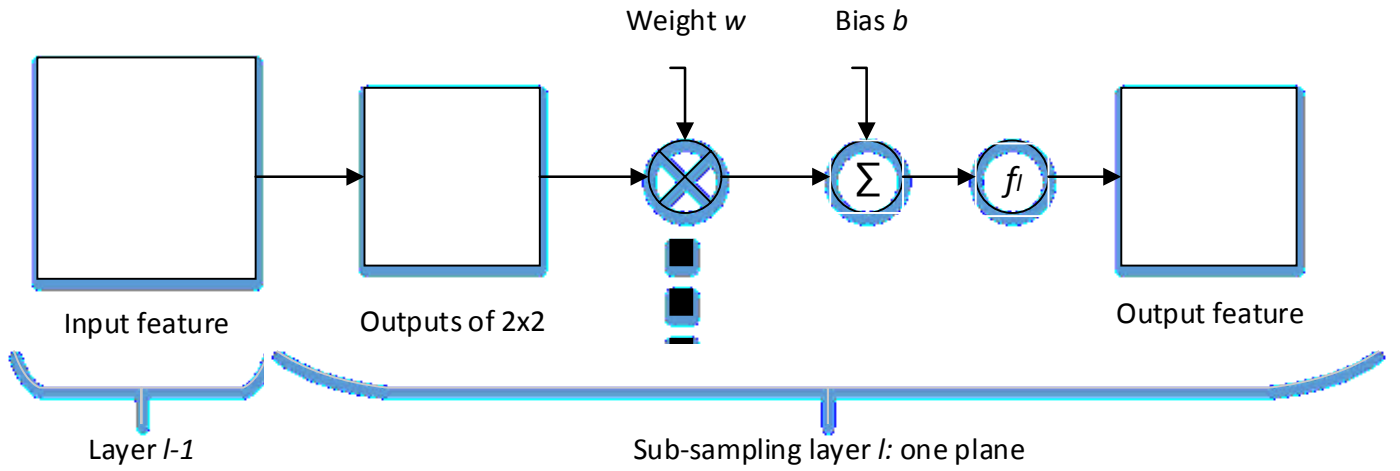


Figure III. 11. One plane of a sub-sampling layer in CNN.

Output (fully connected) layer: this type of layer captures the relationship between the final layer feature maps and class labels. The output of the layer is a vector of K elements, each one representing the score of a class. Fully-connected layers can be seen as convolution operations, in which filters have the same size as their input maps. Knowing that its type depends on the type of the application, it is expressed as follows:

$$y = [y_1^L, y_2^L, \dots, y_{N_L}^L] \quad (\text{III.8})$$

Where, the output of sigmoidal neuron neuron n expressed as follows:

$$y_n^L = f^L \left(\sum_{m=1}^{N^{L-1}} y_m^{L-1} w_{m,n}^L + b_n^L \right) \quad (\text{III.9})$$

Where L represents the output layer, N^L represents the number of output neurons, $w_{m,n}^L$ represents the weight from feature map m of the last convolution layer to neuron n on the output layer, and b_n^L represents the bias of neuron n of layer L . During the training process, the parameters of the network will be updated according to the training data set using the RPROP (Resilient Back-propagation) algorithm [19]. Where the output of the image using CNN is compared to the desired output, as there are differences between them, the network weights and biases will be updated. This function will be repeated until obtaining a minimum error between them as shown in figure III.12, where ϵ represent a very small number which will be determined by the user (usually $\epsilon = 0.001$).

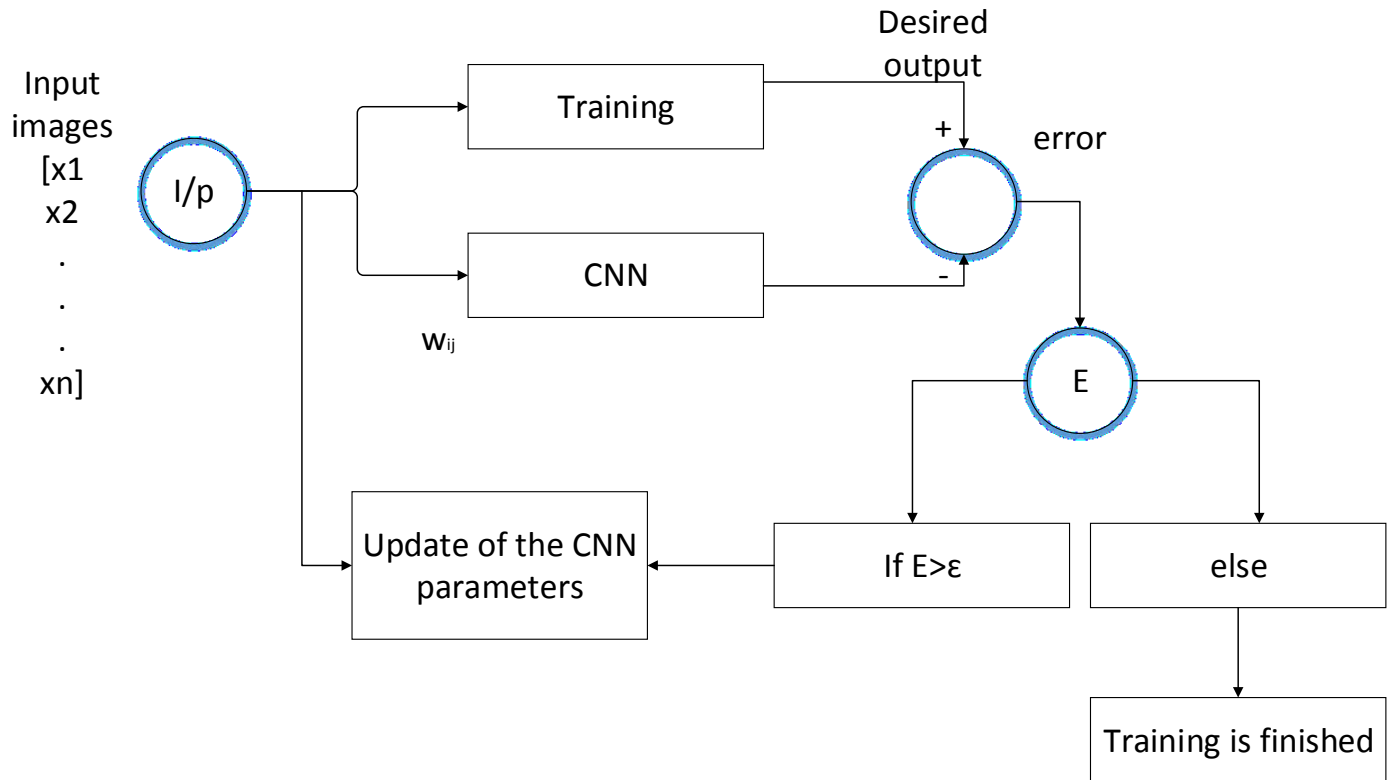


Figure III. 12. Training system of the CNN classifier.

The error function mse (mean squared error) can be defined as follows:

$$mse = \frac{1}{N_L K} \sum_{k=1}^K \sum_{n=1}^{N_L} (y_n^k - d_n^k)^2 = \frac{1}{N_L K} \sum_{k=1}^K \sum_{n=1}^{N_L} (CNN(x_k, W) - d_n^k)^2 \quad (III.10)$$

Where, K is the size of the training data set or the number of input training images, W is the vector that contains all the parameters of the network, x_k is the k^{th} input training image of the network, d_n^k is the

corresponding desired output vector and $y_n^k = CNN(x_k, W)$ is the response obtained at the output of the network [19].

2.3. Implementation of CNN

Figure III.13 presents the pipeline of the proposed approach. Where histological CRC data are obtained from anatomical pathology at the CHU Nancy-Brabois Hospital. Part of these data were used in a previous study for classifying the abnormal PT from texture features [8]. Tissue samples were obtained from sequential colon resections of 40 patients with colorectal cancer. Sections of 5 μm thickness were extracted and stained using haematoxylin and eosin to reduce image processing requirements. Multispectral images of 512×512 pixels were then acquired using a charge coupled device (CCD) camera integrated with a liquid crystal tunable filter (LCTF) in an optical microscopy system [20]. For each tissue sample, the LCTF was used to provide 16 multispectral images sampled uniformly across the wavelength range of 500-650 nm [21]. Since multispectral imaging considers a broader range of wavelengths, it can capture physiological characteristics of tissues beyond those provided by standard grey scale or trichromatic photography.

These images are then used as input to the CNN classifier, both for training the model and classifying the tissue type of a new image. Alternatively, a segmentation technique based on active contours can be used to extract regions of interest corresponding to pathological tissues, before the classification step. Although non-segmented images can also be used directly, a segmentation step is added in the proposed pipeline to isolate the CRC tissues from non-relevant tissues and structures such as lumen. For this step, we used a semi-automatic segmentation technique based on the active contour algorithm, which can accurately delineate the boundaries of irregularly shapes and has been shown to perform well for tissue segmentation [22].

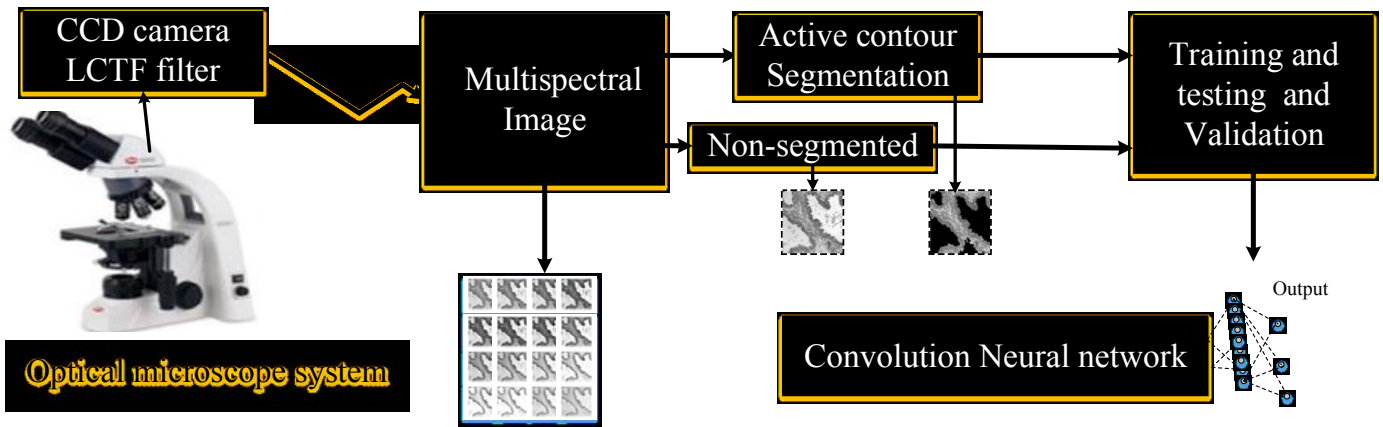


Figure III. 13. Proposed flowchart for automated detection of CRC progression using CNN comprises: 1) multispectral images of PT, and 2) Convolution neural network to classify each CRC image from segmented and non-segmented PT.

These images were applied on the proposed CNN, where it is chosen after study of many networks. The study of the network begins by trying to find the smallest one with the perfect performance, that's why we begin by the less number of layers (table III.1.a) and begin increase it until the performance begin to decrease (table III.1.d), then we come to fixing the number of layers (table III.1.f, g &h). After that we will study the different connections between these layers until we reach the one with the best performance. Table III.1 shows these eight networks, and shows its accuracy values and mean squared error after applying it on our data (training and test data set) which are 28 patients images for training and 12 for testing. Note that, we used the same training algorithm during the training process and the same number of training epochs. The network shown in (c) gives the best result, where it reaches 100% and 99.625% as training and testing accuracy values, and 3.259×10^{-5} and 10^{-4} for training and testing mean squared error in case of segmented images.

CNN	Classification rate		mse	
	(Accuracy)			
	Training 21 patients	Test 9 patients	Training 21 patients	Test 9 patients

	<p>C1 5x5 56x56</p> <p>S2 2x2 28x28</p> <p>C3 3x3 26x26</p> <p>S4 2x2 13x13</p> <p>C5 6x6 8x8</p> <p>Output Layer F6</p>				
(a)	<p>Input image</p> <p>Network output</p>	87.52	85.34	11×10^{-4}	14×10^{-4}
(b)	<p>Input image</p> <p>Network output</p>	83.23	80.12	29×10^{-4}	31×10^{-4}
(c)	<p>Input image</p> <p>Network output</p>	100	99.16	3.259×10^{-5}	1×10^{-4}

(d)	<p>Diagram (d) illustrates a CNN architecture with the following layers and parameters:</p> <ul style="list-style-type: none"> C1: 5x5 kernel, 56x56 spatial dimensions S2: 2x2 stride, 28x28 spatial dimensions C3: 3x3 kernel, 26x26 spatial dimensions S4: 2x2 stride, 13x13 spatial dimensions C5: 6x6 kernel, 8x8 spatial dimensions Output Layer F6: Final output layer <p>Network output: 87.95</p>	87.95	86.52	3×10^{-3}	1×10^{-3}
(e)	<p>Diagram (e) illustrates a CNN architecture with the following layers and parameters:</p> <ul style="list-style-type: none"> C1: 5x5 kernel, 56x56 spatial dimensions S2: 2x2 stride, 28x28 spatial dimensions C3: 3x3 kernel, 26x26 spatial dimensions S4: 2x2 stride, 13x13 spatial dimensions C5: 6x6 kernel, 8x8 spatial dimensions Output Layer F6: Final output layer <p>Network output: 75.91</p>	75.91	74.69	19×10^{-3}	23×10^{-3}

(f)	<p>Diagram of CNN (f) architecture. It shows an input image feeding into two parallel paths. The top path has layers C1 (5x5, 56x56), S2 (2x2, 28x28), C3 (3x3, 26x26), S4 (2x2, 13x13), and C5 (6x6, 8x8). The bottom path has layers S2 (2x2, 28x28), C3 (3x3, 26x26), S4 (2x2, 13x13), and C5 (6x6, 8x8). Both paths converge into an Output Layer F6 (6x6, 8x8).</p>	86.75	85.42	12×10^{-4}	14×10^{-4}
(g)	<p>Diagram of CNN (g) architecture. It shows an input image feeding into two parallel paths. The top path has layers C1 (5x5, 56x56), S2 (2x2, 28x28), C3 (3x3, 26x26), S4 (2x2, 13x13), and C5 (6x6, 8x8). The bottom path has layers S2 (2x2, 28x28), C3 (3x3, 26x26), S4 (2x2, 13x13), and C5 (6x6, 8x8). Both paths converge into an Output Layer F6 (6x6, 8x8).</p>	86.22	84.91	16×10^{-4}	18×10^{-4}
(h)	<p>Diagram of CNN (h) architecture. It shows an input image feeding into two parallel paths. The top path has layers C1 (5x5, 56x56), S2 (2x2, 28x28), C3 (3x3, 26x26), S4 (2x2, 13x13), and C5 (6x6, 8x8). The bottom path has layers S2 (2x2, 28x28), C3 (3x3, 26x26), S4 (2x2, 13x13), and C5 (6x6, 8x8). Both paths converge into an Output Layer F6 (6x6, 8x8).</p>	88.62	86.31	9×10^{-4}	11×10^{-4}

Table III. 1: The composition of eight CNNs showing its accuracy and its mean squared error

The proposed and the best CNN transform the dimension of the input image to be 60x60 pixels, it consists then of 6 layers (table III.1.c):

- Convolution layer C1 uses receptive field of size 5×5 . It produces two feature maps, each consisting of 56×56 pixels.
- Sub-sampling layer S2 uses receptive field of size 2×2 , this applies to all sub-sampling layers. This layer produces feature maps of size 28×28 pixels. Note that feature maps in a sub-sampling layer always have one-to-one connections to feature maps of the previous convolution layer.
- Convolution layer C3 uses receptive field of size 3×3 . It produces five feature maps, each consisting of 26×26 pixels.
- Sub-sampling layer S4 uses a receptive field of size 2×2 and produces five feature maps of size 13×13 pixels.
- Convolution layer C5 uses receptive field of size 6×6 . It produces five feature maps, each consisting of 8×8 pixels.
- Output layer F6 has three neurons that are fully connected to the output of C5.

This network contains three types of connections between CNN layers: one-to-one connection, full connection and custom connection. The number of feature maps in each layer is specified by the connections:

- One-to-one connection: this is a connection from a convolution layer to the next sub-sampling layer. That is, a feature map of a convolution layer connected to exactly one feature map of the next sub-sampling layer. It is shown in C1 to S2, C3 and S4.
- Custom connection: this is a connection from a sub-sampling layer to the next convolution layer. It is shown in the connection from S2 to C3 and S4 to C5 in our network. For example, in the case from S2 to C3, the feature map 1 of layer S2 is connected to feature maps 1, 2 and 5 of layer C3. Feature map 2 of layer S2 is connected to feature maps 3, 4 and 5 of layer C3.
- Full connection: It represents the connection from the input to the first convolution layer C1, and from the last convolution layer to the output layer. That is, each feature produced by the last convolution layer is connected to all neurons in the output layer. It is shown in C5 to F6.

This proposed method will be evaluated using the mean squared error (*mse*) and accuracy [23], for the classification method.

The performance of CNN is decomposed into two parts:

- Training performance, which gives the performance of the trained images (training data set) after applying it many times (according to the number of epochs given initially) and comparing the results to the saved one.
- Testing performance, which gives the performance of the tested images (tested data set).

In both cases, the performance metrics used in this paper are the *mse* and *accuracy*. Where the *mse* measures the average of the squares of the errors or deviations, that is, the difference between the estimator and what is estimated. Knowing that as *mse* tends to zero, the classification will be improved, knowing that the number of samples presented as n , Y_i and Y_i' represent the ground truth and trained outputs, respectively, it is expressed as follows:

$$mse = \frac{1}{n} \sum_{i=1}^n (Y_i' - Y_i)^2 \quad (\text{III.11})$$

Another performance tool is the accuracy, which represents the degree of closeness of measurements of a quantity to that quantity's true value, it represents the correctly classified samples, knowing that as accuracy tends to 1, the classification will be improved, it is calculated according to the following expression:

$$\text{Accuracy} = \frac{\text{number of samples correctly classified}}{n} \quad (\text{III.12})$$

Knowing that each image can be taken as 16 images of different frequencies, to study the performance of our method we use 7ST, 7 BH, 7IN and 7Ca images are used for training, and 3ST, 3 BH, 3IN and 3Ca images are used for testing.

3. Extraction of Features

Four methods are studied, to be applied on the segmented images, in order to extract their features.

3.1. Gray-level run length matrix

The Gray Level Run Length Matrix (GLRLM), which is also known as a gray-level co-occurrence matrix can be viewed as a statistical texture characterization method [24]. The Gray Level Run Length Matrix (GLRLM), which is also known as a gray-level co-occurrence matrix can be viewed as a statistical texture characterization method [24]. Where its function shows in counting the number of pixels in an image that have the same intensity in a given direction. Before having the results in a matrix which is calculating how

often a pixel with gray-level (grayscale intensity) value i occurs horizontally adjacent to a pixel with the value j . This matrix is represented as (l,n) , which is equal to the number of segments of length l and gray level n . Figure III.14 shows an example of the calculation of a Run Length Matrix for a 4x4 image in 0° direction and for 4 gray levels:

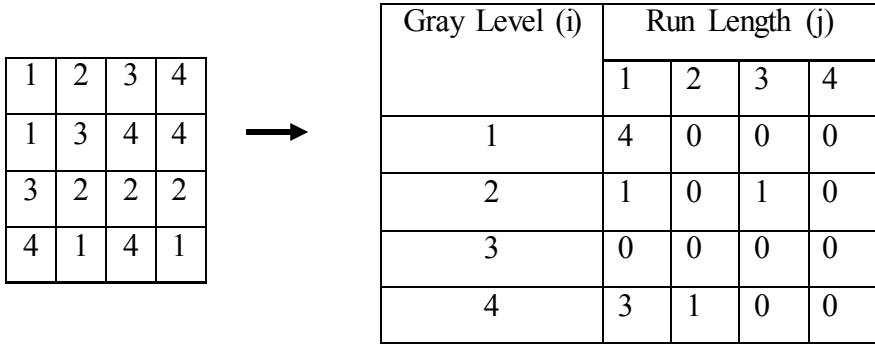


Figure III. 14. Example of the calculation of a run length matrix for a 4x4 image in 0° directions and for 4 gray levels.

3.2. Gray-level size zone matrix

The Gray Level Size Zone Matrix (GLSZM), which is calculated after decomposing the homogeneous texture into areas with pixels of the same intensity level, and not of small groups of pixels or segments in any given direction. It is calculated according to GLRLM principle, where the value of the matrices is equal to the number of areas of size s and of gray level n . This matrix is represented as (s,n) , which is equal to the number of areas of size s and of gray level n . Figure III.15 shows an example of the calculation of such a matrix:

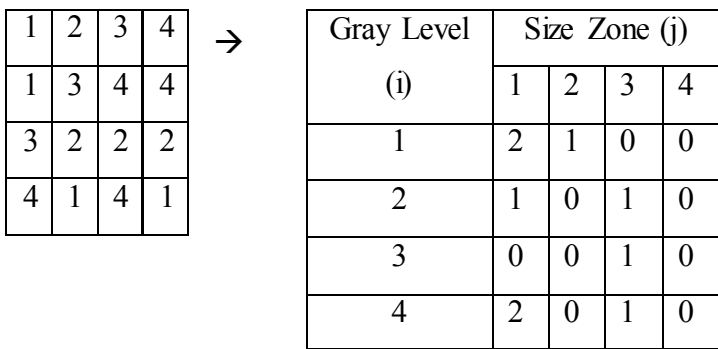


Figure III. 15. Example of the calculation of a run length matrix for a 4x4 image with 4 gray levels

This matrix has a fixed number of lines, which refers to the number of gray levels, and a variable number of columns that are determined by the size of the largest area. Knowing that large homogeneous areas, but with high variations in the intensity between the areas, making them inhomogeneous textured. Therefore, in order to characterize these types, two new indexes are studied (variances) as follows:

$$Var_N = \sqrt{\frac{1}{NxS} \sum_{n=1}^N \sum_{s=1}^S (nxM(n,s) - \mu_N)^2} \quad (III.13)$$

$$Var_S = \sqrt{\frac{1}{NxS} \sum_{n=1}^N \sum_{s=1}^S (sxM(n,s) - \mu_S)^2} \quad (III.14)$$

Where,

$$\mu_N = \frac{1}{NxS} \sum_{n=1}^N \sum_{s=1}^S nxM(n,s) \quad (III.15)$$

$$\mu_S = \frac{1}{NxS} \sum_{n=1}^N \sum_{s=1}^S sxM(n,s) \quad (III.16)$$

with N and S the dimensions of the matrix and $M(n,s)$ the matrix's element of coordinates (n,s) . As the large areas with high intensity vary between them, the value of the variance is higher. To classify the types of images, four different classification methods are studied, such as: logistic regression, k-nearest neighbors, random forests and neural networks.

3.3. Scale Invariant Feature Transformation (SIFT)

Scale invariant feature transformation (SIFT) is an algorithm used to detect and describe local features in images, in which it provides the underlying image patch descriptor for matching scale invariant key points [27]. These features are based on the particular interest points, and it is invariant to image scale, and has minor changes in viewpoints.

Its algorithm begins by determining the key points initially in the SIFT framework, and the image is then convolved with Gaussian filters at different scales. And the update key points will be taken as maxima/minima of the difference of Gaussians (DOG).

Knowing that the convolution of the original image $I(x,y)$ with the Gaussian blur $G(x,y,k\sigma)$ at scale $k\sigma$ is represented as follows:

$$L(x, y, k\sigma) = G(x, y, k\sigma) * I(x, y) \quad (\text{III.17})$$

The DoG image is represented as follows:

$$D(x, y, \sigma) = L(x, y, k_i\sigma) - L(x, y, k_j\sigma) \quad (\text{III.18})$$

Knowing that the DoG image between scales $k_i\sigma$ and $k_j\sigma$ represents the difference of the Gaussian-blurred images at these scales [27].

3.4. Features extracted from CNN

In this case we are going to take the features from the proposed CNN studied above, where the features extracted from the final convolution layer (C5 in our network). In this case we study the CNN and we just take the features from it without the need to classify it from the same application, but we apply it on other classification methods which are two classifier models of SVM, such as treebagger and K-Nearest Neighbor (KNN).

4. SVM Classifier

Two types of SVM are studied and applied on our data.

4.1. Treebagger SVM

Random decision forests are ensemble learning method for classification and other tasks, where it operates by constructing decision trees at training time, and output the classes for individual trees. Bagged decision trees reduces the effects of over fitting, due to the combination of the results of many decision trees [28]. Knowing that bootstrap is a machine learning ensemble meta-algorithm designed to improve the stability and accuracy of machine learning algorithms used in statistical classification and regression [29], using a bootstrap samples of the data, treebagger grows the decision tree in the ensemble, and selects a random subset of predictors in order to use at each decision split as in the random forest algorithm [30].

4.2. KNN SVM

The Support Vector Machine (SVM), is defined as supervised learning models that analyze data used for classification [31]. Initially, SVM is trained using a set of training examples, then SVM will build its model that assigns new examples into one category or the other, making it a non-probabilistic binary linear classifier. SVM constructs a hyperplane or set hyperplanes which can be used for the classification, knowing that, a good separation is achieved by the hyperplane that has the largest distance to the nearest training-data point of any class, the larger the margin the lower the generalization error of the classifier.

The main problem is that the sets of discrimination are not linearly separable in that space. Knowing that the mappings used by SVM schemes are designed to allow the dot product to be computed easily in terms of the variables in the original space, which is defined in terms of a kernel function $k(x,y)$. The hyperplanes defined by vectors, which represent a linear combination with parameters α_i of images of feature vectors x_i that occur in the data base. And the points x are defined as follows:

$$\sum_i \alpha_i k(x_i, x) = constant \quad (III.19)$$

Therefore, the sum of kernels are used to measure the relative nearness of each test point to the data points originating in one or other sets to be discriminated.

KNN is a classifying method that is based on the closest training examples in the features. It can be described as the simplest of all machine learning algorithms [32], where an object is classified by the majority with its neighbors, and every training example is stored with its label and pick the nearest K neighbors ($K \geq 1$). In order to test the example, the distance (Euclidean distance) to every training example is computed.

Therefore, the SVM-KNN method can be described as follows:

- Initially, construct the feature vector for the given image,
- Compute the Euclidean distance, and pick the nearest K neighbors,
- If K have the same labels, otherwise it computes the pairwise distances between K-neighbors,
- Convert the distance matrix to kernel one, and apply SVM.

Also these classifier methods use *mse* and *accuracy* which are expressed in III.11 and III.12 In order to study its performance. In order to study its performance, we also use the same number of image as in CNN, where we use 7ST, 7 BH, 7IN and 7Ca images are used for training, and 3ST, 3 BH, 3IN and 3Ca images are used for testing.

5. Conclusion

Colorectal Cancer is one of the major leading causes of cancer-related deaths all around the world. However, its detection at early stages gives a chance for an effective treatment. To overcome this problem, several computer-aided diagnostic pattern recognition systems are introduced, but until now, no such system did reach a high reliability in classification, due to the hard choice of appropriate features and algorithms.

In this chapter, we have initially had a brief description of machine learning, and then CNN is studied after showing its importance in machine learning. Then proposed to work with CNN as a colon cancer cells classifier that automatically learns local feature extractors. Where we have implemented several network architectures, and compared their performances, to find the CNN that provides the highest accuracy reaching 100% during the training phase, and 96.97% during the test phase. On the other side, the feature extraction of four types is studied such as GLRLM, GLSZM, SIFT and features extracted from CNN. These features extracted from the images in order to be applied also in two different types of SVM classifiers, such as treebagger and KNN. The two types of SVM will be compared to the CNN classifier in order to compare the better method between them, where it will be applied on 40 multi-spectral image textured sound like cells (ST) or abnormal (BH, IN and Ca), which will be our work in next chapter.

References of Chapter III

- [1] J. J. Fu, Y.-W. Yu, H.-M. Lin, J.-W. Chai, and C. C.-C. Chen, "Feature extraction and pattern classification of colorectal polyps in colonoscopic imaging," *Computerized Medical Imaging and Graphics*, vol. 38, pp. 267-275, 2014.
- [2] R. Kumar, R. Srivastava, and S. Srivastava, "Detection and Classification of Cancer from Microscopic Biopsy Images Using Clinically Significant and Biologically Interpretable Features," *Journal of Medical Engineering*, vol. 2015, 2015.
- [3] M. Mookiah, P. Shah, C. Chakraborty, and A. K. Ray, "Brownian motion curve-based textural classification and its application in cancer diagnosis," *Analytical and quantitative cytology and histology/the International Academy of Cytology [and] American Society of Cytology*, vol. 33, pp. 158-168, 2011.
- [4] J. Jass, "Classification of colorectal cancer based on correlation of clinical, morphological and molecular features," *Histopathology*, vol. 50, pp. 113-130, 2007.
- [5] S. Rathore, M. Hussain, and A. Khan, "Automated colon cancer detection using hybrid of novel geometric features and some traditional features," *Computers in biology and medicine*, vol. 65, pp. 279-296, 2015.
- [6] S. Rathore, M. A. Ifikhar, M. Hussain, and A. Jalil, "Classification of colon biopsy images based on novel structural features," in *Emerging Technologies (ICET), 2013 IEEE 9th International Conference on*, 2013, pp. 1-6.
- [7] S. Rathore, M. Hussain, M. A. Ifikhar, and A. Jalil, "Ensemble classification of colon biopsy images based on information rich hybrid features," *Computers in biology and medicine*, vol. 47, pp. 76-92, 2014.

- [8] A. Chaddad, C. Desrosiers, A. Bouridane, M. Toews, L. Hassan, and C. Tanougast, "Multi Texture Analysis of Colorectal Cancer Continuum Using Multispectral Imagery," *PloS one*, vol. 11, p. e0149893, 2016.
- [9] Y. LeCun, L. Bottou, Y. Bengio, and P. Haffner, "Gradient-based learning applied to document recognition," *Proceedings of the IEEE*, vol. 86, pp. 2278-2324, 1998.
- [10] S. Lawrence, C. L. Giles, A. C. Tsoi, and A. D. Back, "Face recognition: A convolutional neural-network approach," *Neural Networks, IEEE Transactions on*, vol. 8, pp. 98-113, 1997.
- [11] A. Krizhevsky, I. Sutskever, and G. E. Hinton, "Imagenet classification with deep convolutional neural networks," in *Advances in neural information processing systems*, 2012, pp. 1097-1105.
- [12] B. Sahiner, H.-P. Chan, N. Petrick, D. Wei, M. A. Helvie, D. D. Adler, *et al.*, "Classification of mass and normal breast tissue: a convolution neural network classifier with spatial domain and texture images," *Medical Imaging, IEEE Transactions on*, vol. 15, pp. 598-610, 1996.
- [13] P. Y. Simard, D. Steinkraus, and J. C. Platt, "Best practices for convolutional neural networks applied to visual document analysis," in *null*, 2003, p. 958.
- [14] S.-C. B. Lo, S.-L. A. Lou, J.-S. Lin, M. T. Freedman, M. V. Chien, and S. K. Mun, "Artificial convolution neural network techniques and applications for lung nodule detection," *Medical Imaging, IEEE Transactions on*, vol. 14, pp. 711-718, 1995.
- [15] D. Stutz, "Understanding Convolutional Neural Networks," 2014.
- [16] S. S. Haykin, S. S. Haykin, S. S. Haykin, and S. S. Haykin, *Neural networks and learning machines* vol. 3: Pearson Upper Saddle River, NJ, USA; 2009.
- [17] D. H. Hubel and T. N. Wiesel, "Receptive fields of single neurones in the cat's striate cortex," *The Journal of physiology*, vol. 148, pp. 574-591, 1959.
- [18] S. L. Phung and A. Bouzerdoun, "MATLAB library for convolutional neural networks," *University of Wollongong, Tech. Rep.*, URL: <http://www.elec.uow.edu.au/staff/sphung>, 2009.
- [19] M. Riedmiller and H. Braun, "A direct adaptive method for faster backpropagation learning: The RPROP algorithm," in *Neural Networks, 1993., IEEE Int. Conference on*, 1993, pp. 586-591.
- [20] A. Chaddad, C. Tanougast, A. Dandache, and A. Bouridane, "Extracted Haralick's Texture Features and Morphological Parameters from Segmented Multispectrale Texture Bio-Images for Classification of Colon Cancer Cells," *WSEAS Transaction on Biology and Biomedicine Journal*, vol. 8, pp. 39-50, 2011.
- [21] P. J. Miller and C. C. Hoyt, "Multispectral imaging with a liquid crystal tunable filter," in *Photonics for Industrial Applications*, 1995, pp. 354-365.
- [22] D. L. Pham, C. Xu, and J. L. Prince, "Current methods in medical image segmentation 1," *Annual review of biomedical engineering*, vol. 2, pp. 315-337, 2000.
- [23] I. H. Witten and E. Frank, *Data Mining: Practical machine learning tools and techniques*: Morgan Kaufmann, 2005.
- [24] G. Thibault, B. Fertl, C. Navarro, S. Pereira, P. Cau, N. Levy, *et al.*, "Texture indexes and gray level size zone matrix application to cell nuclei classification," 2009.
- [25] N. Dalal and B. Triggs, "Histograms of oriented gradients for human detection," in *2005 IEEE Computer Society Conference on Computer Vision and Pattern Recognition (CVPR'05)*, 2005, pp. 886-893.
- [26] D. G. Lowe, "Distinctive image features from scale-invariant keypoints," *International journal of computer vision*, vol. 60, pp. 91-110, 2004.
- [27] D. G. Lowe, "Object recognition from local scale-invariant features," in *Computer vision, 1999. The proceedings of the seventh IEEE international conference on*, 1999, pp. 1150-1157.
- [28] L. Breiman, "Random forests," *Machine learning*, vol. 45, pp. 5-32, 2001.
- [29] L. Breiman, "Bagging predictors," *Machine learning*, vol. 24, pp. 123-140, 1996.

- [30] H. Ishwaran and U. B. Kogalur, "Consistency of random survival forests," *Statistics & probability letters*, vol. 80, pp. 1056-1064, 2010.
- [31] C. Cortes and V. Vapnik, "Support-vector networks," *Machine learning*, vol. 20, pp. 273-297, 1995.
- [32] R. Muralidharan and C. Chandrasekar, "Object Recognition using SVM-KNN based on geometric moment invariant," *International Journal of Computer Trends and Technology-July to Aug*, pp. 215-220, 2011.

CHAPTER IV - RESULTS AND DISCUSSION

1. Introduction

Cancer is a silent disease that should be fought once discovered, and the danger of this war increase with the progression of the disease. The early diagnosis of colorectal cancer presented a challenge to scientists in the last centuries, since it increases the percentage of its treatment, where many studies are taken into consideration such as feature extraction and using many types of classifiers. In order to try making a push for the diagnosis, we try to apply the data in a convenient method, where the classification using CNN and treebagger- SVM [1-3] and KNN- SVM [4, 5] classifiers which uses many types of features are studied in the previous chapter. Its result will be obtained and discussed in this chapter, where it is applied on the same data, in order to know which one is more convenient to our data. CNN initially applied on segmented and non-segmented images to improve the importance of segmentation, where snake method is used after it improved its high performance in chapter II. In this work, we consider a supervised segmentation step similar to a clinical scenario where a pathologist decides which of the segmented regions can be a region of interest for further processing. This method will be compared with some methods that uses the same data and with many other classification methods in order to improve its high performance. Then, treebagger- SVM and KNN-SVM are applied on three features such as SIFT [6] , GLSZM [7] and GLRLM [8] and CNN feature [9], which is extracted from the last feature layer in the proposed CNN, where its result changes with the change of the band number (between 1 and 16). These methods use a new feature type which is extracted from CNN trying to increase the performance of these classifiers which give its importance, taking into consideration the variation of the band number which is also affected even though a little with the results. Finally, the SVM classifier with a feature type and certain band number that gives the best performance is compared with the result taken from CNN. During this work the importance of CNN as features that are extracted automatically

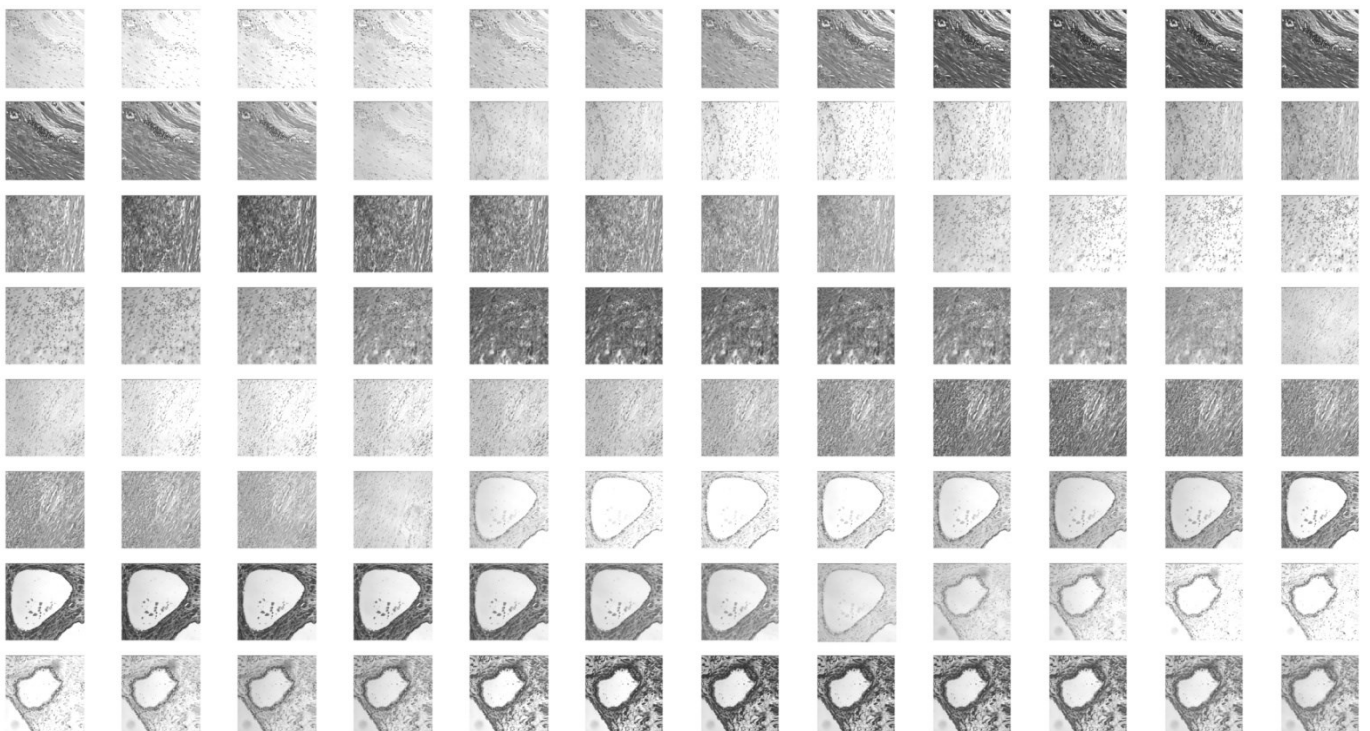
according to the given data, and also as a classifier will be studied, where these methods improve its high performance, which will have a good signs for treatment of colorectal cancer.

2. Classification Results

After the study of the proposed CNN, the data will be applied on it before and after segmentation in order to study the importance of segmenting the image before using it, and another types of classifiers will be used in addition to CNN features in order to study the importance of CNN in both its feature and classifier.

2.1. CNN

In order to study the performance of our proposed classification method CNN, we used 448 images which represents 28 multispectral images (7ST, 7BH, 7IN and 7Ca) for training, and then we used 192 images presented from 12 multispectral images (3ST, 3BH, 3IN and 3Ca) for testing it. Initially in the training algorithm the outputs of the training images are compared to the ground truth (target) and updated the parameters of the network in order to assess the feasibility of CRC progression study. Figure IV.1 shows an example of 256 non-segmented images (64ST, 64BH, 64IN and 64Ca), which shows the difference between images of different frequencies, which may affect the parameters of the network; where this difference is clear especially in the intensity of the image (grey level).



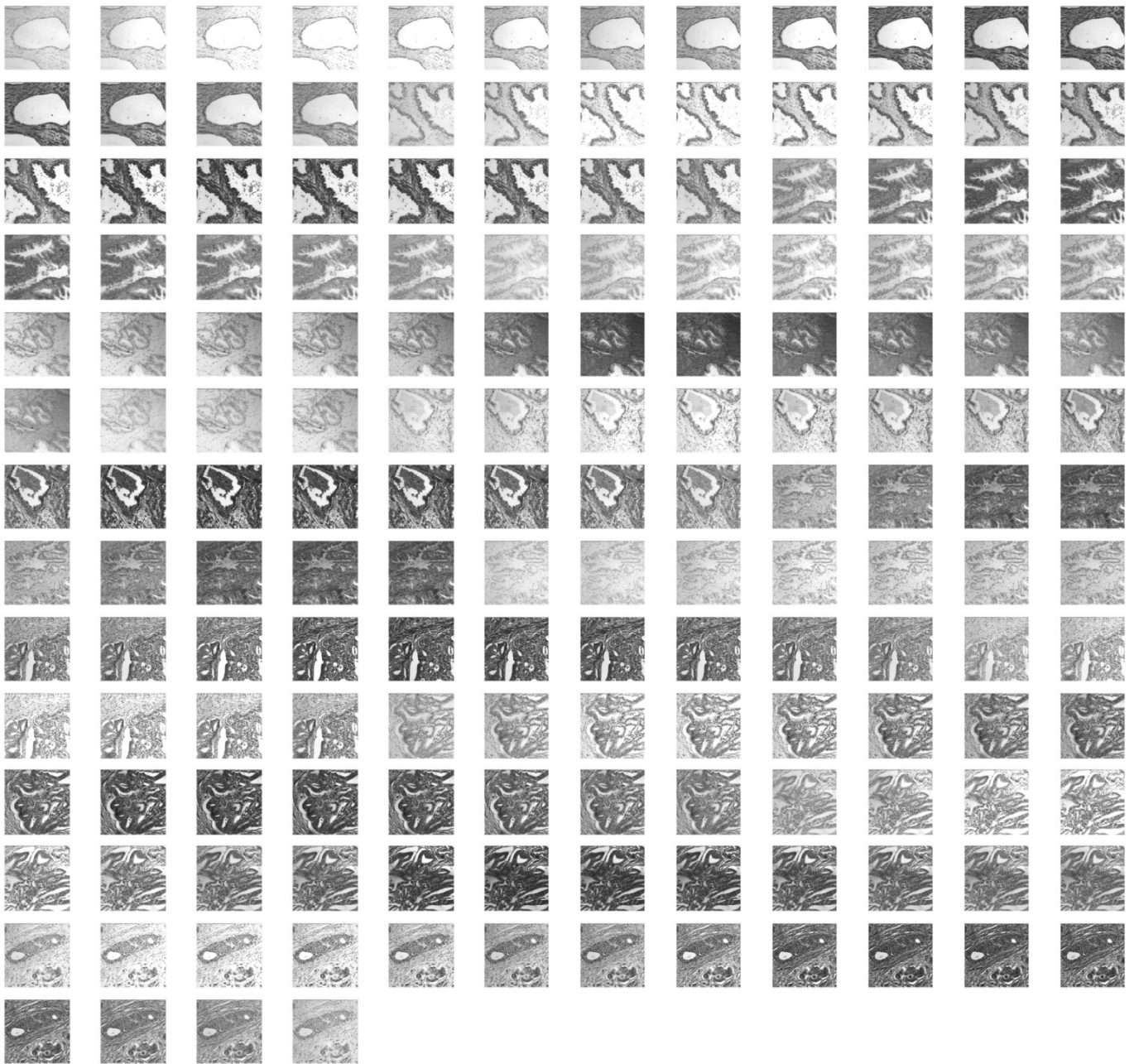


Figure IV. 1. Example of 256 non-segmented images of types ST, BH, IN and Ca

To improve the performance of this method, the variation of MSE during the training process for microscopic images (non-segmented) with respect to the number of epochs, where it represents the number of cycles or training. The variation of the MSE is presented in figure IV.2, where the training in this case reaches 1500 epochs trying to reach a minimum value of the error. As it is shown, the error initially is high (greater than 1.4) and begin to decrease with the increase of training times, until reaching approximately 500 epochs, it will become stable ,consequently it will never changes with the increase of the training samples. The value then

finally reaches approximately 0.205, where this error need to be diminished to validate our work, then there is a need for segmenting the images before classifying it trying to get better performance.

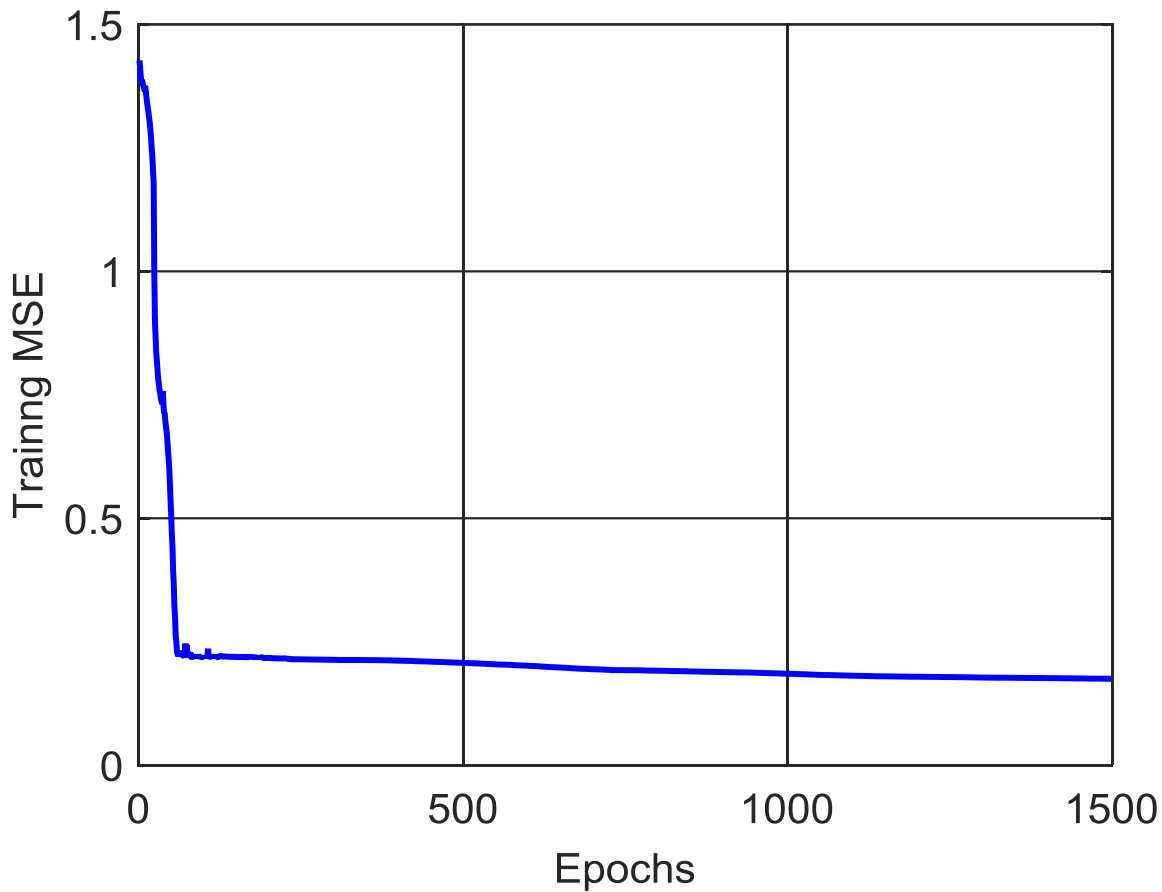
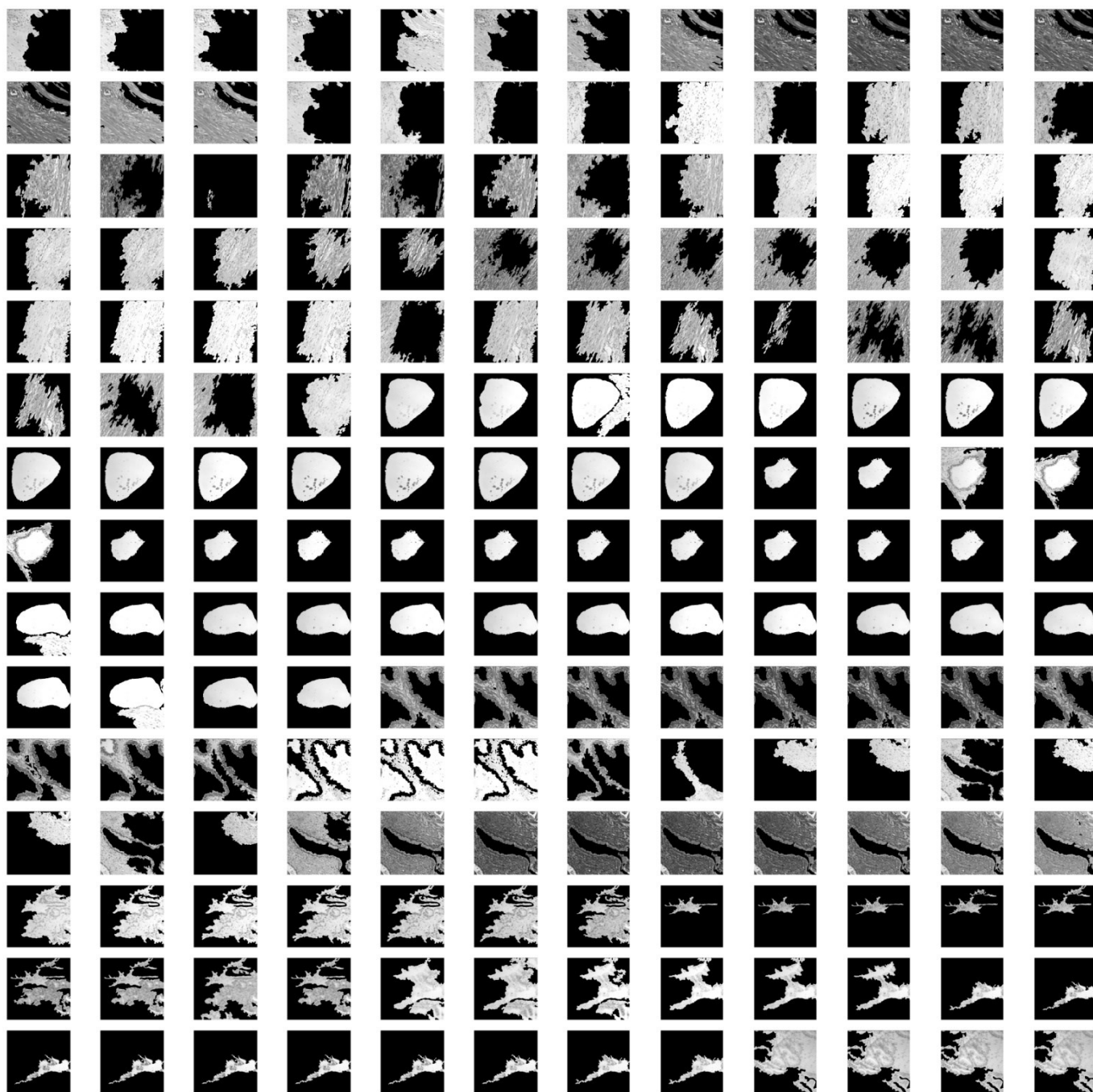


Figure IV. 2. Variation of MSE during the training process of non-segmented images

The same images are segmented using snake method (after improving its high performance with respect to many other methods), where figure IV.3 gives the segmented images of figure IV.1. This segmentation help in limiting the image through its cells that exist among it. Also our data are segmented and applied on the proposed CNN using the same number of images 28 multispectral segmented images (7ST, 7BH, 7IN and 7Ca), and testing case using 12 multispectral images (3ST, 3BH, 3IN and 3Ca). The variation of its MSE during the training process with respect to the number of epochs is shown in figure IV.4. Knowing that the

number of epochs studies are the same as in the case of non-segmented images (1500 epochs), the error reaches a very low value with respect to the previous one, where it is clear that as the number of epochs increases the error decrease rapidly until reaches a very low value (approximately zero) after 500 epochs, to continue its stability.



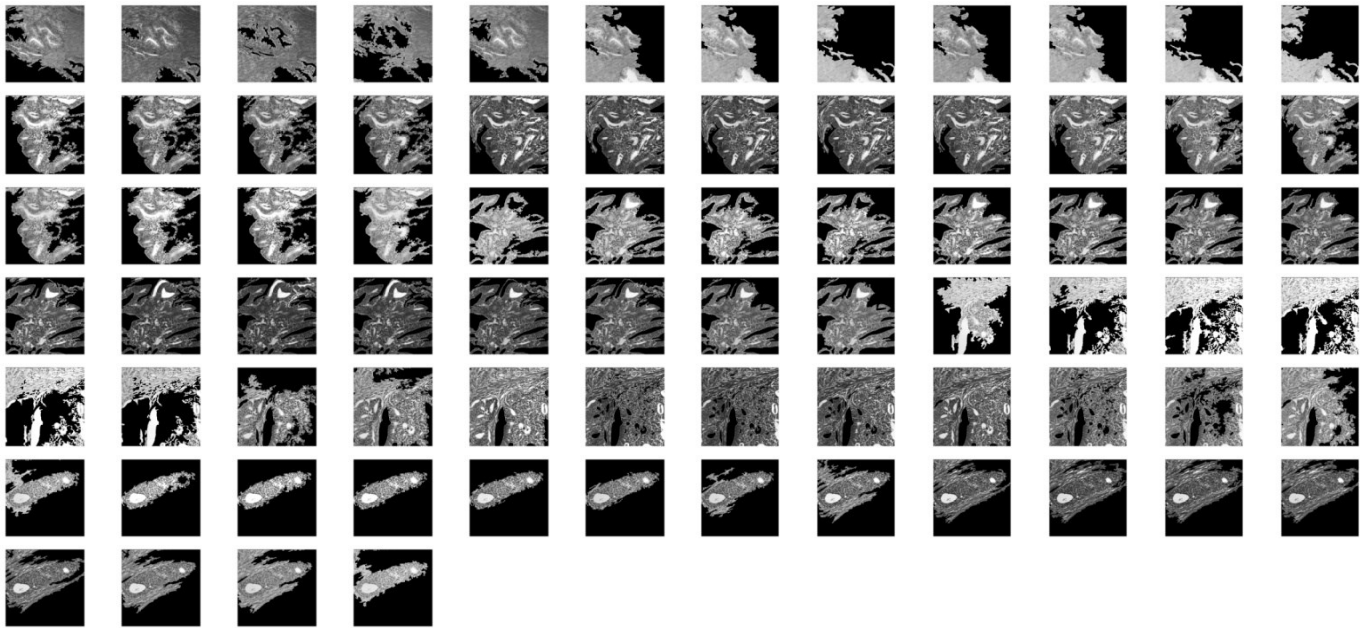


Figure IV. 3. Example of 256 segmented images of types ST, BH, IN and Ca

This difference in the errors between segmented and non-segmented images is clear, where the MSE value achieved 0.205 and 3.259×10^{-5} for microscopic (non-segmented) and segmented images, respectively. This difference improves the importance of the segmentation in our work, since it limits the classification to the cells themselves instead of using the whole image, where it helps in decreasing the false signs and also decrease the duration of classification.

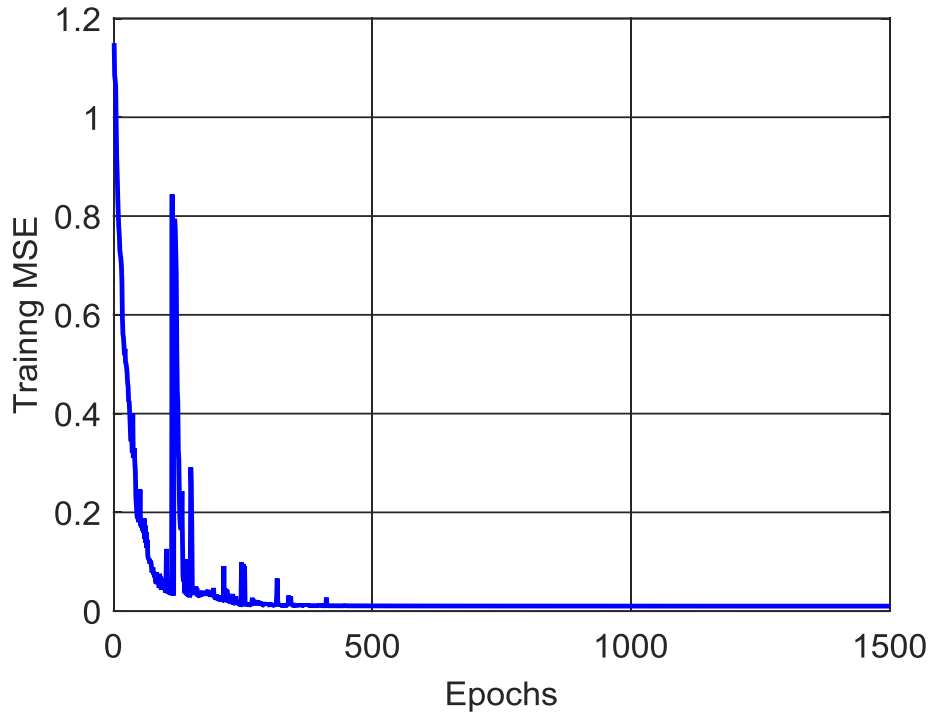


Figure IV. 4. Variation of MSE during the training process of segmented images

Table IV.1 gives a brief result of the accuracy and MSE of the microscopic and segmented images in both training and testing cases. Where the classification rate showed a best accuracy classifier of 100% using segmented images, while the accuracy decreased to 88.52% for non-segmented images during the training, and its MSE 0.205 and 3.259×10^{-5} for microscopic and segmented images, respectively. And the CNN is tested using 192 images which is 12 multispectral (3ST, 3BH, 3IN and 3Ca), where in the case of non-segmented images, the performance metrics showed an MSE of 0.2435 and accuracy of 79.23%. However, the same images are segmented and tested, and the performance metrics were increased with MSE and accuracy value of 0.0001 and 99.168%, respectively.

		MSE	Accuracy (%)
<i>Training</i>	Microscopic images	0.205	88.52%
	Segmented images	3.259×10^{-5}	100%
<i>Testing</i>	Microscopic images	0.2435	79.23%
	Segmented images	1×10^{-4}	99.17%

Table IV. 1: Summary of training and testing of the proposed CNN.

To evaluate our method, we compare it with other methods. The table IV.2 shows the accuracy obtained by Chaddad et al. [10], and Peyret et al. [11], that uses the same data that we use in our proposed method, where it approves the high performance value of our method. Also, Table IV.3, showing the accuracy obtained on examples of the test set by our proposed CNN model, with and without the image segmentation step. For comparison, we also report accuracy values obtained by various tissue classification approaches on the same data. These approaches are categorized according to the type of texture or shape features used (e.g., GLCM, statistical moments, etc.), classifier model (e.g., SVM, nearest-neighbors, etc.), and whether image segmentation is required or not. Note that these approaches work by quantifying a region (segmented or the whole image) with generic features, and using these features as input to a classifier. In contrast, our proposed CNN method learns the features from training data, providing a better representation of the different CRC tissue types.

Classification Techniques	Accuracy%
Chaddad et al. [10]	98.92
Peyret et al. [11]	91.3
Proposed Method	99.168

Table IV. 2: Comparison of classification methods in the same type of data.

From these results, we observe that extracting regions of interest through segmentation enhances the accuracy of our method. Thus, while an accuracy of 79.23% is obtained without segmentation, the accuracy of our method reaches 99.17% on pre-segmented images. While this could be due to various other factors, extracting regions corresponding to CRC tissues provides more discriminative examples to train the CNN. In comparison to other tissue segmentation approaches, our CNN method with segmentation provides the highest accuracy (i.e., 99.17% versus 98.92% for Chaddad et al.). Although relatively small, such improvement in accuracy can have a significant impact considering that the problem is cancer detection. To illustrate the convergence of the parameter optimization phase (i.e., stochastic gradient optimization), we see that the optimization converges after 500 epochs, and that the MSE upon convergence is nearly zero.

This shows that the proposed architecture is complex enough to learn a discriminative representation of tissue types, and that the learning rate is adequate. In practice, the best number of epochs is selected based on the validation accuracy. However, eight segmented images were tested, and the performance metrics were increased with MSE and accuracy value of 0.0001 and 99.168%, respectively.

	Accuracy	Feature types	Classifier models	Segmentation
Chaddad et al. [10]	98.92%	Laplacian of Gaussian filter Discrete wavelets GLCM	LDA Decision trees Nearest neighbors	Yes
Peyret et al. [11]	91.30%	Local binary patterns GLCM Local intensity order patterns	SVM Random forest	No
Kumar et al. [12]	92.19%	Clinically significant biologically features	Nearest neighbors SVM	Yes
Rathore et al. [13]	98.85%	Statistical moments GLCM	SVM	No
Elgamal et al. [14]	97.50%	Discrete wavelets	Nearest neighbors Neural Networks	Yes
Ours (unsegmented)	79.23%	CNN	CNN	No
Ours (segmented)	99.17%	CNN	CNN	Yes

Table IV. 3: Comparison of tissue classification methods on the same data.

2.2. SVM

The SVM classifier is used by many studies from a long time, and it improves its performance in many types of data especially in cancer ones. In the previous chapter, we studied the two types of SVM such as treebagger-SVM and KNN- SVM, using four types of features such as SIFT, GLSZM, GLRLM and CNN. They are trained using the same data used in CNN training which are 28 multispectral segmented images (7ST, 7BH, 7IN and 7Ca), where their outputs are compared to the ground truth in order to evaluate this study, and its testing using 12 multispectral images (3ST, 3BH, 3IN and 3Ca). Table IV.4 shows the average MSE and accuracy values of the four feature methods using treebagger- SVM. Initially by applying these data to the treebagger- SVM, where it gives the average value of the MSE and the accuracy by taking each time a fixed band number for all images for feature type. Beginning by applying GLRLM on treebagger- SVM, it reached its highest performance in the last four bands (13th, 14th, 15th and 16th), where it reached 75.9% and 0.18 as

accuracy and MSE values respectively. The performance increases while applying GLSZM on treebagger-SVM, where it improves its better performance in the 16th band resulting 82.8% as accuracy value and 0.17 as MSE.

Applying SIFT on treebagger- SVM, gives performance better than the previous two features, while it approved its better performance during the last four bands, its accuracy reaches 93.8%, and the MSE is between 0.09 and 0.10 during it. The fourth type of feature presented by CNN features, headway the other three features reaching 94.2% as accuracy value and 0.07 as MSE value during the 16th band. Therefore, the 16th band always gives a better performance than the other 15 bands, and the classification rate showed that the performance reaches its lower value when using GLRLM, and it is increased more using GLSZM, and it still increases using SIFT till reach its better performance for the CNN.

Band	Treebagger- SVM							
	MSE				Accuracy (%)			
	GLRLM	GLSZM	SIFT	CNN	GLRLM	GLSZM	SIFT	CNN
1	0.33	0.27	0.14	0.10	75.7%	82.4%	93.3%	94.0%
2	0.34	0.25	0.14	0.10	75.7%	82.4%	93.3%	94.0%
3	0.33	0.24	0.13	0.09	75.6%	82.6%	93.4%	94.1%
4	0.31	0.26	0.12	0.09	75.6%	82.5%	93.4%	94.1%
5	0.31	0.24	0.14	0.08	75.7%	82.4%	93.5%	94.0%
6	0.28	0.22	0.12	0.09	75.7%	82.4%	93.6%	94.0%
7	0.27	0.21	0.10	0.09	75.6%	82.5%	93.6%	94.1%
8	0.25	0.21	0.10	0.09	75.8%	82.5%	93.5%	94.1%
9	0.25	0.21	0.10	0.08	75.8%	82.5%	93.5%	94.1%
10	0.26	0.19	0.10	0.08	75.7%	82.6%	93.6%	94.2%
11	0.25	0.18	0.08	0.09	75.8%	82.6%	93.7%	94.1%
12	0.22	0.19	0.08	0.09	75.7%	82.7%	93.7%	94.0%
13	0.22	0.17	0.09	0.07	75.9%	82.6%	93.8%	94.1%
14	0.19	0.18	0.09	0.09	75.9%	82.8%	93.8%	94.1%
15	0.19	0.18	0.10	0.08	75.9%	82.7%	93.8%	94.2%
16	0.18	0.17	0.10	0.07	75.9%	82.8%	93.8%	94.2%

Table IV. 4: Performance metrics for multispectral texture of CRC cells using Treebagger SVM classifier.

Applying the same data and the same features on KNN- SVM as a classifier gives a brief result on Table IV.5, where it gives the average MSE and accuracy values of the four feature methods after applying this classifier, and determine at each time a fixed band number for all images.

The first feature applied on KNN-SVM classifier is the GLRLM, where it reaches its highest performance values using 15th and 16th bands which are 73.7% and 0.32 as accuracy and MSE values respectively. While using GLSZM, the performance reaches its highest value which is 80.8% and 0.26 as accuracy and MSE values respectively in the case of the 16th band. The performance increases to 92.7% and 0.15 as accuracy and MSE respectively for both 15th and 16th band using SIFT features. Where finally it reaches 93.8% and 0.10 as accuracy and MSE values respectively in the last four bands (13th, 14th, 15th and 16th bands) using CNN features. Therefore, also the 16th band always give a better performance than the other 15 bands, and the performance increases using the GLRLM, GLSZM, SIFT and CNN respectively. So as a result, between the previous methods, the Treebagger- SVM classification method using CNN features and using the 16th band gives the highest performance between it.

Band	KNN- SVM							
	MSE				Accuracy (%)			
	GLRLM	GLSZM	SIFT	CNN	GLRLM	GLSZM	SIFT	CNN
1	0.41	0.32	0.20	0.18	73.4%	80.1%	92.2%	93.4%
2	0.41	0.32	0.20	0.18	73.3%	80.1%	92.2%	93.6%
3	0.40	0.32	0.19	0.18	73.6%	80.3%	92.2%	93.6%
4	0.40	0.30	0.19	0.18	73.6%	80.5%	92.2%	93.5%
5	0.39	0.30	0.19	0.17	73.6%	80.5%	92.4%	93.6%
6	0.39	0.31	0.19	0.17	73.5%	80.5%	92.4%	93.4%
7	0.40	0.29	0.17	0.17	73.5%	80.6%	92.4%	93.6%
8	0.38	0.29	0.17	0.16	73.7%	80.5%	92.5%	93.5%
9	0.38	0.27	0.17	0.16	73.7%	80.6%	92.6%	93.6%
10	0.37	0.28	0.18	0.14	73.8%	80.8%	92.8%	93.5%
11	0.36	0.27	0.17	0.14	73.9%	80.8%	92.8%	93.6%
12	0.36	0.26	0.16	0.14	73.8%	80.6%	92.8%	93.6%
13	0.36	0.26	0.16	0.10	73.7%	80.7%	92.8%	93.8%
14	0.34	0.26	0.15	0.10	73.7%	80.7%	92.7%	93.8%
15	0.32	0.27	0.15	0.10	73.7%	80.8%	92.7%	93.8%
16	0.32	0.26	0.15	0.10	73.7%	80.8%	92.7%	93.8%

Table IV. 5: Performance metrics for multispectral texture of CRC cells using KNN SVM Classifier.

The above result improves the importance of the features extracted from the images in classifying it, and its bands. Knowing that the two classifying methods are used, the result shows the variation of the accuracy values with the variation of the type of features extracted from the images, and its band number. Where the

features extracted from CNN improves its high performance with respect to the other methods. Therefore, as the convenient features are extracted, the diagnosis of CRC will advance more.

Table IV.6 shows some examples that use different types of features. Chaddad et al. used three types of features such as: gray level co-occurrence matrix (GLCM), Discrete Wavelet (DW) Transform and LoG based Texture on the segmented images. Also Peyret et al. used different techniques for texture feature extraction including local binary patterns, Harlick features and local intensity order patterns, taking in consideration that it didn't apply the segmentation on the data. Kumar et al. used clinically significant and biologically interpretable features, and it was applied on the segmented images.

And Color components based statistical moments (CCSM) and Harlick features, which was studied by Rathore et al., and applied on the initial images. Also, Elgamal et al. used discrete wavelet transforms DWT feature for the segmented images.

	feature based method	Segmented PT
Chaddad et al.[10]	Laplacian of Gaussian filter Discrete wavelet transforms Gray level co-occurrence matrix	Yes
Peyret et al. [11]	Local binary patterns Gray level co-occurrence matrix local intensity order patterns	Non
Kumar et al. [12]	Clinically significant biologically features	Yes
Rathore et al. [13]	Statistical moments Gray level co-occurrence matrix	Non
Elgamal et al.[14]	Discrete wavelet transforms	Yes
Our work	Convolution neural network	Yes

Table IV. 6: Examples of some methods using different feature in the same type of data.

2.3. Comparison between CNN and SVM

Table IV.7 presents a brief result of applying our proposed CNN on our data without the need for using features, since it is automatically extracted by itself according to the data used. And also it shows the accuracy of the treebagger-SVM and KNN-SVM using the CNN features, applying on the same data used in CNN classifier which is presented in 40 multispectral images. It is clear that CNN gives the better performance with

respect to the other, which is due to the network resulted initially, and also to the importance of automatic detection of features.

Classification Techniques	Accuracy%	Feature used
CNN	99.168	Automatically extracted
Treebagger- SVM	94.2	CNN
KNN- SVM	93.8	CNN

Table IV. 7: Comparison of CNN and SVM.

2.4. Discussion

In our work, we initially make a comparison between segmented and non-segmented images during classification technique, using the snake segmentation algorithm studied in chapter II and it proved its high performance. This comparison is done to visualize the effect of segmentation on the performance of the classification task, and facilitate its work in limiting the size and needed items in the images and decrease its time. It's highly remarkable that the performance of the classification task is improved when the input images are segmented before classified. This proves the importance and effectiveness of segmentation before classification providing a better performance.

These segmented images applied on our proposed CNN, after studying of many networks in order to get the more applicable one for our data. Since the network is important, our primary design aim was to obtain the best performance vs. the network size. Specifically, we increased the number of layers until near-maximal performance was achieved. We also experimented with layer-to-layer connections to improve performance. The proposed CNN is compared to many different classifier methods, where most of them classify according to a certain types of features which should be determined before. The proposed CNN proves its strength over the previously-used classifiers, where the main difference between our approach and other methods, is their choice of manual feature extraction algorithms separate from the classifier itself, which gives error according to the type of features extracted (if it is convenient to the data), while the CNN automatically learn local feature extractors, as explained earlier.

And on other side, applying treebagger- SVM and KNN- SVM on four different types of features such as GLRLM, GLSZM, SIFT and features extracted from our proposed CNN, using 16 bands number on each image which is between 1 and 16. The features taken from CNN give higher performance than the other types of features in both classifier methods (treebagger- SVM and KNN- SVM) and on the 16th band. This is due

to the automatic features which are extracted to be convenient according to the types of images which is not available in manual features extraction. Between these two classification methods, the treebagger- SVM classifier using the CNN features gives the better performance in the 16th band.

However, we study the CNN as a classifier and also we take its features and apply it on two different types of classifiers such as treebagger- SVM and KNN- SVM. This method improves its high strength and performance in both its features and its classifier. Where during the use of treebagger- SVM and KNN- SVM the CNN features reaches the highest performance with respect to the others and its performance increase while using CNN classifier.

The CRC tissue classification approaches presented in Table IV.3 are based on the assumption that such tissues can be effectively described using generic texture or morphological features. For example, Chaddad et al. used texture features derived from gray level co-occurrence matrices (GLCM), discrete wavelet transforms and Laplacian of Gaussian filters, computed on pre-segmented regions, to classify the same images with an accuracy of 98.92% [10]. Likewise, Peyret et al. computed texture features such as local binary and local intensity order patterns, on non-segmented to images, obtaining an accuracy of 91.3% [11]. In contrast, we proposed a data-driven method, based on CNNs, to learn an optimal representation of tissues from training data. Our experiments showed this method outperforms existing approaches, even with a small number of tissue samples, with an accuracy of 99.17%. Results have also shown the usefulness of using pre-segmented images, which significantly improves the accuracy by focusing computation on relevant tissue regions within the image.

While results are promising, this study also has several limitations. First it is based on a single small cohort of 40 patients. Having a larger set of biopsy images from different patients would help capture the full variability of tissues in the progression of CRC. Moreover, to obtain an optimal accuracy, our method currently requires the pathologist to select the region of interest from a segmented image. In order to have a fully automated pipeline, this step should be replaced by a supervised learning model which would determine the region of interest from training data.

3. Conclusion

In this chapter we have presented a method for the classification of CRC tissues from multispectral biopsy images, based on active contour segmentation and on three classifiers such as: CNN, treebagger- SVM and KNN- SVM after extracting features from the proposed CNN, which learn a discriminative representation

directly from the data. Experiments of these methods are done on multispectral images of 40 patients, and CNN outperform traditional approaches when using pre-segmented images, and also outperform the two other classifiers which scored the top ranking in the last century. Also the testing accuracy of our proposed approach is compared with that of other methods applied either on the same type of data or not, and in both cases, it proves the strength of the CNN classifier over other used classifiers. CNN improves its strength in extracting its features and also in classifying it.

In future work, we will extend this study by including a larger number of patients and using a fully automated segmentation step.

References of Chapter IV

- [1] H. Ishwaran and U. B. Kogalur, "Consistency of random survival forests," *Statistics & probability letters*, vol. 80, pp. 1056-1064, 2010.
- [2] L. Breiman, "Random forests," *Machine learning*, vol. 45, pp. 5-32, 2001.
- [3] L. Breiman, "Bagging predictors," *Machine learning*, vol. 24, pp. 123-140, 1996.
- [4] C. Cortes and V. Vapnik, "Support-vector networks," *Machine learning*, vol. 20, pp. 273-297, 1995.
- [5] R. Muralidharan and C. Chandrasekar, "Object Recognition using SVM-KNN based on geometric moment invariant," *International Journal of Computer Trends and Technology-July to Aug*, pp. 215-220, 2011.
- [6] D. G. Lowe, "Object recognition from local scale-invariant features," in *Computer vision, 1999. The proceedings of the seventh IEEE international conference on*, 1999, pp. 1150-1157.
- [7] D. G. Lowe, "Distinctive image features from scale-invariant keypoints," *International journal of computer vision*, vol. 60, pp. 91-110, 2004.
- [8] G. Thibault, B. Fertil, C. Navarro, S. Pereira, P. Cau, N. Levy, *et al.*, "Texture indexes and gray level size zone matrix application to cell nuclei classification," 2009.
- [9] S. L. Phung and A. Bouzerdoum, "MATLAB library for convolutional neural networks," *University of Wollongong, Tech. Rep.*, URL: <http://www.elec.uow.edu.au/staff/sphung>, 2009.
- [10] A. Chaddad, C. Desrosiers, A. Bouridane, M. Toews, L. Hassan, and C. Tanougast, "Multi Texture Analysis of Colorectal Cancer Continuum Using Multispectral Imagery," *PloS one*, vol. 11, p. e0149893, 2016.
- [11] R. Peyret, A. Bouridane, S. A. Al-Maadeed, S. Kunhoth, and F. Khelifi, "Texture analysis for colorectal tumour biopsies using multispectral imagery," in *Engineering in Medicine and Biology Society (EMBC), 2015 37th Annual International Conference of the IEEE*, 2015, pp. 7218-7221.
- [12] R. Kumar, R. Srivastava, and S. Srivastava, "Detection and Classification of Cancer from Microscopic Biopsy Images Using Clinically Significant and Biologically Interpretable Features," *Journal of Medical Engineering*, vol. 2015, 2015.
- [13] S. Rathore, M. Hussain, M. A. Iftikhar, and A. Jalil, "Ensemble classification of colon biopsy images based on information rich hybrid features," *Computers in biology and medicine*, vol. 47, pp. 76-92, 2014.
- [14] M. Elgamal, "Automatic skin cancer images classification," *IJACSA) International Journal of Advanced Computer Science and Applications*, vol. 4, 2013.

CONCLUSION AND PERSPECTIVES

People were concerned about cancer over years, and billions of dollars were spent to find a treatment for it. And colorectal cancer is one of the most dangerous types of cancer, where it is expected to have 50,260 deaths during 2017 due to it, the thing that makes it urgent to find an anticipated detection and treatment for it to prevent its advance. In general, the detection of this cancer cells are based on microscopic observation of the cells, where this method is done manually which makes it depends majorly on the medical staff and it needs high time for computation. Knowing that these cells can be decomposed into normal cells (ST) and abnormal cells (BH, IN and Ca), there is a big need to update the detection and classification of these cells images, where this change begins by an intimate selection of the camera type, image type and a convenient filter for it, then optimizing an automatic detection and classification that meets our need.

The importance of the work done in this paper is shown in the high performance of the proposed method used and also in the comparison done between it and many other methods. Where initially we studied and applied many segmentation methods on our data such as: snake, thresholding, edge based, and region based

segmentation images. After applying the same data to these methods, we concluded that the snake method is more convenient among other segmentation methods, where it takes 16 images of different bands for every multispectral image, and it reaches the highest performance value. But the importance of segmentation appears when each classification method applied on the same segmented and non segmented data, and produced its highest performance among segmented images, since it was applied only on the segmented parts of the images, which help it to avoid a lot of mistakes and noises during the classification method. Till this step we convert the image into a filtered one that contains the selected cells that are ready to be selected according to their types as normal cells (ST) and abnormal cells (BH, IN and Ca), the challenge then begins by finding a good classification method that improves its high performance in our data.

Over years, many classification studies depended on the features extracted from data, where the selection of these features in each application is very important. In our work ,two types of SVM classification are studied such as Treebagger-SVM and KNN-SVM, and each was applied on three different types of features such as SIFT, GLSZM, GLRLM and also on the feature extracted from CNN that is automatically selected according to the type of data. Since the CNN features are extracted automatically, the two classification types give the best results when applied to it compared to other feature types, the thing that concludes its importance with respect to other feature types. Then the comparison was done between the two classifiers Treebagger-SVM and KNN-SVM that applied on CNN features, where Treebagger classifier reached the highest performance comparing to KNN one. But our work does not stop in this point, since the features extracted from CNN give the best result; we study the classification of CNN too in order to find if it can give better performance than the studied techniques.

CNN improves its importance over years due to the self adaption of its characteristics, according to the type of data used. The precise work begins in choosing the perfect network that will meet our needs, so we study many networks, where we search for the smallest one with perfect result in order to decrease the time computation of the process. The proposed network consists of 6 layers, and when our data is applied it reaches 100% and 99.625% as training and testing accuracy values, and 3.259×10^{-5} and 10^{-4} for training and testing mean squared error in case of segmented images respectively. This CNN is compared to the Treebagger classifier after applying to CNN features, and it improves its high performance with respect to it, so improving the power of CNN classification too. Therefore, CNN improves its efficiency in our data in both features and classification of the images after segmenting it, which can help in a true early diagnosis of CRC which will help in decreasing the number of deaths due to it.

As a future work, we are going to make a combination of many segmented methods that will produce a new one that takes the advantages from them and decrease the problems facing them in order to get the highest performance in segmenting an image. Then we are going to extend our study by increasing the number of patients in order to increase our data, and this method will not be monopolized on colorectal cancer, but it will be applied on many other types of cancer. In order to have a quick diagnosis that will make the humankind benefit from it, we are going to transform our proposed work into hardware implementation in a fast technology such as FPGA technology.

List of Publications

Articles in internationally reviewed academic journals

H. Haj-Hassan, A. Chaddad, Y. Harkouss, C. Desrosiers, M. Toews, C. Tanougast. “*Classifications of multispectral colorectal cancer tissues using convolution neural network*”. Journal of Pathology Informatics, Vol.8, No.1, Published online 2017 Feb 28

Papers at international science conferences published in full in proceedings

H. Haj-Hassan, A. Chaddad, C. Tanougast, and Y. Harkouss. “*Hybrid segmentation of bio-images*”. In 45th International Conference on Computers & Industrial Engineering Digital Information and Communication Technology on 2015, Vol.2, 2015, pp. 1431-1437.

H. Haj-Hassan, A. Chaddad, C. Tanougast, and Y. Harkouss. “*Comparison of segmentation techniques for histopathological images*”. In Digital Information and Communication Technology and its Applications (DICTAP), 2015 Fifth International Conference on, 2015, pp. 80-85.

H. Haj-Hassan, A. Chaddad, C. Tanougast, and Y. Harkouss. “*Segmentation of abnormal cells by using level set model*”. In Control, Decision and Information Technologies (CoDIT), 2014 International Conference on, 2014, pp. 770-773.

